MIGRATION OF DREDGED MATERIAL MOUNDS: PREDICTIONS BASED ON FIELD MEASUREMENTS OF WAVES, CURRENTS, AND SUSPENDED SEDIMENTS, BRUNSWICK, GA

A Thesis
Presented to
The Academic Faculty

By

Charley R. Johnson

In Partial Fulfillment
Of the Requirements for the Degree
Master of Science in Environmental Engineering

Georgia Institute of Technology

May, 2005

MIGRATION OF DREDGED MATERIAL MOUNDS: PREDICTIONS BASED ON FIELD MEASUREMENTS OF WAVES, CURRENTS, AND SUSPENDED SEDIMENTS, BRUNSWICK, GA

Approved by:

Dr. Paul A. Work, Advisor
School of Civil and Environmental Engineering
Georgia Institute of Technology--Savannah

Dr. Kevin Haas
School of Civil and Environmental Engineering
Georgia Institute of Technology – Savannah

Dr. F. Michael Saunders
School of Civil and Environmental Engineering
Georgia Institute of Technology

Date Approved: April 8, 2005

ACKNOWLEDGEMENTS

This study was supported by the United States Army Corps of Engineers, Coastal and Hydraulics Laboratory, Waterways Experiment Station, Vicksburg, Mississippi. Jarrell Smith and Joseph Gailani from the Corps are thanked for their input along with Trap Puckette and Carol Coomes of Evans-Hamilton, Inc. who assisted with the interpretation of data. I would like to thank Dr. Paul Work who served as the advisor on my research committee and guided me through the Master's program. I appreciate Dr. Kevin Haas who gave insight which helped in the completion of the project, and Dr. Michael Saunders who, among other things, fielded numerous logistical and administrative questions during the course of my studies.

Many other people were a part of my life as a graduate student, and they made it a more enjoyable experience. They include Lindsay Check, my main cohort and homework buddy; Huseyin Demir, my office mate who answered numerous research oriented and MatLAB questions every day; and Brian Sapp, Kemal Cambazoglu, Jason Check, Heath Lloyd, Bobby Wellman, and Doug Curtis, the weekly basketball crew. My second family, the Harpers, and friends like Joey also helped to divert my mind from some of the stresses of school. But, if it were not for my professors and many friends from Mercer University, this endeavor would have never been successful.

Finally many thanks to my parents, sister, and grandparents in Jesup and the Big-O, who have always supported me through all my endeavors and pushed me to accomplish much more than I could alone.

TABLE OF CONTENTS

LIST OF TABLES

LIST OF FIGURES

SUMMARY

Along the coastline of the United States there are many harbors, inlets, and channels that must be dredged in order to maintain navigability. Most of these operations are managed by the United States Army Corps of Engineers (USACE). The sediments removed from these areas have typically been disposed of far from the shore at depths which remove them from the littoral cycle. This offshore disposal, while being the easiest and most economical method, often causes enhanced erosion downdrift of the dredging activity. In Georgia there are two entrance channels that are maintained via periodic dredging. Sediments removed from the channel at Brunswick, Georgia have typically been disposed of in deep water, which has caused added erosion on the downdrift (south) side of the channel or along Jekyll Island in this case (Griffin and Henry 1984).

A potentially viable alternative to offshore disposal is placement of sediments in the nearshore region. Sediments placed in the nearshore can then be acted on by waves and currents and possibly be pushed ashore, thereby benefiting the shoreline. Sediments from the Brunswick Entrance Channel were dredged in the winter of 2002-2003 and placed in several mounds adjacent to the entrance channel. An experiment was initiated following the dredged material placement to assess the feasibility of a nearshore mound providing material to the downdrift beaches along Jekyll Island. This thesis, which addresses the movement of sediments away from one of these dredged material mounds

adjacent to the entrance channel, is one component of that study The hope is that if the efforts to predict sediment transport at Brunswick are successful, this placement option might be used to mitigate erosion at other locations.

Following dredged material placement in Brunswick, several optical and acoustic instrument packages were deployed to collect data describing waves, currents, and sediments. Two sizes of fluorescent tracer, one sand-sized (d_{50}=240 μm) and one mud-sized (d_{50}=65 μm), were also deployed over the crest of the mound. Several bathymetric surveys and the subsequent sampling of fluorescent tracer material placed in the mound were conducted to give an additional picture of sediment transport trends in the area. Results of the tracer study indicated that the mud-sized tracer was winnowed away quickly (i.e., in a matter of days) while the sand size fraction remained. Additional sampling is needed to determine the fate of the sand sized tracer material.

After the data describing waves, sediments, and mean velocities at the mound were collected, quality control procedures were employed to eliminate erroneous data points. Four techniques were then employed using the data to compute sediment transport rate and direction, and predictions into the fate of the placed sediments were made. Two of the methods used only mean currents to make sediment transport predictions while one method estimated suspended sediment flux solely from measured quantities. The most physically correct method considered both waves and currents for transport predictions. Results indicate that the channel steers the flow of water and sediment, with net transport of sediments being nearly parallel to the channel as they leave the mound.

Sediment transport calculations suggest that transport directions were independent of sediment size, with all sand-sized sediments predicted to move in the onshore direction. Predictions indicate that sediment transport rates are size- and time-dependent with more significant movement occurring in the spring over the summer. The predictive methods considered suggest that the mound will deflate at a rate of 8-30 cm/month while the bathymetric survey data gives an average erosion rate of 20-45 cm/month over the crest of the mound. The predictions assume that no sediment is deposited on the mound (i.e., the mound serves as a sediment source only).

Predicting the ultimate fate of sediments after they leave the dredged material mound is beyond the scope of this study; however, the results of this study will be used for calibration and validation of large-scale hydrodynamic modeling efforts currently underway by the United States Army Corps of Engineers. These models will then be used to assess the likelihood of materials from the mound making their way onto Jekyll Island. If efforts to predict dredged material movement at Brunswick are successful and nearshore placement proves to be a feasible option, it is possible that this method could be applied at other locations where similar problems exist.

CHAPTER 1

INTRODUCTION

For many years, material dredged from coastal navigation channels was simply disposed of via the most economical means, which typically meant offshore placement at depths such that the dredged sediments were removed from the littoral cycle. This offshore disposal, while often being the most economically viable method, can negatively impact the sediment budget of the coastal region and lead to shoreline retreat on the downdrift side of the dredged channel. Examples of this exist throughout the world (Dean and Dalrymple 2002).

The United States Army Corps of Engineers (USACE) is currently responsible for maintenance of over 40,000 km of dredged channels, serving 400 major U.S. ports, including Brunswick Harbor in Georgia (USACE 1999). Natural depth of the channel is not adequate to accommodate large ships, thus dredging has been conducted to give a depth in excess of 9 m mean lower low water level (MLLW), which allows for safe passage of ships into and out of the port regardless of tidal stage. The harbor at Brunswick is very important for commerce in Georgia, as well as the United States, as many ships carrying cars and other goods arrive daily. Sediments removed from the channel are typically pumped several kilometers offshore and placed adjacent to the Brunswick Entrance Channel in mounds such as those shown in Figure 1.

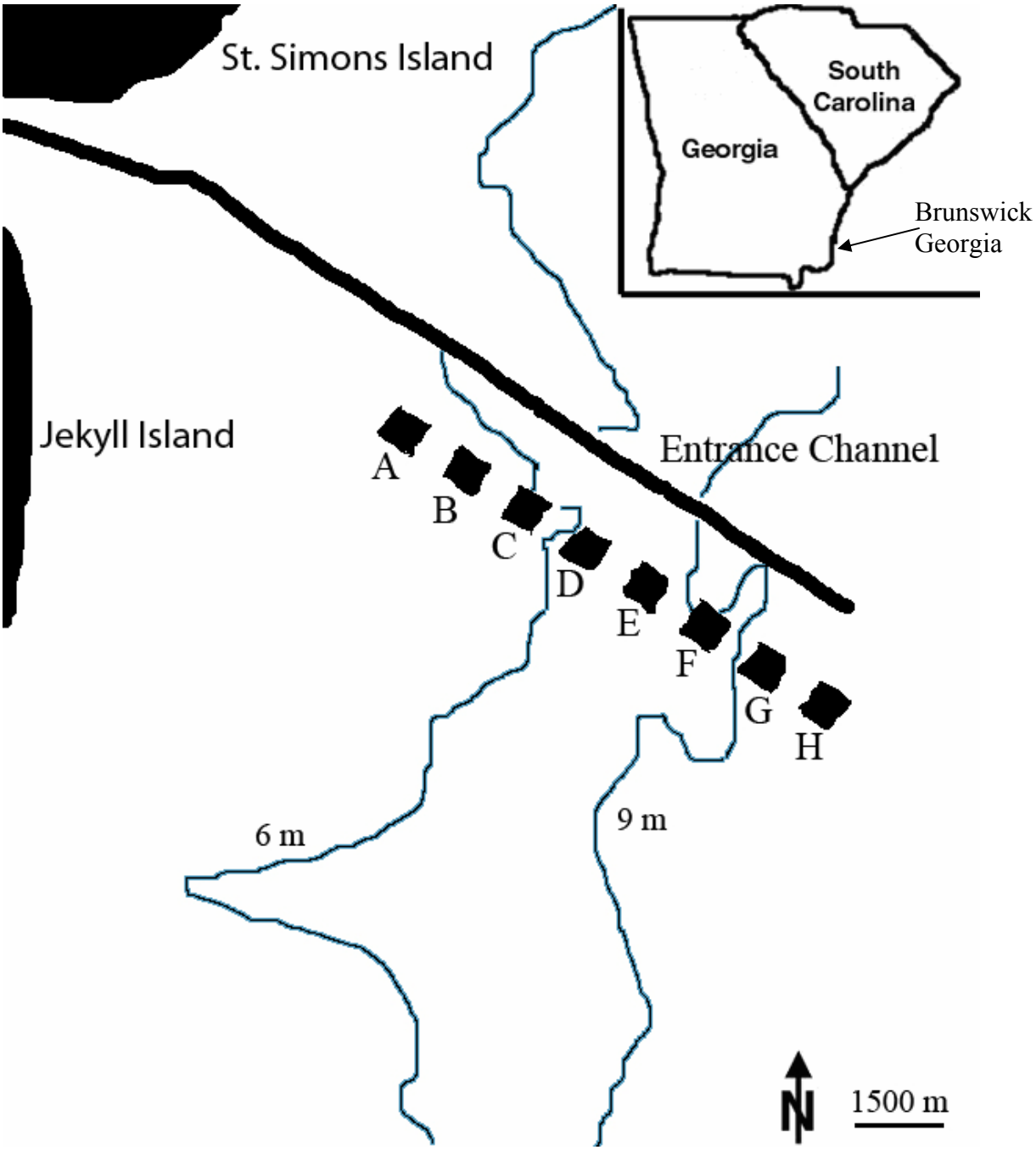

Figure 1. Brunswick Harbor Entrance Channel. St. Simons Island is located to the north while Jekyll Island is located to the south. Dredged material mounds (labeled A-H) are located adjacent to the entrance channel on the downdrift (south) side.

The USACE are investigating methods for reducing dredging costs and minimizing potential negative impacts of dredging. One approach that may reduce downdrift impacts of dredging without incurring higher costs associated with onshore placement is placement of dredged material in nearshore mounds. If a mound is placed in the nearshore region (close to the shoreline), natural processes may sort the material in the mound, removing fines. Beach grade material, sand suitable for placement on the beach, may then be washed ashore, thus lessening the negative impacts of dredging and providing additional storm protection to properties near the coast (e.g. Hands 1992).

In order to assess the feasibility of a nearshore placement program at Brunswick, the USACE initiated a study in 2002 to collect data describing sediments, bathymetry, waves, and currents in the area. The USACE and subcontractors deployed instruments around several of the existing dredged material mounds to collect these data. The USACE have also applied a large-scale numerical model for currents, waves, and sediment transport trends in the area (USACE 2004). Fluorescent tracer was also mixed with sediments placed on the crest of the mound, and subsequent sampling three months later revealed that little to no movement of the sand-sized tracer material had occurred (ETS 2004). A tracer is an identifiable material that is introduced and followed through a system in order to learn about a process. For this study, the tracer was synthetic fluorescent sand used to learn about sediment transport patterns.

The project described in this thesis focused on the interpretation of the collected data describing waves, currents, and sediments near the Brunswick mounds. The primary project objective was to use the data, along with appropriate wave theories and sediment transport equations, to describe long-term movement, on the order of months to years, of

the sediment in the dredged material mound. The two dominant sediment transport modes, bed load transport and suspended sediment transport, were treated separately and combined to give estimation of total load. Bed load is sediment transport within a certain distance of the sea floor, suspended load is material carried within the fluid column, and total load is the sum of the two. From the data collected by the instruments, a sediment transport rate and direction for each mode and for various sediment size fractions were calculated to give net sediment transport trends. Instances where waves and currents are not collinear and the influence of wave nonlinearities on transport are both considered. The influences of different predictive methodologies and sediment sizes are also explored.

The sediment transport rates calculated using the predictive methodologies were then compared to bathymetric survey data in an effort to validate the results and methodologies used for sediment transport predictions. The ultimate goal was to assess the likelihood of sediments placed in the mound being sorted and washed ashore, thus re-entering the littoral cycle, so that the beaches of Jekyll Island might benefit. The sediment transport trends obtained from this study will also be used to validate and calibrate the results of the hydrodynamic and sediment transport models developed by the USACE (USACE 2004).

The background material, methodologies, and results of this study are presented in six chapters. Previous relevant studies are summarized in the literature review in Chapter 2. Chapter 3 discusses the field instrumentation used to collect the data for sediment transport predictions. In this chapter the operating principles of each instrument, deployment configurations, type of data collected, limitations, and error

bounds are also discussed. In Chapter 4, quality assurance procedures and the methodology used for sediment transport predictions are presented along with the results of each method. Chapter 5 includes predictions of long-term transport trends at the dredged material placement site. Bathymetric survey data are presented in Chapter 5 in an effort to validate the methodologies and results from Chapter 4. Finally in Chapter 6 a summary of the results found in this study and suggestions for further work and improvements are presented.

CHAPTER 2

LITERATURE REVIEW

The feasibility of nearshore placement of dredged material has been investigated previously, via prototype scale experiments as well as laboratory, analytical and numerical studies. This chapter reviews some of those previous studies. Several sediment transport equations are discussed along with options for describing the vertical profile of suspended sediment concentration. Finally, previous studies of currents and sediments near Brunswick, Georgia are reviewed.

2.1 Evolution of Placed Dredged Material

Before dredging of an entrance channel or harbor can occur, the placement of the dredged material must be considered. Dredged materials can be placed onshore or offshore in open water dredged material placement sites. While studying dredging operations in the coastal arena, it is important to understand terminology used in the literature. Hands (1992) defined several terms that are useful and will be used throughout this report. A berm is a prominent, submerged, man-made, positive-relief feature created intentionally on the sea floor. If a berm has fairly equidimensional sides then it is known as a mound. If a berm is elongated in one direction it is termed a bar or ridge. Finally, a berm can be placed such that it provides sediments to the littoral system; this is termed a feeder berm or feeder mound.

The Handbook of Coastal Engineering describes three steps that dredged material goes through when placed offshore in open water (Moritz et al. 2000):

1. Convective descent—material descends through the water column due to gravity;
2. Dynamic collapse—the sediment either reaches neutral buoyancy or arrives at the bottom;
3. Passive transport or dispersion—material is transported due to ambient processes such as currents and waves rather than due to the placement operation.

In an effort to describe the entire placement operation fully, many numerical models have been developed to describe the transport of sediments during each of these steps. Such models include the Short-Term Fate (STFATE), Long-Term Fate (LTFATE), and Multiple-Dump (MDFATE) models developed by the USACE (Moritz et al. 2000). Each of these models focuses on a specific phase of the process. For the study employed here, the focus will be on step 3, or the evolution of an existing offshore dredged material mound.

Once material is placed in an open water mound, the site can either be dispersive or non-dispersive. Moritz et al. (2000) classified a non-dispersive site as one in which 95-99% of the dredged material placed stays in the immediate vicinity. When mounds are located closer to shore, in shallower water, as they are at Brunswick, Georgia, it is expected that they will be dispersive and possibly provide sediment to the littoral cycle. Moritz explains that when a mound is dispersive, one of the key issues is that the placed dredged material must be transported away from the point of dredging. In Georgia, the

predominant transport along the coast is from north to south, so dredged material should be placed downdrift of the entrance channel to minimize infilling. There are often local or seasonal sediment transport reversals, at inlets which have to be considered. Mound placement can also modify hydrodynamic trends in an area, so studies should be conducted to investigate how dredged material placement affects sediment transport trends.

Kraus (1992) outlined several factors that should be taken into account when placing berms such that they might be "active" and benefit the nearshore environment. One factor to consider when placing a feeder berm is the location or depth of placement. A feeder berm should be placed in sufficiently shallow depths to maximize wave breaking over the berm. If placed properly the berm can help the nearshore region in two ways. First wave breaking over the berm promotes the movement of sediment away from the mound, maximizing the chance of sediments reaching the littoral system and indirectly nourishing the beaches. Second, such a placement scheme gives added protection to the beach by dissipating wave energy. The mounds at Brunswick were placed so that they would serve these purposes.

A second issue Kraus discussed in his paper is the timing of dredged material placement. He explained that in the northern hemisphere sand is typically transported toward shore in the summer when ocean swell dominates. In the winter, local storms, hurricanes, and extratropical events cause steeper waves which tend to push sand offshore; therefore, dredged material placed in the nearshore is more likely to nourish the beach if placed in the early to mid-summer period.

Kraus et al. (1991) studied erosion and accretion of beach profiles by plotting non-dimensional sediment fall speed, H_o/wT, versus a sediment Froude parameter $w/(gH_o)^{1/2}$, noting whether a bar moved on- or offshore. Both wave tank and field data were considered with the goal being to develop a method to quickly predict onshore/offshore movement of bars on a beach or within offshore dredged material mounds.

Ahrens and Hands (1998) also tried to predict onshore/offshore movement of sediments using an approach similar to that of Kraus et al. (1991). Their method was also intended to predict erosion/accretion conditions for beach profiles but extension to offshore dredged mounds was investigated. Ahrens and Hands (1998) plotted Mobility Number, N_s, versus deep-water wave steepness, H_o/L_o, where H_o is the deep water wave height and L_o is the deep water wave length. Mobility Number is given in Equation (1) as:

$$N_s = \frac{H}{(s-1)d_{50}} \tag{1}$$

H = representative wave height [L];

s = specific gravity;

d_{50} = median sediment diameter [L].

The graph was then divided into four sections depending on experimental observations. These sections included: no sediment movement, accretion of sediments, transition, and erosion of sediments. A study by Zenovich and Schwartz (1987) was then used to see if the graph could be extended to predict movement of materials placed offshore. In the Zenovich and Schwartz study, gravel was dumped offshore in 4-6 m of water and storm conditions moved the material onshore over the next year. The

conditions described by the authors were plotted on the Ahrens and Hands graph and found to fall in the accretion region which matched observations. Note that both the Kraus et al. (1991) and Ahrens and Hands (1998) studies base sediment transport on wave height and do not consider tidal or wind-driven flows.

Douglass et al. (1995) studied the movement of several dredged material mounds offshore of Mobile, Alabama. The mounds were placed south Dauphin Island in the Gulf of Mexico. The largest mound (13 million m^3) is near the 15 m depth contour and consists primarily of fine grained material. Two smaller sand berms were located closer to shore in depths similar to the Brunswick dredged material mounds. These berms were placed in the nearshore region to save beach quality sand from traditional deep-water disposal and study the effects of Gulf waves on the berms.

Instruments were installed in the area for a 4-year monitoring period and included wave gauges and near bottom electromagnetic current meters. The authors also had ample survey data to show how the dredged mounds evolved over time. The goal of the study was to learn the dominant mechanisms for movement so that depths, locations, and configurations of future berms could be predicted with greater success. The authors investigated several movement mechanisms including: mean currents, wave nonlinearities, temporal organization of the currents, entrainment and advection, storms, and feedback between berm and flow field. They found that the mean currents were directed predominantly offshore, while the berm consistently moved toward shore in a north-northwesterly direction. The berm was dispersive to the point that it eventually connected with the Mobile Bay ebb-tidal delta. The onshore movement was attributed to

nonlinearity in the wave field, while feedback between the waves and berm shape may have amplified this tendency.

Scheffner (1996) used a database of wave and current information coupled with the Ackers and White (1973) sediment transport method to model the movement of another mound offshore of Mobile Bay. The sediment transport methodology was slightly modified by incorporating surface waves with currents based on the work of Bijker (1967) and Swart (1976). Scheffner found that this methodology was applicable for non-cohesive sediments with a grain size between 40 and 4000 μm and it was applied to the mound offshore of Mobile.

Measurements of sediment transport rate and direction determinations have also been made using fluorescent tracers. Munoz-Perez et al. (1999) explains the methodology for a successful tracer experiment. First, native sediment samples from the area where the tracer is to be deployed are collected to determine background fluorescent levels. The tracer sand grains are coated with a fluorescent resin that can be illuminated under ultraviolet light. The sand is then sieved to get a grain-size distribution similar to the native sand where the tracer will be deployed. Synthetic sand with similar characteristics to the native sand can also be created for use as a tracer. The tracer is then introduced to an aquatic environment and after a period of time sampling occurs. The sampling is conducted to see how the tracer spreads from the point it was introduced to reveal sediment transport patterns of the area. Munoz-Perez et al. (1999) outlined that while being a viable method, tracer studies contain several of their own complexities such as difficulties in detection and location of the tracer, gathering of samples, and counting of the particles. The biggest advantage of the method is that if done correctly an

excellent picture of transport trends in the area is displayed, with no reliance on predictive equations or calibration.

It is important to note that most of the papers reviewed were studies of whether or not a mound was active. This assessment was usually made based on bathymetric survey data or on wave heights over the mound. The Douglass et al. (1995) study was the only one found which used a combination of instrumentation and surveys for understanding the rate and direction of sediment transport.

2.2 Predictions of Sediment Transport as Bed Load

There are a variety of methods for describing incipient sediment motion as well as for estimating the rate of sediment transport as bed load. Bed load transport was defined by Bagnold (1956) as the part of the total sediment load that is supported by intergranular forces. Others have defined it as the portion of the total load within a certain distance to the sea floor. Shields (1936) developed one of the first, and probably the most widely used method for describing incipient motion of sediments. One of the results of his study was the formulation of a dimensionless shear stress now known as the Shields Parameter, Θ :

$$\Theta = \frac{\tau}{(\gamma_s - \gamma)d} \tag{2}$$

where,

τ = shear stress [F/L^2];

γ_s = specific weight of sediment [F/L^3];

γ = specific weight of water [F/L^3];

d = diameter of particle [L].

Shields (1936) used a variety of sediment transport data from uniform steady flow laboratory experiments to plot the non-dimensional shear stress (Shields Parameter), versus the non-dimensional shear velocity or Boundary Reynolds number, Re_b:

$$\mathrm{Re}_b = \frac{U_* d}{\nu} \tag{3}$$

where,

U_* = shear velocity [L/T];

ν = kinematic viscosity of water [L^2/T].

A curve drawn through the data defines a threshold dimensionless shear stress which must be exceeded in order to initiate sediment motion. The original Shields Diagram was difficult to use due to the fact that the dependent variable appears on both the ordinate and abscissa; therefore, the American Society of Civil Engineers Task Committee added a third parameter, $d/\nu\left[(s-1)gd\right]^{0.5}$, to the curve to facilitate the use of the Shields Diagram (Vanoni 1977). The Shields diagram will be displayed and discussed further in Chapter 4.

Following the work of Shields (1936), many later sediment transport equations incorporated an excess dimensionless shear stress into their predictive methodology. Meyer-Peter and Muller (1948) developed an equation for non-dimensional sediment transport as a function of the excess Shields Parameter:

$$\Phi_B = 8\left(\Theta - \Theta_c\right)^{1.5} \tag{4}$$

where, Φ_B is the bed load sediment transport non-dimensionalized by $d\sqrt{(s-1)gd}$, with d being the diameter of the sediment, g is the acceleration due to gravity, and s the

specific gravity of the sediment. The critical Shields Parameter, Θ_c, is simply the nondimensional critical shear required to initiate sediment motion, as given by the Shields curve. The Shields diagram was developed for steady unidirectional flow and Equation (4) was calibrated using similar flow experiments conducted in the laboratory. Nielsen (1992) conducted further experiments and found that the Meyer-Peter and Muller equation did not accurately simulate the sediment transport trends under high stress conditions; therefore he modified the formula to better match data:

$$\Phi_B = 12(\Theta - \Theta_c)\sqrt{\Theta} \tag{5}$$

Soulsby (1997) developed a formula for bed load transport due to combined waves and currents. The formula was developed by integrating the Nielsen bed load equation over a wave cycle. When no wave forcing is present the Soulsby equation reverts back to the Nielsen formula. Soulsby's transport rates are a function of a variety of Shields Parameters that can be calculated from velocity data or known wave information. The formula also incorporates the effects of non-collinear currents and waves, but does not describe suspended sediment transport. The application of this method will be discussed in Chapter 4.

Quick et al. (1986) studied, in the laboratory, how different flow types cause sediments to become mobile. They used a laser Doppler anemometer to measure the flow velocity several millimeters from the sea floor. Flows included: steady currents only, waves only, waves and currents traveling in the same direction, and waves and currents traveling in opposite directions. The authors varied current velocities and wave heights while measuring the instantaneous velocities with the laser instrument. They found that the same maximum instantaneous velocity produced sediment motion, "no

matter whether the velocity was produced by turbulent steady flow or by waves alone, or by combined waves and currents" (Quick et al. 1986). This suggests that incipient motion can be predicted if the critical velocity is known and accurate high frequency measurements of velocity are taken very close to the sea floor.

An opinion contrary to Quick et al. (1986) was expressed in a previous work by Komar and Miller (1973), who suggest that initiation of sediment motion depends not only on diameter of a sediment and flow speed, but also the wave period, and by extension, flow acceleration. They show that sediments tend to be more mobile for shorter wave periods due to a larger associated acceleration.

Van Rijn (1984) conducted sediment transport studies and developed equations for bed load and suspended load transport. Those equations were calibrated for a riverine environment and for sediments with mean diameters between 200-2000 μm, but they are often used in marine environments when the current is considered to dominate the sediment transport. The two modes of transport were separated by defining a maximum saltation height. Particles rising above this height were considered suspended load while other particles were considered to be bed load. The Van Rijn bed load equation describes transport rate as a function of particle velocity, the saltation height (depth of bed load layer), and the concentration of particles in the bed load layer. He developed expressions for each of these components and parameterized them into two separate equations for bed load and suspended load.

2.3 Predictions of Suspended Sediment Transport

Several methods exist for predicting sediment transport away from the bed in the suspended mode. Instantaneous suspended load can be calculated by integrating the product of the velocity and suspended sediment profile according to Equation (6),

$$q_{ss} = \int c(z)u(z)dz \tag{6}$$

where *c(z)* is the concentration profile and *u(z)* is the velocity profile. In order to achieve this, measurement techniques or theories have to be developed to describe the velocity and concentration profiles over the water column.

One widely used conceptual model of the suspended sediment concentration profile was developed by Rouse (1937). He developed an equation assuming steady equilibrium conditions for sediments. The Rouse equation balances the downward movement of sediment particles, due to gravity, with the upward movement of particles, caused by turbulent velocity fluctuations. The result describes the profile of sediment concentration, which decreases with height above the bed. The solution contains simple parameters such as the sediment fall speed, flow shear velocity, depth, and a reference concentration. Decay of concentration above the seafloor is controlled by a dimensionless quantity known as the Rouse Parameter. The reference concentration is an assumed value or measured concentration at some point within the water column. Combining a Rouse distribution of sediments with water velocity measurements from an ADV or ADCP gives an easy method in which suspended load can be predicted. The Rouse equation is discussed further in Chapter 4.

Suspended sediment concentration profiles and sediment size distributions can be measured using a variety of methodologies and instruments. These include, but are not

limited to: bottle and pump samplers; acoustic, nuclear, and optical methods; focused beam and remote spectral reflectance methods. Wren et al. (2000) briefly discusses each of these methods along with the advantages and disadvantages for each. Two of the methods/instruments discussed by Wren et al. are the optical backscatter sensor (OBS) and laser in-situ sediment transmissometer (LISST), both of which were deployed for this study and will be discussed further in Chapter 3. Wren et al. also state that using OBS and LISST devices together can give better data than if either one were to be used alone.

Other methods such as the equation developed by Van Rijn (1984), do not directly assume a suspended sediment profile when making sediment transport predictions. His equations were developed and fit to 800 data sets, but the potential for large error in sediment transport predictions still exists. During verification of his equation, Van Rijn found that error between 50% and 100% could occur; therefore, it is important to realize the potential for large inaccuracies when using any predictive sediment transport methodology.

2.4 Previous Relevant Studies near Brunswick, Georgia

There have been studies of the bathymetry, tide, wind, and wave conditions typical in the coastal Georgia region. The barrier islands of Georgia are located in an embayment called the Georgia Bight. Griffin and Henry (1984) detail some of the characteristics of the Georgia Bight such as typical tidal range, wave heights, wind and wave directions, as well as bathymetry. These parameters are discussed further in the site description section in Chapter 4. In general in the Georgia Bight, the dominant onshore wave direction is from the northeast in the winter and from the southeast in the summer.

In the winter, winds and waves are also typically larger than the wind and waves in the summer months (Griffin and Henry 1984).

Due to the relatively large tidal range and relatively small waves present in the Georgia Bight region, it is typically considered to be tidally dominated. This tidal dominance causes a large amount of sediment to be moved during each tidal cycle. During the flood tide, sediments are moved inland, and in the associated ebb-flow, much of these sediments are returned seaward to form large ebb-tidal shoals adjacent to the channels. Typically, the ebb-tidal shoals are more developed on the north side of the tidal inlets, which suggests a north to south littoral transport of these sediments along the coastline (Griffin and Henry 1984, Hayes 1994). Other studies have also shown that the barrier islands of Georgia typically migrate in a southerly direction due to erosion on the north ends of the islands, with deposition on the south ends (Hoyt and Henry 1967). The USACE dredging records suggest that the annual longshore transport of sediment in the Brunswick Entrance Channel area is approximately 330000 m^3 (USACE 1971).

The main sources of sediment to the coastal region of Georgia are the Altamaha and Savannah Rivers (Kingery 1973, Griffin and Henry 1984, Hayes 1994). These rivers bring sand down from Piedmont Region of Georgia and deposit it offshore. These sediments then act as a source to the barrier islands which are continually being eroded. As sediment conservation programs and reservoirs are built on the rivers, sediment supply to the coastal region is diminished, causing the islands to "feed" on themselves in areas where a negative sediment budget results (Griffin and Henry 1984, Hayes 1994). Meade (1976) has shown that the Hartwell and Clarks Hill Reservoirs cut off most of the Piedmont sediment to the lower Savannah River. Other anthropogenic activities such as

construction of groins and jetties and the dredging of entrance channels reduce the sediment supply to areas downdrift of the activity or structure (Dean and Dalrymple 2002).

The Brunswick Entrance Channel passes through the St. Simons Sound between two barrier islands as it reaches from the Brunswick Harbor to the open ocean. The two islands adjacent to the channel are St. Simons Island to the north and Jekyll Island to the south. St. Simons Island is approximately 19 km long and 6 km wide with a total area of 94 km^2 (Griffin and Henry 1984). Much of the island's primary dune system has been destroyed by recreational and residential development. This development has also caused changes in the sediment transport patterns on the island due to the addition of seawalls, revetments, and other beach stabilization and storm protection structures.

Dredging of the Brunswick Entrance Channel began in 1904. By 1937 the channel had been deepened to 9.8 m below MLW. The channel is oriented in a northwest to southeast manner and passes within 1.3 miles of the south end of St. Simons Island. From 1968 to 1977 dredging operations removed approximately 557,000 m^3 of sediment annually. Records also indicated that for several years more than 760,000 m^3 of sediment were removed from the channel (Griffin and Henry 1984).

South of the sound and entrance channel is Jekyll Island. Jekyll Island is about 12 km long and 4 km wide. This island has been operated as a state park since 1947 but has had major development along its central section, part of which is being eroded. While the total length of Jekyll Island's beach did not significantly change between 1857 and 1980, the island has migrated southward due to erosion on the north end of the island and deposition on the southern end as shown in Figure 2.

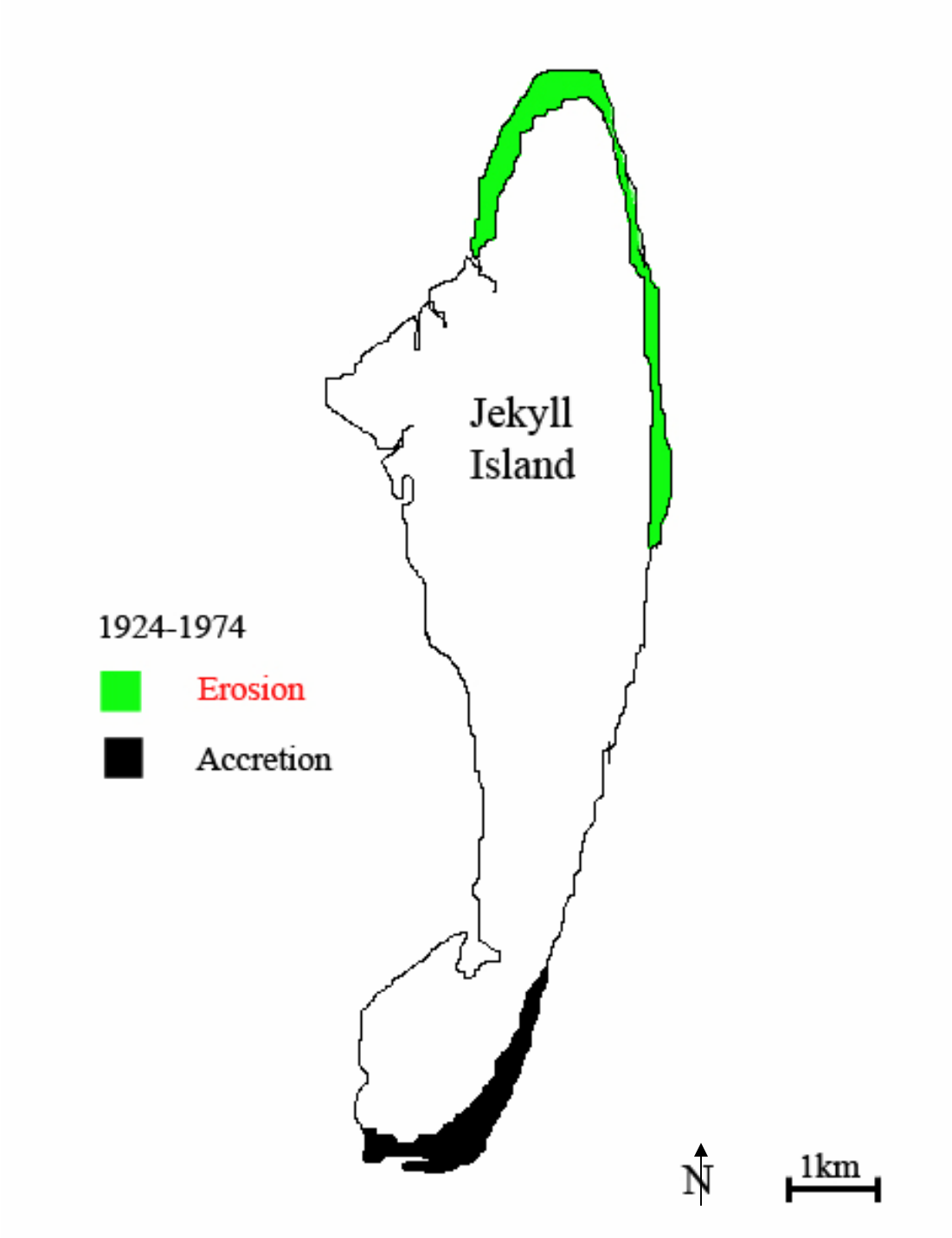

Figure 2. Erosion and accretion patterns experienced at Jekyll Island from 1924-1974. Erosion occurs at the north end of the island due to source sediments being deposited in the entrance channel. Accretion occurs at the south end of the island. Figure adapted from Griffin and Henry (1984).

Sediments from the north end of Jekyll Island are continually eroded. Just south of the entrance channel, the shoreline retreated approximately 260 m between 1860 and 1974 (Griffin and Henry 1984). Similar erosion patterns can be expected to have existed from 1974 to the present time, since dredging of the entrance channel has continued. This dredged entrance channel intercepts and cuts off most of the source sediment from reaching the north end of Jekyll Island.

The USACE began a National Berm Demonstration Program off the coast of Alabama in 1987 to aid in the understanding of the long-term fate of dredged material placed in mounds (Douglass et al. 1995). The current efforts to predict and confirm sediment transport and large-scale hydrodynamic trends at Brunswick, GA are some of the first to be undertaken for the area. In the past, when dredged materials from the Brunswick Entrance Channel were disposed of, no study was undertaken to observe the movement of those sediments. This study is the first to incorporate the placement of dredged material, tracer, and simultaneous collection of wave and current data near the mounds for the purpose of documenting and predicting mound migration.

CHAPTER 3

FIELD INSTRUMENTATION AND AVAILABLE DATA

In 2002, a study was initiated by the United States Army Corps of Engineers (USACE) to collect data describing sediments, bathymetry, and the hydrodynamics of the dredged material placement site near Brunswick, Georgia. The placement area, adjacent to the Brunswick Entrance Channel, consists of several dredged material mounds. A second component of the study was also initiated to develop and apply numerical models to describe the hydrodynamics and sediment transport trends in the area.

The goal of the instrument deployment was to collect data such that the hydrodynamics and sediment transport trends of the area might be described. The collected data would then be used to calibrate and validate the numerical models developed by the USACE. In order to achieve this goal, data were collected near several existing dredged material mounds. Over one particular mound ("C" in Figure 3), data were collected using several instruments including Sontek Acoustic Doppler Velocimeters (ADV), an RDI Acoustic Doppler Current Profiler (ADCP), D&A Optical Backscatter Sensors (OBS), and Sequoia Scientific Laser In-Situ Sediment Transmissometers (LISST). In this chapter, the site, deployment location, instrument operating principles, and types of data collected by each of these instruments are described.

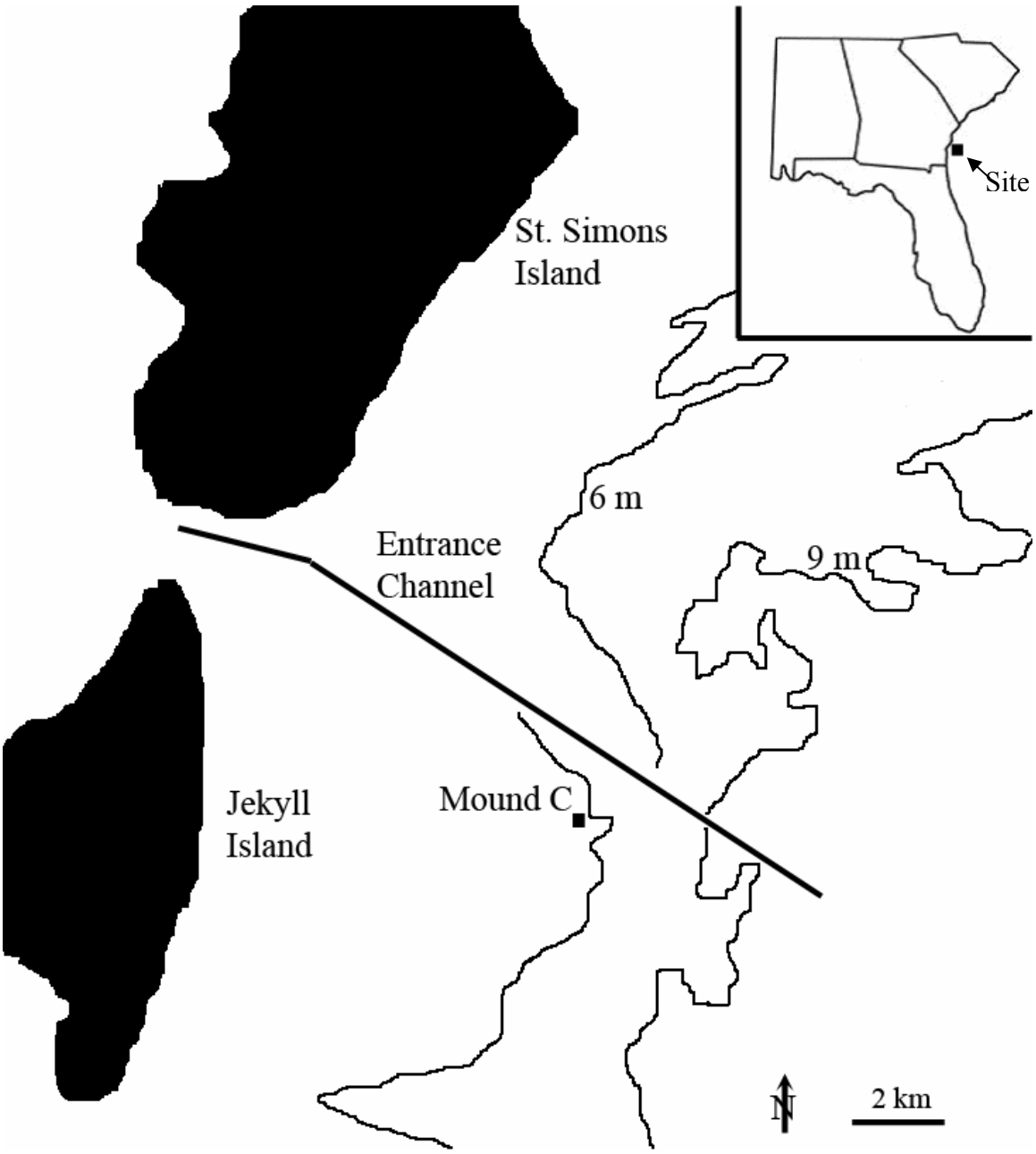

Figure 3. Brunswick Harbor Entrance Channel. St. Simons Island is located to the north while Jekyll Island is located to the south. Mound C is located adjacent to the entrance channel on the downdrift (south) side.

3.1 Site Description

There have been studies of the bathymetry, tide, wind, and wave conditions typical in coastal Georgia (Hayes 1994). Coastal Georgia lies within an embayment known as the Georgia Bight. The Georgia Bight has the largest tides in the southern United States (Hubbard and Oertel 1979). Tides within this embayment are semi-diurnal and average 2 m in range, with spring tides up to 3 m being frequent. Tidal currents are sufficient to maintain many channels to depths up to 20 m (Griffin and Henry 1984).

The continental shelf off the coast of Georgia is relatively shallow and wide, extending approximately 120 km (75 mi) offshore. The bottom slope over the shelf is typically 0.4-0.8 m/km. The broad continental shelf tends to dampen wave energy and reduce the wave heights reaching the Georgia coast (Tanner 1960). Wind and wave directions are seasonally dependent. The seasonal dependence of winds and waves will be investigated later in this chapter. Hurricanes also significantly affect the sediment distribution patterns of the coastal Georgia area, and on average, a severe hurricane strikes Georgia every ten years (Carter 1970).

The dredged material mound addressed in this study is denoted Mound C and located approximately 8 km offshore and adjacent to the Brunswick Entrance Channel (Figure 3). Nominal depth at the mound location is 6-8 m; however, over the crest the depth is only 2-3 m. The mound has a crescentic shape, and fits within a 600 m X 1100 m box. The crest of the mound, where most of the instrumentation was located, has approximate dimensions of 600 m X 600 m (Figure 4).

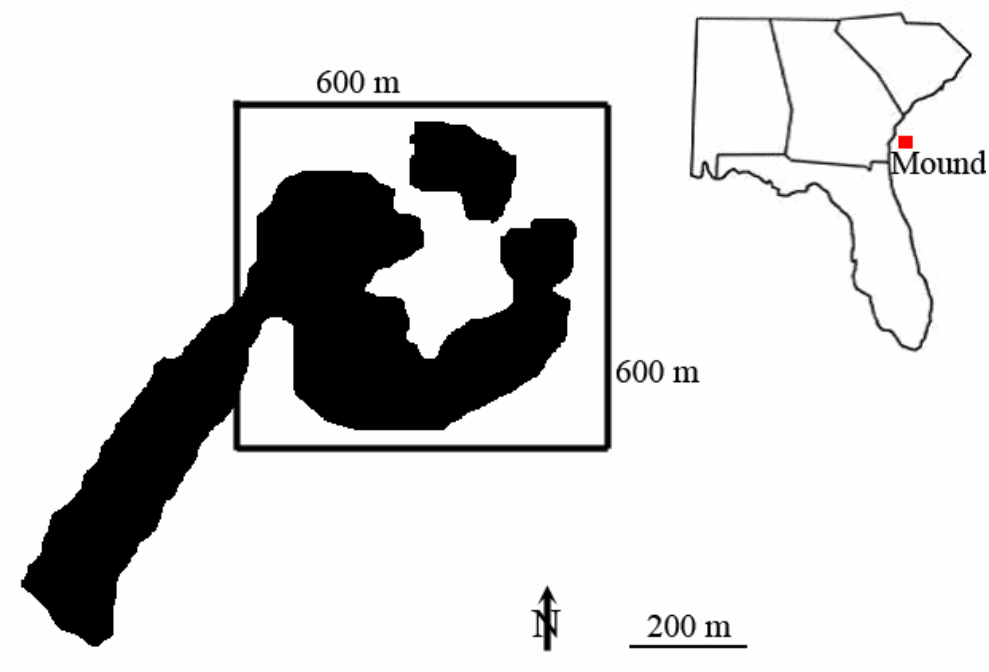

Figure 4. The dredged material mound has a cresentic shape and the crest can be contained within a box of dimensions 600 m X 600 m. The mound is located offshore of Brunswick, GA.

The USACE subcontracted Evans-Hamilton, Inc. (EHI) to conduct sediment sampling campaigns and characterize sediments placed in the mound. Seven Vibracore samples were collected at various locations on the mound and sent to the Virginia Institute of Marine Science (VIMS) for analysis. Each Vibracore sample was divided into multiple horizons and grain size distributions were determined for thirty-two sediment sub-samples using a wet sieve method. Within the crest of Mound C, VIMS found that the sand fraction of the sediment had a d_{50} of approximately 350 μm, and a d_{90} of approximately 1400 μm (Cartwright and Friedrichs 2003).

In addition to instrument placement, two colors of fluorescent tracer were deployed over the mound in February of 2003 to give an additional method for

determination of sediment transport trends. The different colors were used to differentiate between different sediment sizes. The fine or mud-sized tracer was yellow with sizes of 0.4-111 μm and a d_{50} of approximately 65 μm. The coarse of sand-sized material was violet with sizes of 101-542 μm and a d_{50} of approximately 240 μm. Subsequent sampling, over the next four months, revealed that the fine tracer was dispersed rapidly, while the sand sized tracer moved very little. Personnel from The Georgia Institute of Technology also collected data in September 2003 defining bathymetry and tidal hydrodynamics in and near the Brunswick Harbor entrance channel. Those data were later used by the USACE to calibrate hydrodynamic models for the region. Table 1 details the chronology of the experiment.

Table 1. Timeline of events for the Brunswick dredged material placement experiment.

Event	**Date**
Placement of Dredged Material	10/2002—1/2003
Sampling for Background Fluorescence	12/2002
Instruments Deployed	1/30/2003
Tracer Deployed	2/5/2003
Tracer Sampling Event I	2/7/2003
Tracer Sampling Event II	2/17/2003
Instrument Service I	3/11/2003
Instrument Service II	4/1/2003
Tracer Sampling Event III	4/3/2003
Instrument Service III	6/4/2003
Tracer Sampling Event IV	6/23/2003
Tracer Sampling Event V	8/25/2003
Instruments Retrieved	8/27/2003
GA Tech Hydrodynamics and Bathymetry Survey	9/4/2003—9/5/2003

The timeline outlines the deployment, retrieval, and cleaning schedule for the instruments. The operating principles, error bounds, and type of data collected by each of these instruments are described in the following sections.

3.2 Acoustic Doppler Velocimeter

The Acoustic Doppler Velocimeter (ADV) is an instrument that calculates the velocity of suspended particles within one discrete sampling volume in the water column using the Doppler principle. The Doppler principle describes how sound undergoes a frequency shift when the source is moving relative to a receiver or vice versa. The ADV uses this principle to measure water velocity by transmitting an acoustic beam through the water column and measuring the frequency shift of sound reflected off scatterers in the water. Scatterers are small particles or plankton in the water column that reflect sound back toward the ADV. A picture of an ADV mounted in a tripod is shown in Figure 5.

Figure 5. Photograph of a Sontek ADV similar to the one used at Brunswick.

Typically, the sampling volume for an ADV is a few cubic centimeters (cc) or less, and it is assumed that the particles within this sampling volume move at the same speed as the water. The sound reflected off the scatterers is received and measured by transducers as shown in Figure 6.

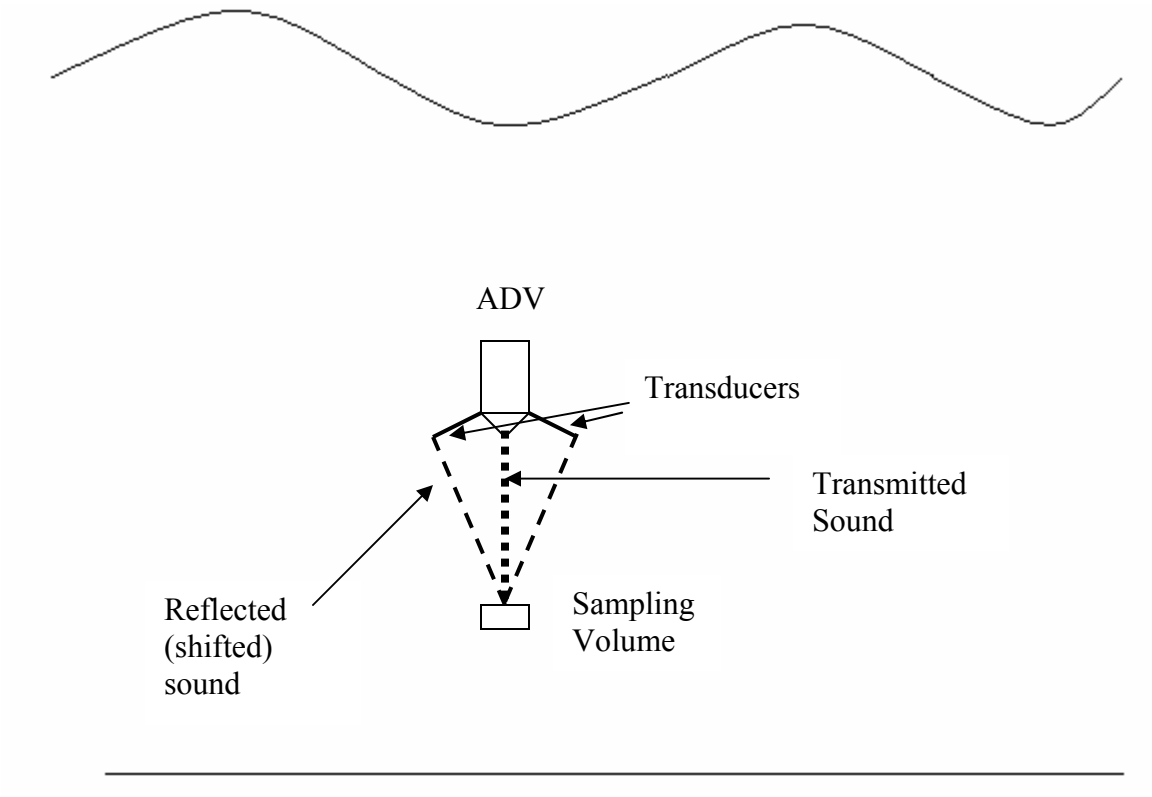

Figure 6. Sound is transmitted by the ADV where it is reflected back to the receiving transducers by scatterers in the sampling volume. The known geometry of the instrument and output from an onboard compass allows the instrument to relate the Doppler shift of the sound to North, East, and vertical components of velocity.

Using the principle of the Doppler shift, the frequency difference between transmitted sound and the sound reflected back to the ADV by the scatterers can be related to the along-beam water velocity according to Equation (7).

$$F_{doppler} = -F_{source}\left(\frac{2V}{C}\right) \tag{7}$$

where,

$F_{doppler}$ = Doppler shift or change in received frequency [1/T];

F_{source} = frequency of transmitted sound [1/T];

V = velocity of the object relative to the receiver [L/T];

C = speed of sound [L/T].

Since a compass is used for the conversion of velocity from beam coordinates to earth coordinates, the magnetic declination experienced at the deployment site has to be considered. The magnetic declination angle for Brunswick is relatively small, with magnetic North being approximately 6^{o} west of true North. The declination does change at a rate of about 7' per year for this region. If the magnetic declination were not taken into account, the velocity directions would have an error equal to the declination angle. Also included on many ADVs are temperature and pressure sensors to give water temperature and water level measurements.

The ADV used at Brunswick was designed to ping the water column as fast as possible, approximately 150-250 times per second. Due to large errors in the single ping data, temporal averaging is done to reduce the noise in each velocity measurement. Averaging reduces the standard deviation of the estimated velocity error according to Equation (8).

$$\sigma \propto \frac{1}{\sqrt{N}} \tag{8}$$

where,

σ = standard deviation of velocity error;

N = number of pings averaged to compute one velocity estimate.

The value of N is specified indirectly by the user through choice of a sampling rate. For example, if the sample rate is set to 25 Hz, the ADV records as many velocity values as possible over a 40 ms period and then averages those results together for output as one sample. Therefore, a 1 Hz output signal has about one-fifth the noise of a 25 Hz output signal. Sontek estimates that the noise in a 25 Hz output signal is approximately 1% of the velocity range measurable by the instrument. Accuracy of the ADV is a function of user-specified speed of sound and probe geometry. Probe geometry is set and calibrated for each ADV at the factory such that it measures within 1% of the actual velocity (Sontek 2001). If the speed of sound or salinity is specified incorrectly, it can be corrected during post processing. Speed of sound can also be calculated internally using the instrument's onboard temperature sensor. This option is often used for long deployments where large temperature shifts are likely. The typical range of temperatures for ADV sampling is 0-50^{o} C, which results in a speed of sound range of 1450-1565 m/s.

One advantage of ADVs, as with all Doppler instruments, is that there is no possibility for zero drift. This is because Doppler instruments measure the change in frequency between transmitted and received signals. Other advantages of the ADV include its ability to resolve velocity very close to the seafloor, at very low velocities, and ability to perform well when fouled; however, its inability to measure velocities at multiple locations in the water column is a disadvantage.

3.3 Acoustic Doppler Current Profiler

The Acoustic Doppler Current Profiler (ADCP) is an acoustic instrument that uses the same operating principle as the ADV, except that it measures velocity of suspended particles throughout a water column instead of within a single sampling volume. The ADCP is a versatile instrument that can be mounted on a boat in a downward looking configuration, or on the seafloor facing upward through the water column (Figure 7). Other advantages of an ADCP are its ability to measure currents many meters away from the transducer faces, and the high degree of temporal and vertical resolution it provides.

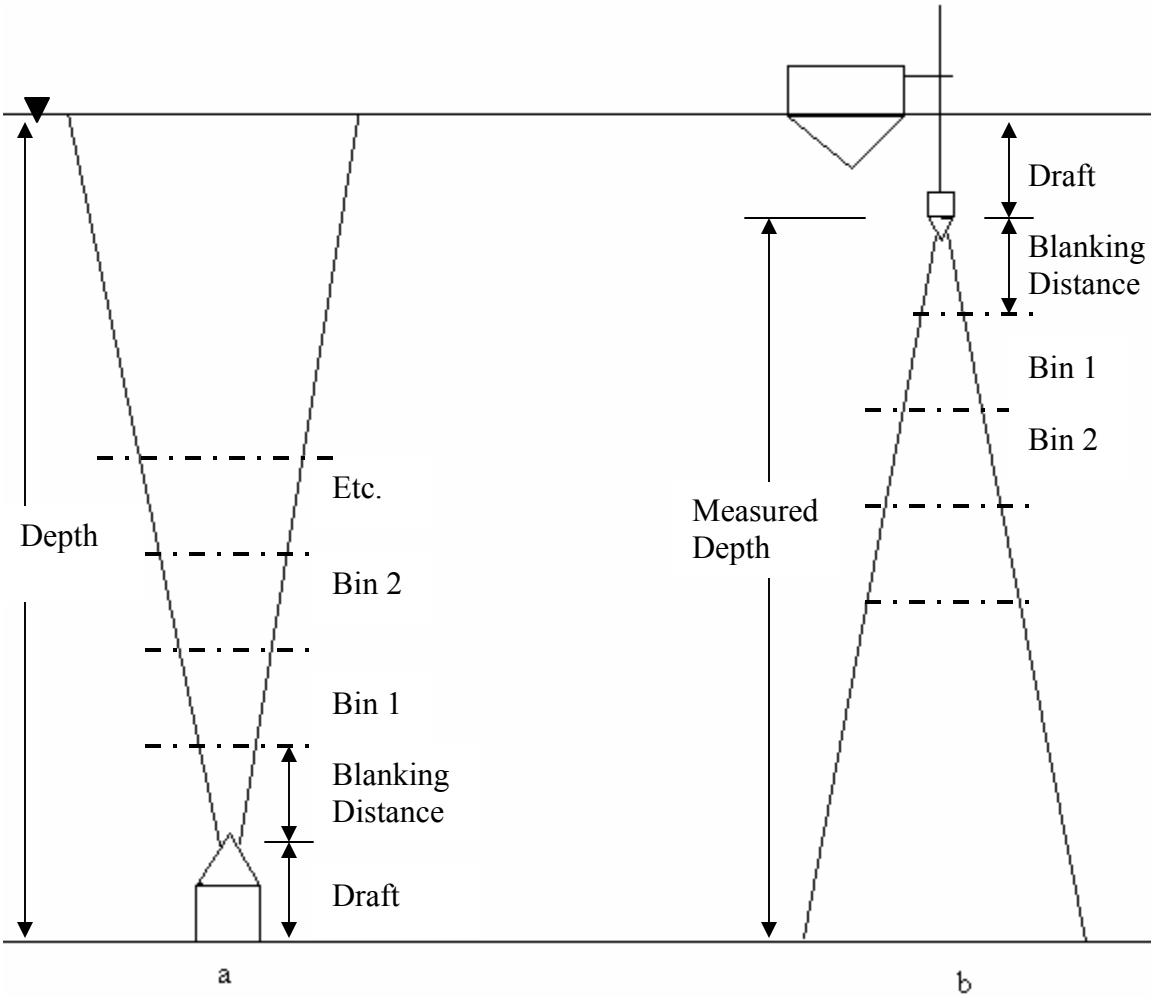

Figure 7. Illustration of upward-looking (a) and downward-looking (b) ADCP configurations. ADCPs cannot measure within the blanking distance.

Three acoustic beams are required to resolve the three velocity components; however, many ADCPs utilize four acoustic beams to provide redundancy and to allow an added estimate of error. The ADCP sends beams through the water column in different directions (angles) and measures the frequency shift of the sound along each beam. The returned acoustic signal is divided up into segments called bins through a process called range-gating. Using the speed of sound and time between transmission and reception of a ping, the ADCP calculates the distance from the instrument to each

bin. The user can configure the height of each depth cell depending on the application. The distance the ADCP can "see" into the water column is dependent on the turbidity of the water and the frequency of the instrument being used. A 1200 kHz ADCP is usually limited to about a 12 m range. If greater penetration into the water column is desired, then an ADCP with a lower frequency is needed. If the user is more interested in greater resolution of the velocity, then smaller depth cells can be chosen but that results in reduced range.

The ADCP is a semi intrusive instrument in that it must be in the water to measure, but the velocities it measures are remote to the sensor. There is a region close to the ADCP that cannot be measured due to signal processing limitations. This distance is called the "blanking distance" and is frequency dependent. The blanking distance can be specified by the user and varies depending on application, but is typically around 1 m in length. ADCPs also typically have onboard compass and heave-pitch-roll sensors. This gives the instrument the ability to compensate for motion of the instrument, resolve its orientation with respect to magnetic North, and convert the velocity measurements to the earth coordinate system. As with the ADV, magnetic declination can be entered to convert direction from magnetic to true coordinates.

An onboard pressure transducer is also used to measure water depth when deployed in an up looking configuration. Atmospheric pressure fluctuations will affect reported head, and may be important depending on application. At Brunswick, this change in reported head was typically less than 5 cm.

There are two potential sources of error within the velocity measurements: random error and systematic error. The single ping velocity data can have a large amount

of random error, up to 0.5 m/s. As with the ADV, this error is reduced by averaging over many pings. The noise is inversely proportional to the square root of the number of pings averaged together (RDI 1996).

At some point, averaging reduces the random error below that of the systematic error. At this point further averaging does not significantly reduce the overall error. The error present after averaging is the systematic error or bias. The size of the bias is dependent on several factors such as temperature variability, mean current speed, signal-to-noise ratio, and beam geometry. It is not yet possible to measure or remove ADCP velocity bias, but RDI has estimated it to be less than 10 mm/s. The random error is dependent on ADCP frequency, depth cell size, number of pings averaged together, beam geometry, flow turbulence, and ADCP motion, and can be approximated by computing the standard deviation of the error velocity. The error velocity is the difference between two estimates of vertical velocity and is calculated using the redundant fourth beam (RDI 1996).

3.4 Laser In-Situ Sediment Transmissometer

The Laser In-Situ Sediment Transmissometer (LISST) is a device that measures the volume concentration and size distribution of particles in suspension. It generally consists of a laser, optical lenses, and electronics for data collection and logging (Sequoia 2004). The instrument operates by firing a laser through a sampling volume and measuring how light is diffracted by particles in suspension (Figure 8). The angle of light scattered by particles in suspension is measured by several ring-shaped photodectectors (Wren et al. 2000). This angle of diffraction can then be related to particle size and

ultimately to volume concentration. The optical alignment of the LISST must be checked periodically to ensure that the angle of diffraction is accurate. The instrument also needs to be calibrated before deployment to remove the affects of background scattering which can be due to scratched lenses.

This instrument is used to get in situ sediment characteristics at greater temporal resolution than many traditional grab sampling devices; however, it is a large instrument with a very flow-intrusive nature. Since the operating principles of this instrument are based on the angle of optical scattering, any biofouling of lenses causes errors. It is not possible to apply antifoulant coating/paint to this instrument because it scatters light unpredictably; therefore the amount of useful data collected can be severely reduced in many environments.

Figure 8. Photograph of a Sequoia Scientific LISST Device similar to the one used at the Brunswick dredged material mound. This LISST is approximately 1 m in length and 12 cm across.

3.5 Optical Backscatter Sensors

An Optical Backscatter Sensor (OBS) is an instrument that uses light to measure turbidity of water. "Turbidity is the cloudy appearance of a liquid produced by light scattered from suspended matter. It is an apparent optical property that depends on the size, color, and shape of scattering particles" (D&A Instruments 2000). The OBS operates by transmitting light from a high-intensity infrared-emitting diode (peak wavelength of 875 nm) into a sample volume and sensing the amount reflected back by particles in suspension. The strength of the reflected signal is a measure of turbidity that is related to concentration using a calibration curve. An OBS is good for temporal resolution of turbidity and can be good for spatial resolution if several instruments are used together. The OBS also performs very well when measuring turbidities if the particle size is constant or lies in the 200-400 μm range. Disadvantage of the OBS are its varying sensitivities to differing particle sizes. An OBS also tends to give erroneous results when a mixture of heterogeneous sediments is present, but this problem can be surmounted through a procedure proposed by Green and Boon (1993). They suggest using the OBS in conjunction with acoustic backscatter sensors or in situ particle sizing sensors, such as a LISST, to help resolve the errors associated with sensitivity to differing particle sizes.

The Virginia Institute of Marine Science (VIMS) calibrated the OBS used for this study using sediments taken from St. Simons Sound (Cartwright and Friedrichs 2004). The instrument was calibrated inside a Modified Downing-Beach Calibration Chamber. The OBS was mounted inside this chamber and a known concentration of sediment was added and kept in suspension. The instrument response was then recorded for the known

concentration. This process was repeated for a range of sediment concentrations (0-21 g/L), and from the resulting data, a calibration curve was constructed. The calibration curve was then used to convert instrument response (voltage) to concentration. The sediment used for sand concentration calibration was 99.8% sand (63-500 μm) and had a d_{50} of approximately 200 μm.

D&A Instruments, the supplier of the OBS used for this study, estimates their instruments to be accurate within 3.5% for turbidity measurements. Since the OBS is an instrument dependent on calibration, zero-drift is a possibility. The zero-drift is also estimated to be within 3.5% for the first 2000 hours of operation (D&A 2000).

3.6 Deployment Scheme

The ADV, OBS, and LISST devices described above were deployed at the mound (Mound C), on January 30, 2003 and remained until August 27, 2003. The instruments were mounted together on a frame called a cassette (Figure 9). The cassette was then attached to a trawler-resistant bipod and placed over the crest of the mound in 2-3 m of water. Every three months the cassette would be removed from the bipod and brought to the surface so that data could be downloaded, instruments cleaned, and batteries replaced. The cassette would then be reattached to the bipod for the next round of sampling. Deployment parameters for each of the instruments are summarized in Table 2.

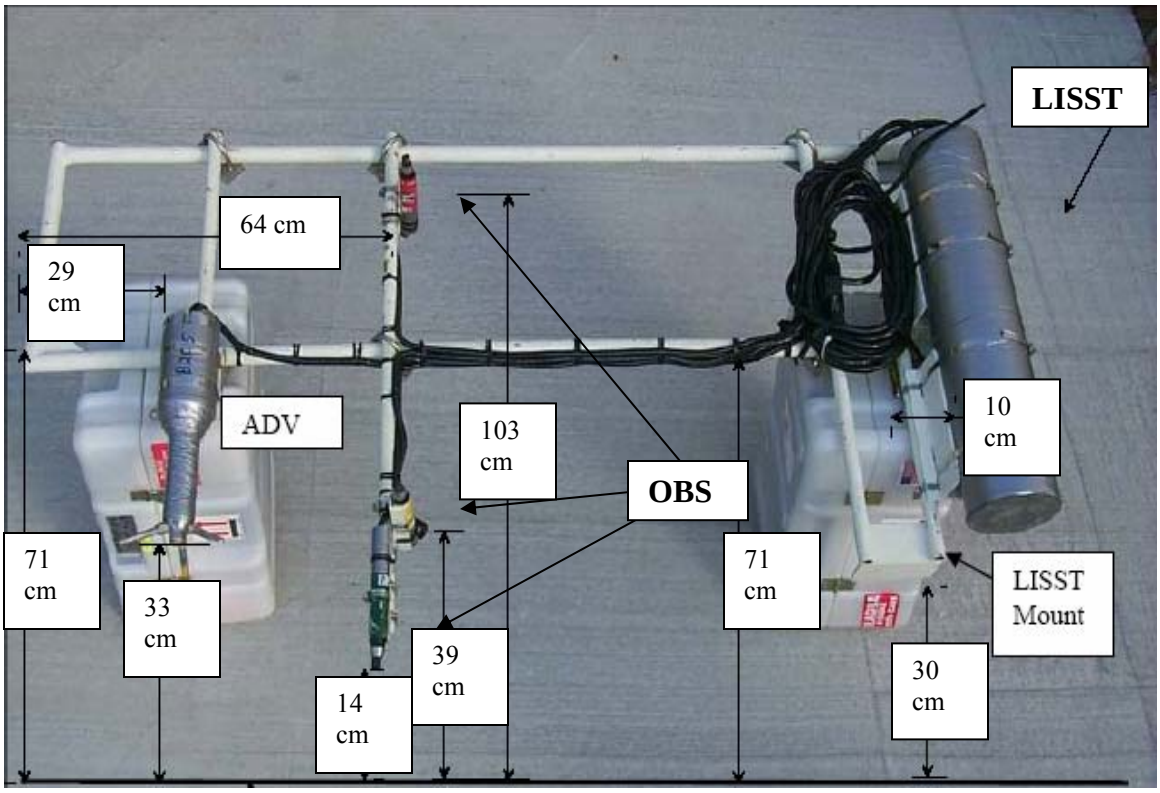

Figure 9. Photograph of the cassette holding the instruments deployed over the crest of Mound C at the Brunswick offshore dredged material site. The bottom of the picture corresponds to the bed when the cassette is deployed.

Table 2. Deployment parameters selected for the ADV, OBS, LISST and ADV located at Mound C offshore of Brunswick GA.

Parameter	ADV (currents)	ADV (waves)	OBS (bottom)	OBS (middle)	OBS(top)	LISST	ADCP (currents)	ADCP (waves)
Location	Crest of Mound C	Crest of Mound C	Crest of Mound C	Crest of Mound C	Crest of Mound C	Crest of Mound C	Offshore of Mound C	Offshore of Mound C
Water Depth	1-3 m	1-3 m	1-3 m	1-3 m	1-3 m	1-3 m	6-8 m	6-8 m
Bin Size	N/A (point meas.)	N/A (point meas.)	N/A (point meas.)	N/A (point meas.)	N/A (point meas.)	N/A (point meas.)	35 cm	35 cm
Number of Bins	1	1	1	1	1	1	30	30
Blanking Distance	N/A	N/A	N/A	N/A	N/A	N/A	87 cm	87 cm
Altitude of Sample Vol. Above Bottom	24 cm	24 cm	14 cm	39.3 cm	102.9 cm	38 cm	45 cm (instr. altitude)	45 cm (instr. altitude)
Turbidity Range	N/A	N/A	0-500 NTU	0-1000 NTU	0-2000 NTU	N/A	N/A	N/A
Sampling Rate	2 Hz	2 Hz	2 Hz	2 Hz	2 Hz	0.5 Hz	0.167 Hz	2 Hz
Sound Frequency	5 MHz	5 MHz	N/A	N/A	N/A	N/A	1.2 MHz	1.2 MHz
Burst Duration	3 min.	20 min.	3 min.	3 min.	3 min.	3 min.	10 min.	20 min.
Samples recorded per Burst	360	2400	360	360	360	70	1	2400
Burst Interval	1 hr	3 hr	1 hr	1 hr	1 hr	1 hr	10 min.	1 hr

The instrument cassette was initially deployed January 29, 2003, however, due to a problem with the digital signal processing board, no useful data were gained from the ADV for the first three months of this deployment. The instrument was repaired and useful data were collected from March 13, 2003 until August 27, 2003. The ADV is an instrument that can function with some biofouling; however, clear antifouling paint was applied to the transducers in order to minimize fouling as much as possible. Every three weeks the transducer faces were wiped clean by divers.

The Sontek Hydra systems have many options that allow the user to adapt them to the type of field data being collected. The ADV used for this study was a 5 MHz system, deployed in a downward looking configuration, which measures current velocities inside a 2 cubic centimeter (cc) volume 18 cm below the transducer faces. For every sampling event or burst, the ADV measured and recorded the component of the current velocity in the north, east, and up directions. The instantaneous pressure, heave, pitch, and roll, as well as the signal strength and correlations calculated for each beam are also measured and recorded by the instrument. Since the ADV was configured to record at 2 Hz, there are 2 records per second for each data stream.

The pressure transducer measures absolute pressure, which is influenced by ambient atmospheric pressure. In order to remove the signal induced by atmospheric pressure fluctuations, the ambient air pressure for each burst was subtracted from the measured pressure record. This left a gage pressure, which represented the height of water over the instrument. The ambient pressure reading, taken from the NOAA website, was measured and recorded by the Grays Reef Buoy located 55 km northeast of the

mound. This correction resulted in the reported head being changed by a maximum of 18 cm.

As with the ADV, clear antifouling paint was applied to the OBS lenses to minimize biofouling. The altitudes of each OBS above the seafloor, and the turbidity range capabilities of each instrument, are summarized in Table 2 and displayed in Figure 9. The table indicates that the instrument nearest the bottom has the greatest turbidity range when compared to the other instruments. This was planned since the highest concentrations of suspended sediments are expected nearest the seafloor. The instrument response (voltage) output by each OBS was recorded by the ADV Hydra system. This response was converted to mass concentration by VIMS using the calibration curves discussed earlier.

The LISST device was supplied by Sequoia Scientific and was also mounted on the cassette. This instrument measured volume concentration (μL/L) over 32 separate size ranges from 2-500 μm (shown in Table 3). The LISST was mounted such that the sampling volume was nominally 38 cm above the ocean floor (Figure 9).

Table 3. Deployment parameters selected for the LISST located over Mound C. The LISST samples the volume concentration (μL/L) of sediments centering on each of these 32 diameters.

	LISST
Sediment Diameters Reported (μm)	2.73, 3.22, 3.8, 4.48, 5.29, 6.24, 7.36, 8.69, 10.2, 12.1, 14.3, 16.8, 19.9, 23.5, 27.7, 32.7, 38.5, 45.5, 53.7, 63.3, 74.7, 88.2, 104, 128, 157, 186, 219, 259, 293, 332, 391, 462

It is impossible to apply an antifoulant coating/paint to the LISST device because it scatters light unpredictably; therefore, biofouling was a problem. This instrument could only collect valid data for a maximum of 1-2 weeks before thorough cleaning was necessary. Due to limited LISST data and sediment size not playing a major role in the prediction of sediment transport direction, the LISST data were not considered.

The ADCP used at Brunswick was a 1200 kHz RDI Workhorse Sentinel. It was mounted in a separate trawler-resistant bipod in approximately 6 m of water (MLLW) just offshore of the mound. The instrument was mounted in an upward looking configuration such that the transducer faces were nominally 45 cm above the seafloor. The ADCP was in a position such that it recorded incident wave parameters before modification by the dredged material mound. Deployment parameters for the ADCP are summarized in Table 2.

Data recorded or calculated by the ADCP include the zero moment wave height (H_{mo}), wave period at spectral peak (T_p), wave direction at peak period (D_p), water level above the instrument, mean period (T_{mean}), and current magnitude and direction in several bins throughout the water column.

3.7 Comparison of measurements to long-term conditions at Grays Reef

The National Oceanic and Atmospheric Administration (NOAA) maintains numerous buoys for collection of oceanographic and meteorological data offshore of the United States coasts. Buoy number 41008 is located within the Grays Reef National Marine Sanctuary, 55 km northeast of the mound (Figure 10).

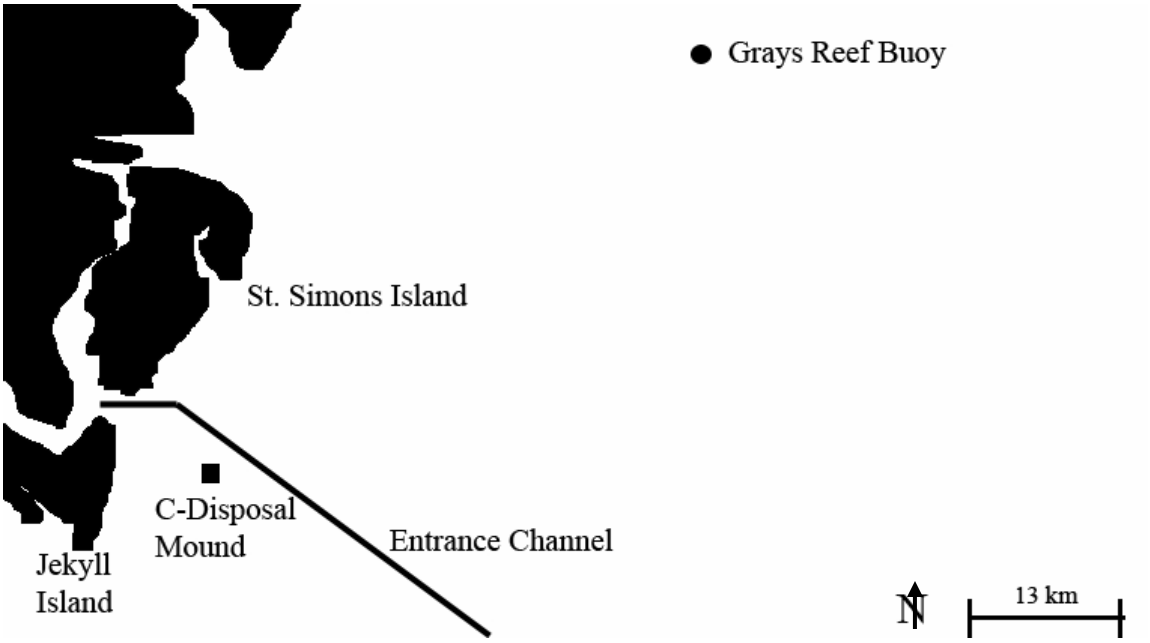

Figure 10. Locator map of NOAA Grays Reef Buoy. The buoy is 55 km northeast of the mound, which is 7 km from Jekyll Island. Depth at the mound is 6 m and depth at Grays Reef Buoy is 18 m.

Station 41008 has been recording data including winds, waves, air and water temperature, and barometric pressure since 1988. The wind and wave data recorded by the buoy were inspected in order to determine if the experiment at Brunswick was conducted during a period of increased, decreased, or typical wind and wave energy.

The wind speed measured by the buoy is an 8-minute average taken every hour, 5 m above sea level, while the wave height data are calculated from the energy spectrum calculated from a 20 minute sampling period every hour. The wind and wave data from 1988 to 2003 were downloaded and monthly averages determined. Monthly averages for 2003 were also calculated (Figure 11).

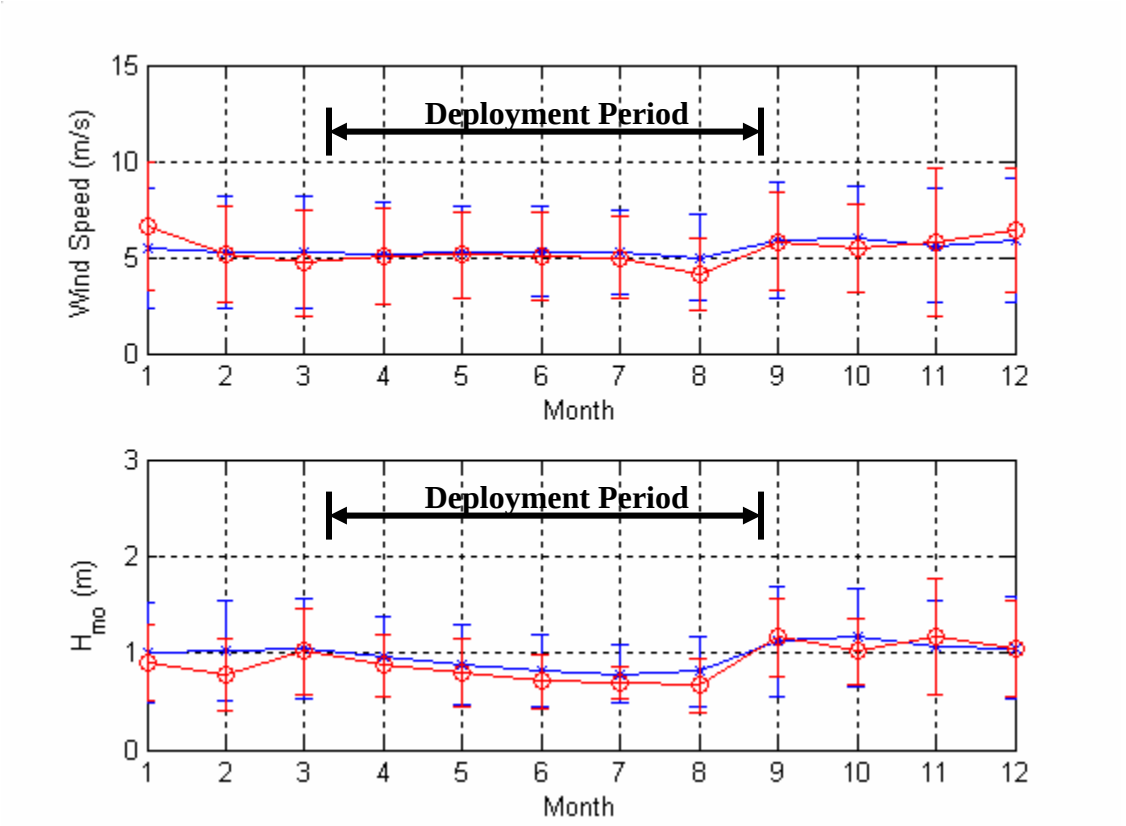

Figure 11. Average 8-minute wind speed measured 5 m above sea level (top) and zero-moment wave height (bottom) at the Grays Reef Buoy based on hourly data for all of 2003 (red circle) and average conditions measured from 1988-2003 (blue x). Error bars indicate one standard deviation away from the mean for each month.

The figures above show that the average wind speed and average wave heights for the 2003 deployment were similar to the long-term average conditions. This suggests that the deployment did not occur during a period in which abnormal wind or wave conditions were present.

The wind and wave directions also display some seasonal trends. In order to observe these variations, the data from the Grays Reef Buoy were divided into seasons according to Table 4. The average zero-moment wave height and wind speed for each season were calculated. Only 10 months of wave direction data were available for

download; therefore, only wind directions were investigated. Wind roses for each season were constructed from the data and the most probable direction displayed in those plots was found. All of the seasonal trends are summarized in Table 4.

Table 4. Average and standard deviation of zero-moment wave height and wind speed. Wind direction is heading from which winds are coming. The average wind direction was determined from wind rose plots. Data are taken from the Grays Reef Buoy for 1988—2003 and averaged over a season.

Season	**Months**	**Mean (Std. Dev.) of H_{mo} (m)**	**Mean (Std. Dev.) of Wind Speed (m/s)**	**Most Probable Wind Direction**
Spring	March—May	0.96 (0.45)	5.2 (2.6)	S & NE
Summer	June—August	0.80 (0.34)	5.2 (2.3)	SSW
Autumn	September—November	1.11 (0.52)	5.8 (2.9)	NE
Winter	December—February	1.03 (0.52)	5.6 (3.1)	NNE

Several seasonal dependencies are apparent in the data. In the autumn and winter months of the year, the wave height and wind speeds are larger, on average, than in the spring and summer months. In addition, the wind direction shifts from a southerly direction in the summer to a more northeasterly direction in the autumn and winter.

The instruments deployed at the Brunswick Offshore Dredged Material Placement Area yielded data describing a variety of hydrodynamic and oceanographic parameters. The data set provides insight regarding sediment transport trends of the area and the fate of the sediments placed in the dredged material mounds. The procedures for sediment transport calculations as well as the results of these analyses are presented in the next chapters.

CHAPTER 4

SEDIMENT TRANSPORT PREDICTIONS DERIVED FROM FIELD MEASUREMENTS

Hydrodynamic, sediment, and bathymetric data were collected with instruments deployed at the dredged material mound. Before analysis of the data for determination of sediment transport trends could commence, an extensive inspection of the files was undertaken to gain an understanding of the extent of the data and remove any points with poor quality. The details of this quality control procedure as well as the methodology used for the estimation of sediment transport, in terms of bed, suspended, and total load transport rates, are discussed in this chapter.

4.1 Quality Control of Data

The ADV served as the main source of data. It recorded data at 2 Hz for 3 minutes every hour. These data include 3 components of velocity and pressure, heave, pitch, and roll of the instrument as well as strength and correlation of the signal. Several methods were used to eliminate poor quality data. First, the heading, heave, pitch, and roll reported by the instrument were investigated for each deployment. This was done to ensure that the instrument remained stationary. The heading, heave, pitch, and roll for all deployments remained essentially constant, indicating that the instrument was stationary during each deployment.

Next, the signal strength and correlation values were checked so that any bad data points could be removed before further analysis. Signal strength is a measure of the intensity of the reflected acoustic signal and is measured in counts. The values for signal strength can range from 0-255 counts (i.e. 8-bits), with one count being equal to 0.43 dB. When signal strength is expressed in dB, it is commonly referred to as the signal-to-noise ratio (SNR). Signal-to-noise ratio is often defined as:

$$SNR = 20\log\left(\frac{E_2}{E_1}\right) \tag{9}$$

where,

$E_1 =$ intensity or energy of the noise;

$E_2 =$ intensity or energy of the reflected signal.

Signal strength of an ADV is a function of the amount and type of particulate matter in the water column; therefore, it is primarily used to verify that there are enough scatterers in the water to provide a strong return signal for velocity determination. With proper calibration procedures, signal strength measurements can be used to determine suspended sediment concentration. Reduced signal strength is typically caused by biofouling but can also be due to very clear water. For the purposes of this project, signal strength was used to verify that the SNR was large enough to ensure good quality data. Sontek (2001) recommended that for high-resolution measurements the signal strength should be at least 15 dB or 35 counts. In order to view typical signal strengths for the deployments, the average signal strength for each burst (3-minute sample) was calculated and plotted. An example of such a plot is shown in Figure 12.

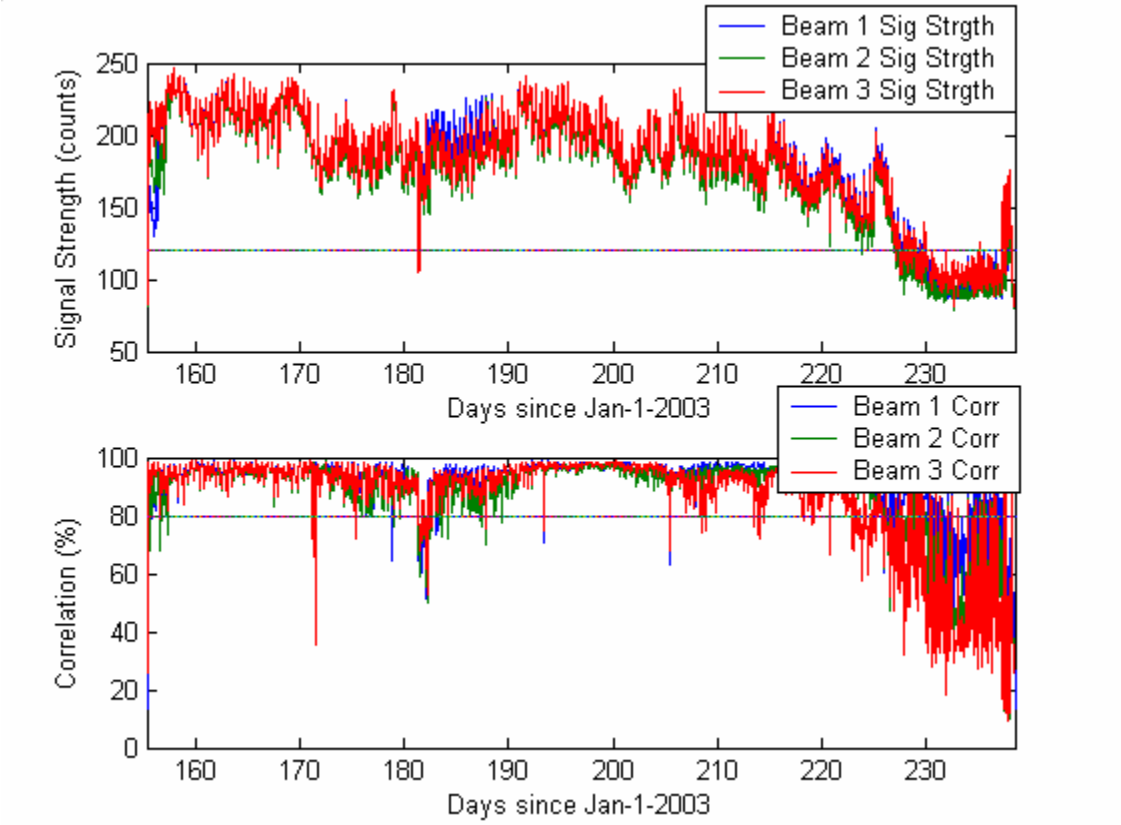

Figure 12. Signal Strength (top) and correlation (bottom) values reported by the C-Crest ADV during Deployment 3. Thresholds are indicated by the horizontal line. The drop in signal strength and correlation after day 220 is likely due to fouling of the instrument.

Near the end of the record above, a drop in the signal strength was observed. This drop in signal strength was also accompanied by a decrease in correlation, which suggests fouling of the transducers. In order to eliminate these points of suspect quality, a cutoff value of 120 counts (52 dB) was chosen. Any burst that had an average associated signal strength value below this threshold was discarded before analysis. This threshold value caused 307 (9%) of the bursts to be discarded.

Correlation is a measure of the coherence of the recorded velocity signal and is a direct output from the Doppler velocity calculations. Correlation is calculated for each beam and can range from 0-100%. A value of 100% indicates high coherence (low

noise) in the velocity measurements while a value of 0% indicates no coherence or a signal dominated by noise. Sontek suggests that correlation be used to monitor data quality during collection and for removing bad quality data points during post processing. Low correlation indicates the instrument is damaged or measuring in a difficult (noisy) environment. Low correlation is often due to: low SNR, highly turbulent flow, highly aerated water, a damaged ADV, or the instrument periodically being exposed to air (Sontek 2001). Sontek suggests that the correlation should be above 70% for measuring wave-induced velocities. A correlation below 70% is indicative of problems with the raw velocity data; therefore, to be conservative, a threshold value of 80% was selected for this study. Any burst with an average correlation below 80% was discarded before analysis commenced. The application of this threshold alone resulted in 625 (18%) of the bursts being discarded.

Finally, the magnitude of the mean velocity in the horizontal plane was used to filter out unreasonable data. Data in which the magnitude of the mean velocity is too large to be reasonable were discarded. Unreasonable velocity magnitudes could be due to fouling of the instrument, low signal to noise ratio, or waves breaking on the instruments that cause interference due to bubbles. A plot of the mean horizontal current speed for one deployment is shown in Figure 13.

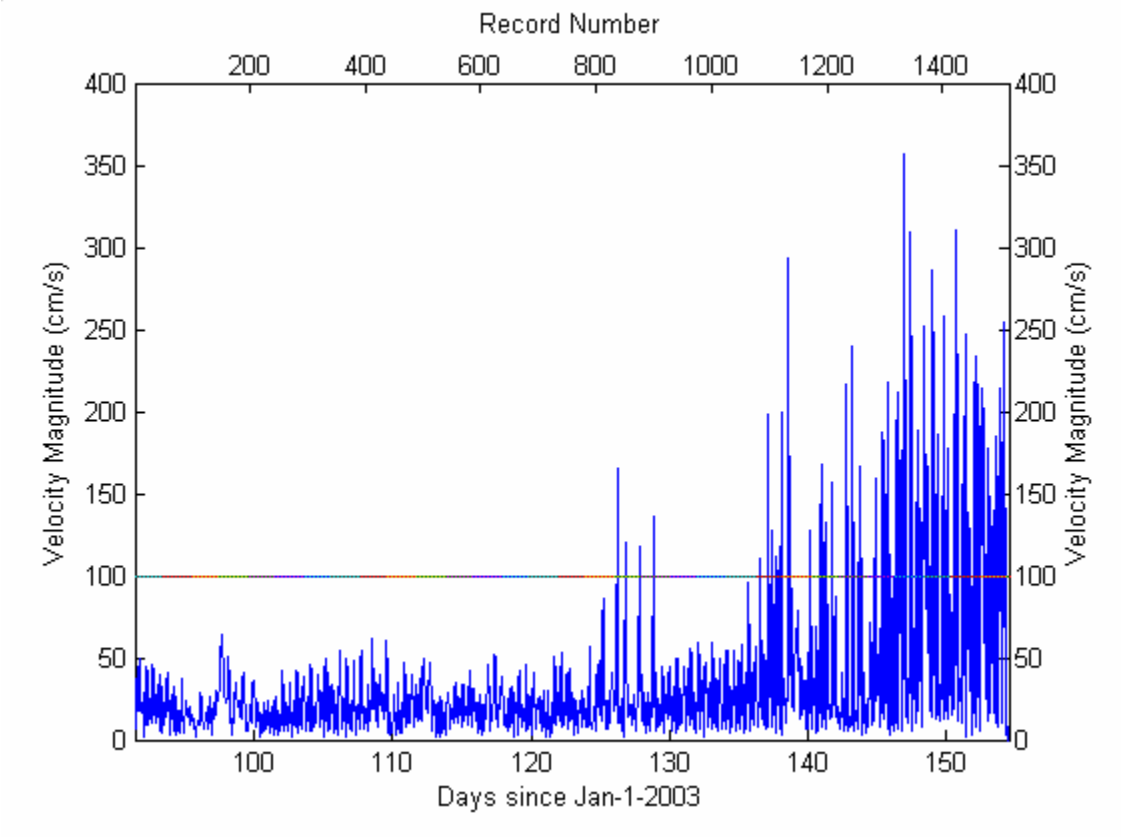

Figure 13. Burst averaged horizontal velocity recorded by C-Crest ADV. Abnormally high magnitudes were eliminated by quality control thresholds indicated here by the horizontal line. The four bursts in the middle of the record that are over the horizontal line also had corresponding correlation values below that threshold.

Looking at Figure 13, the magnitude of the mean velocity throughout the majority of the deployment is below 50 cm/s. Near the end of the deployment, many abnormally high magnitudes are displayed. Most of these large magnitudes would have already been eliminated due to correlation and signal strength thresholds; however, a threshold value of 100 cm/s was selected for redundancy. This cutoff resulted in the discarding of 101 (3%) of the bursts recorded.

Every burst that failed one or more of the quality control thresholds was discarded. Applying all the filters together resulted in the discarding of 711 (20%) of the

total 3511 bursts recorded. Upon completion of the quality checks, there remained two useful data sets. The first set consisted of data collected from April 2, 2003 to June 4, 2003, hereafter referred to as Deployment 2, and a set containing data collected from June 5, 2003 to August 22, 2003, hereafter referred to as Deployment 3. Deployment 1 was discarded due to the limited amount of data it contained after elimination of bad records.

4.2 Harmonic Analysis

Harmonic analysis was employed to reveal the dominant tidal forcing constituents for the two instrument deployments. The analysis was conducted using the M-file t_tide which can be downloaded from the Mathworks website. The tool works by optimizing the amplitude and phase angles, using the known frequency for up to 146 different tidal constituents. The M-file optimizes Equation (10) such that it is as close as possible to the measured water level.

$$\eta_{pred} = \sum_{i=1}^{I} a_i \cos(\omega_i t + \phi_i) \tag{10}$$

η_{pred} = water level predicted by harmonic analysis [L];

a_i = amplitude [L];

ω_i = theoretical frequency of tidal constituent being considered [1/T];

t = time [T];

ϕ_i = phase angle [-];

I = number of constituents [-].

Figure 14 shows the measured tidal stage from the ADV data versus the stages predicted using constituents derived from harmonic analysis for Deployment 2.

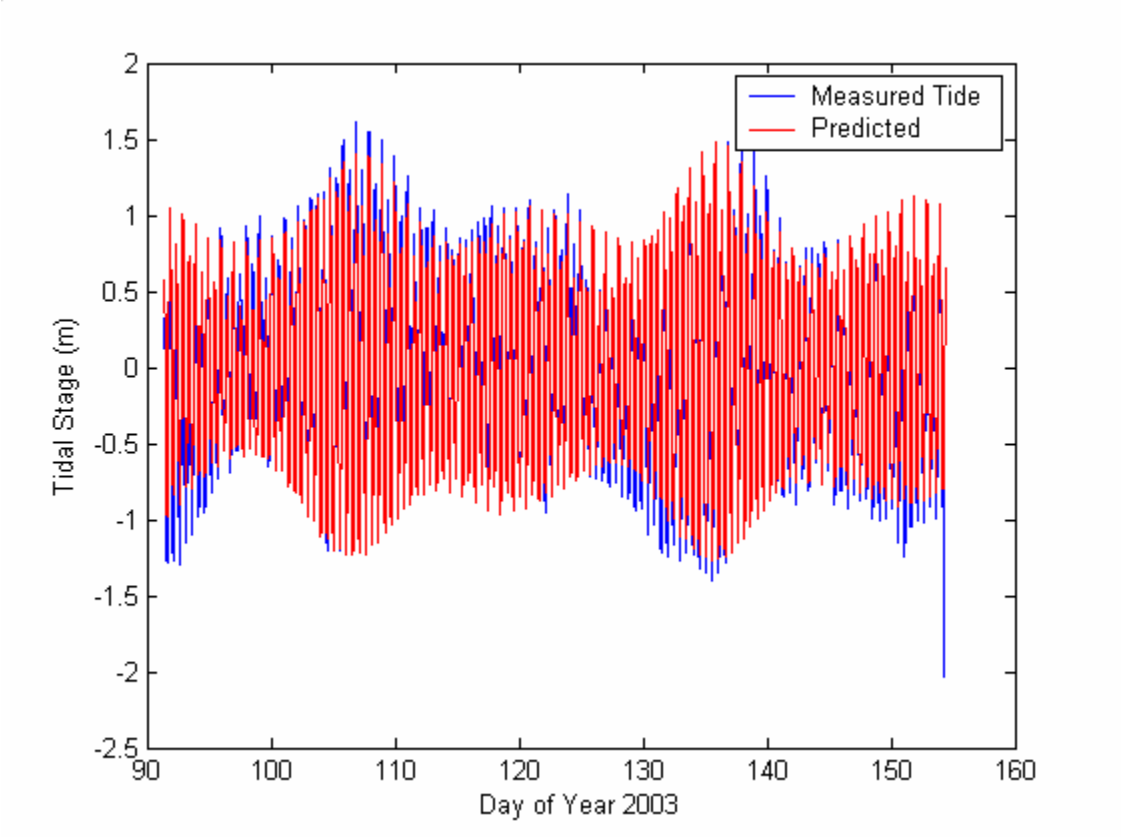

Figure 14. Measured tidal stages versus those predicted by harmonic analysis for Deployment 2.

The measured and predicted tides match well, with harmonic analysis yielding 91.6% of the variance of the measured tide. The corresponding number for Deployment 3 was 93.6%. The tidal stage is dominated by the primary lunar semi-diurnal (M2) constituent. Results derived from the harmonic analysis of the measured tidal stages from the ADV are shown in Table 5. This analysis was also done on the ADCP data and the dominant tidal constituents and corresponding amplitudes were similar.

Table 5. Primary tidal constituents and corresponding amplitudes, periods, and phases at the ADV over the crest of the mound at the Brunswick, GA dredged material placement site. Harmonic analysis of the ADCP data yielded similar results.

Constituent		Deployment 2 (April 2—June 4, 2003)		Deployment 3 (June 5—August 22, 2003)	
	Period (hrs)	Amplitude (m)	Phase (deg)	Amplitude (m)	Phase (deg)
M2	12.42	0.87	327	0.92	359
N2	12.66	0.23	163	0.19	77
S2	12.00	0.16	273	0.11	322
K1	23.93	0.12	350	0.14	321
O1	25.82	0.08	327	0.09	60

Harmonic analysis was also performed on the mean (burst-averaged) velocity records. The results of the harmonic analysis described 69.2% and 84.7% of the variance of the mean flows for Deployment 2 and Deployment 3, respectively. Harmonic analysis did a better job predicting the tidal stage than the mean flows. This is expected since bathymetry and wind modify flows more than water level. Winds were larger for Deployment 2, which may explain some of the reduction in ability to predict the variance; the average wind speed was 5.1 m/s and 4.7 m/s for Deployments 2 and 3, respectively. The standard deviation of the wind speed was 2.3 m/s and 2.2 m/s for Deployments 2 and 3, respectively. This analysis showed that the M2 constituent was again the dominant forcing mechanism for mean flows. Characteristics of the tidal flows are summarized in Table 6.

Table 6. Summary of the results of harmonic analysis of mean (burst averaged) velocity measured for two deployments at the Brunswick dredged material placement site.

	Deployment 2 (April 2—June 4, 2003)	**Deployment 3 (June 5—August 22, 2003)**
Semi-major axis	27 cm/s	22 cm/s
Semi-minor axis	1 cm/s	<1 cm/s
Tilt	133^{o}	136^{o}

These results show that the tidal flow is essentially back-and-forth with the ellipse being rotated approximately 135^{o} clockwise from magnetic North, which is nearly along the same axis as the entrance channel (Figure 15).

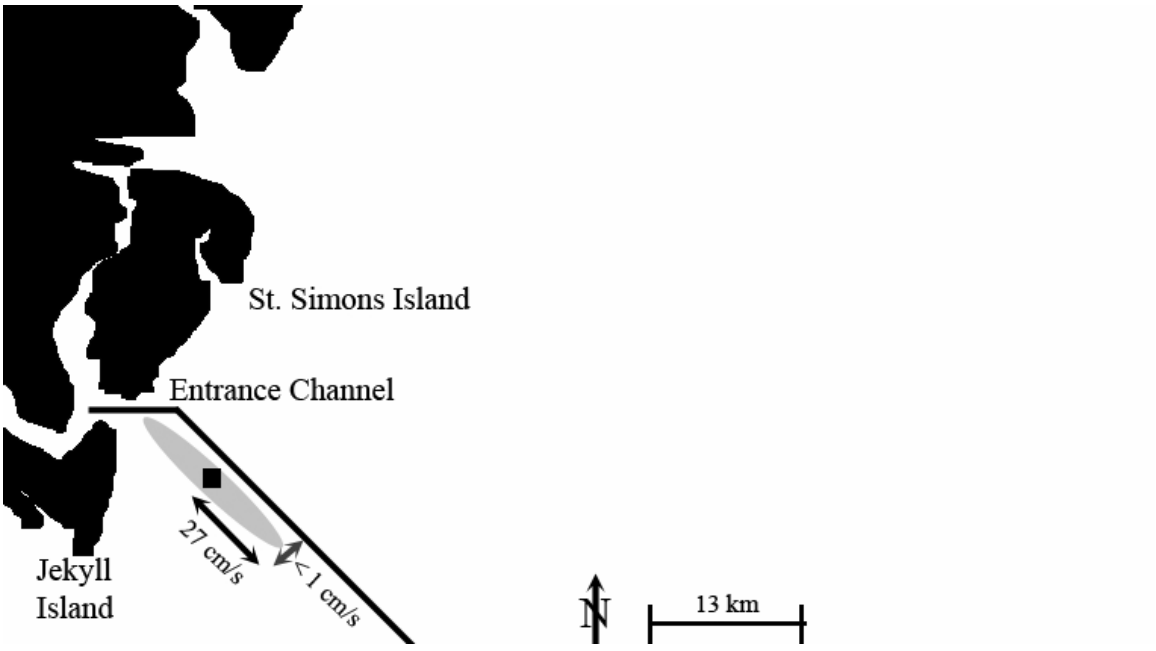

Figure 15. Tidal flows, represented by the ellipse, are essentially back-and-forth along the same axis as the entrance channel dictated by the line. Box indicates the location of the mound.

The same analysis conducted on the ADCP data gave an ellipse with similar semi-major and semi-minor amplitudes but it was tilted 10-15^{o} more westerly such that it pointed more toward Jekyll Island. This suggests that the mound does not greatly modify the flow direction.

4.3 Relative Importance of Waves and Currents

Waves arriving from offshore were measured by the ADCP prior to reaching the mound. The ADCP calculates the full directional energy spectrum, from which many wave parameters are derived, including the zero-moment wave height and average direction of incoming waves. Figure 16 is a plot of those two parameters.

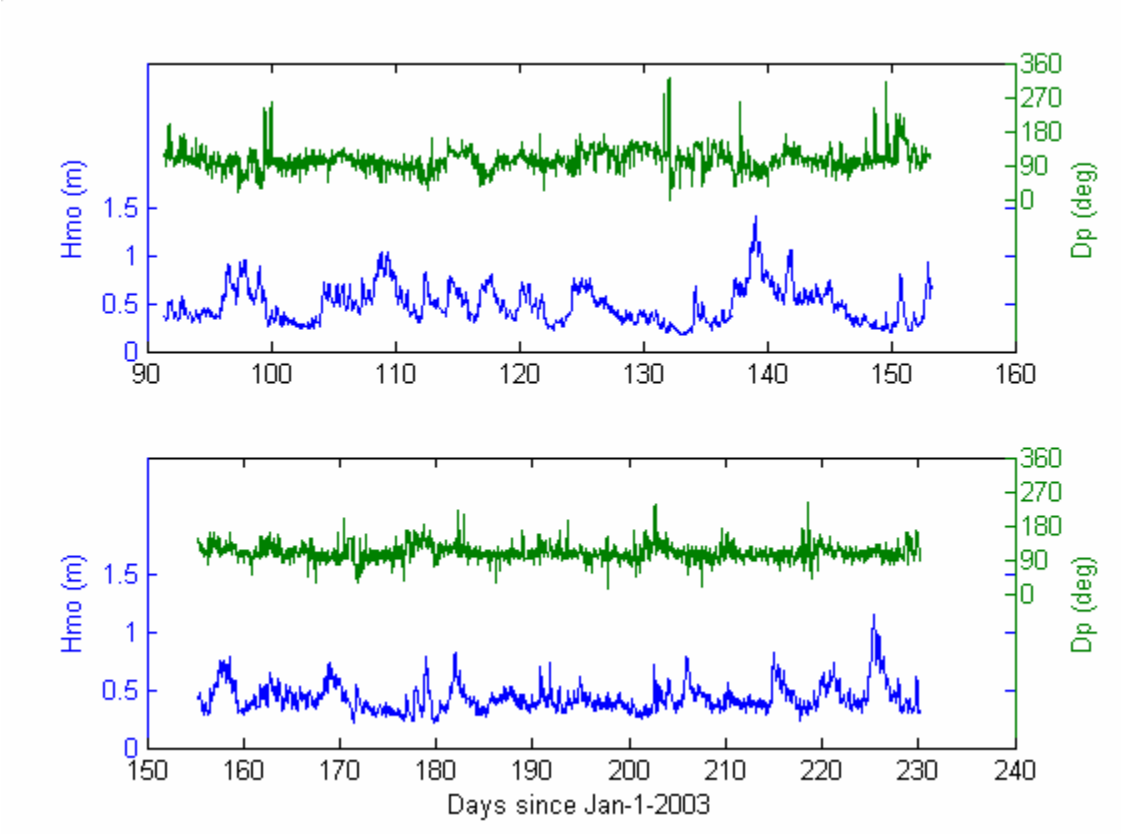

Figure 16. Incident wave heights and directions measured by the ADCP just offshore of the Mound C. Wave direction is the direction waves are coming from, with respect to magnetic North. Top: April 2—June 4, 2003 (Deployment 2). Bottom: June 5—August 22, 2003 (Deployment 3).

The figure shows that, for these deployments, the waves typically come from a direction of about 105^{o} measured clockwise from magnetic North. This corresponds with the summer to autumn wave directions that are usually out of the southeast (Griffin and Henry 1984). The average incident significant wave height has an average value of 46 cm before shoaling over the dredge material mound. As waves shoal, it is possible that they will break while over the mound. One model often used to predict wave breaking is the spilling breaker model given by Equation (11).

$$H_b = \kappa h_b \tag{11}$$

where,

H_b = breaking wave height [L];

κ = wave breaking criterion [-];

h_b = depth of wave breaking [L].

McCowan (1894) estimated that if κ reaches 0.78, waves break. This model was applied to the data by calculating the height of waves as they passed over the ADV. This was done using pressure data recorded by the ADV. The mean was removed from each burst of pressure data. The Fast Fourier Transform was then applied to the pressure time series and the coefficients band pass filtered to remove noise and focus on the wind wave regime. Cutoff frequencies of 0.05 and 0.5 Hz were used. The Fourier coefficients of the pressure time series were then converted to the surface by dividing by the square of the pressure response function. The pressure response function is given by Dean and Dalrymple (1991) as:

$$K_p = \frac{\cosh k(h+z)}{\cosh kh} = \frac{\cosh kz'}{\cosh kh} \tag{12}$$

k = wave number [1/L];

h = water depth [L];

z = distance below the mean water level [L];

z' = elevation of pressure transducer above bottom [L];

The water surface Fourier coefficients were then converted to the water surface time series using the Inverse Fast Fourier Transform. A zero-upcrossing method was employed to isolate waves, and the wave height calculated as the maximum excursion

between two successive upcrossing occurrences (i.e. for each wave). Calculated wave heights were then divided by water depth, which was 2.5 m on average with an average tidal fluctuation of ±1 m from the mean, and if the ratio of wave height to water depth was greater than or equal to 0.78, waves were said to be breaking. Using this simple model, it was found that waves never broke over the instrument location. In some cases, κ can be as low as 0.4. In this case the model predicts that waves are breaking only 2% of the time for this site.

The magnitude of the mean velocity over the mound is strongly dependent on wave conditions. Figure 17 was constructed to show the variation of velocity magnitude on a day with large waves versus a day with smaller waves.

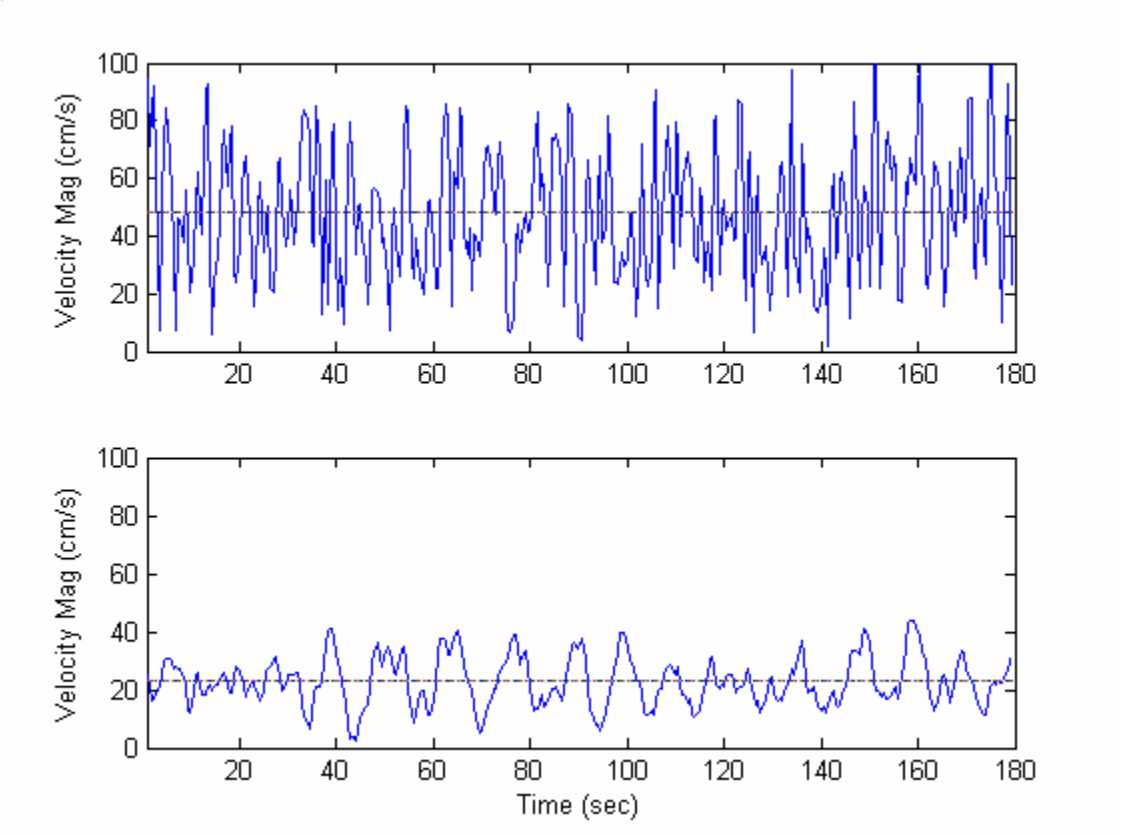

Figure 17. Top graph is the velocity magnitude time series for a 3-minute burst with H_{mo}=85 cm. Bottom is velocity magnitude time series for a burst with H_{mo}=31 cm. Dashed line indicates mean magnitude for the burst: 48 cm/s (top) and 23 cm/s (bottom).

The mean of the magnitude for the burst with larger waves was 48 cm/s and the mean for the small wave burst was 23 cm/s. The differences in the velocity records are probably due to winds, which causes waves to become larger. This shows that wind/wave action can have a significant effect on the velocity over the mound. Varying tidal currents could also have contributed to some of the differences between the mean of the two records.

The relative importance of wave-induced orbital velocities and mean flows on sediment transport was investigated. This was done by calculating the wave-current ratio as given in Equation (13).

$$WC = \frac{\sigma_w}{\overline{V}} \tag{13}$$

where,

WC = relative importance of waves to currents [-];

σ_w = standard deviation of 3-minute velocity magnitude time series [L/T];

$\overline{V} = \sqrt{\left(\overline{V_N}\right)^2 + \left(\overline{V_E}\right)^2}$ = magnitude of the mean velocity vector [L/T].

$\overline{V_N}$ = mean of the north component of velocity for a burst [L/T];

$\overline{V_E}$ = mean of the east component of velocity for a burst [L/T];

The result, shown in Figure 18, is a ratio that can be used to quantify the relative importance of waves and currents. If this ratio is order 1 or greater, it indicates that the deviation of velocities from the mean is great; therefore, wave energy is important. Conversely, if the ratio is small, wave energies are less important and currents dominate.

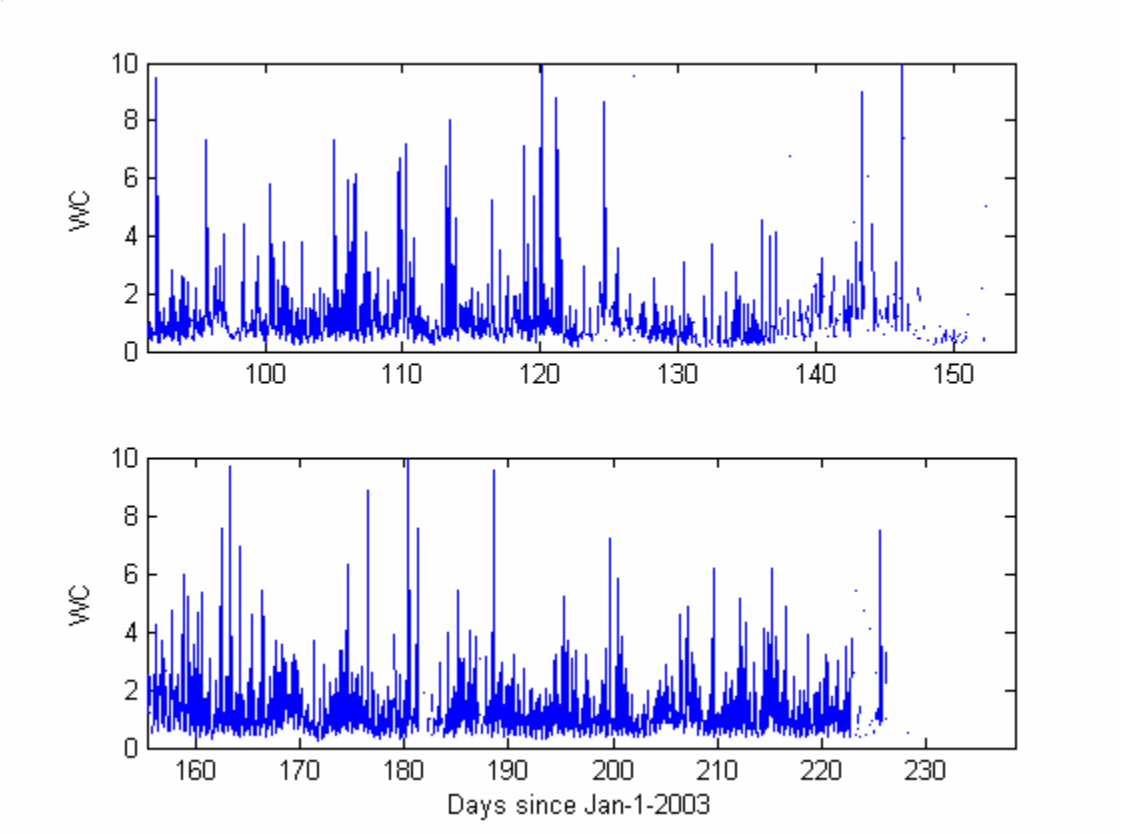

Figure 18. Graph of relative importance of waves and currents at the mound for Deployment 2 (top) and Deployment 3 (bottom). The WC ratio is order 1 for the both deployments which suggests that both waves and currents are important and should be considered in sediment transport calculations.

In Figure 18, a range of WC values are displayed but the ratio is order 1 for most of the deployment. This suggests that both waves and currents are important and should both be considered when modeling sediment transport trends.

4.4 Bed Load Transport Predictions

Bed load transport was defined by Bagnold (1956) as the part of the total sediment load that is supported by intergranular forces. Others have defined it as the part of the total load that occurs within a certain distance of the bed. Of the numerous

methods available for estimation of sediment transport, two relevant equations were selected. One method (Nielsen 1992) was selected to give an estimate of transport based solely on mean flows. The other method (Soulsby 1997), which is derived from the Nielsen equation, was used for two reasons. First, the USACE has used it in their numerical modeling of the Brunswick, GA region, so it was selected to facilitate comparisons and give additional data for calibration of the USACE model. This method also estimates sediment transport due to both waves and currents, so the contribution and importance of wave forcing on sediment transport can be estimated by comparing results from the Soulsby and Nielsen formulae. A more in-depth discussion of each of these methods and results are provided below.

4.4.1 Shields/Nielsen Bed Load Transport Method

Shields (1936) studied incipient motion of particles and developed two relevant dimensionless parameters. One of the parameters on the curve is known as the Shields parameter, Θ, or the dimensionless shear stress, and is a balance between disturbing and stabilizing forces acting on a particle. The Shields parameter is given as:

$$\Theta = \frac{\tau}{(\gamma_s - \gamma)d} \tag{14}$$

where,

τ = shear stress [F/L^2];

γ_s = specific weight of sediment [F/L^3];

γ = specific weight of water [F/L^3];

d_{50} = mean sediment diameter [L];

The critical Shields parameter, Θ_c, is simply the dimensionless shear stress calculated using the critical value of shear stress, τ_c, required to initiate sediment motion.

The other dimensionless parameter is Re_b, the Boundary Reynolds Number which is given as:

$$\mathrm{Re}_b = \frac{U_* d}{\nu} \tag{15}$$

where,

ν = kinematic viscosity [L^2/T];

$$U_* = \sqrt{\frac{\tau}{\rho}} = \text{shear velocity [L/T]}; \tag{16}$$

$$\tau = \frac{1}{2}\rho f U^2 = \text{shear stress [F/L}^2\text{]}; \tag{17}$$

ρ = water mass density [F-T^2/L^4];

U = current speed [L/T];

f = friction factor [-].

Shields plotted several experimental data sets using these dimensionless parameters. The result was the well-known curve for incipient motion shown in Figure 19.

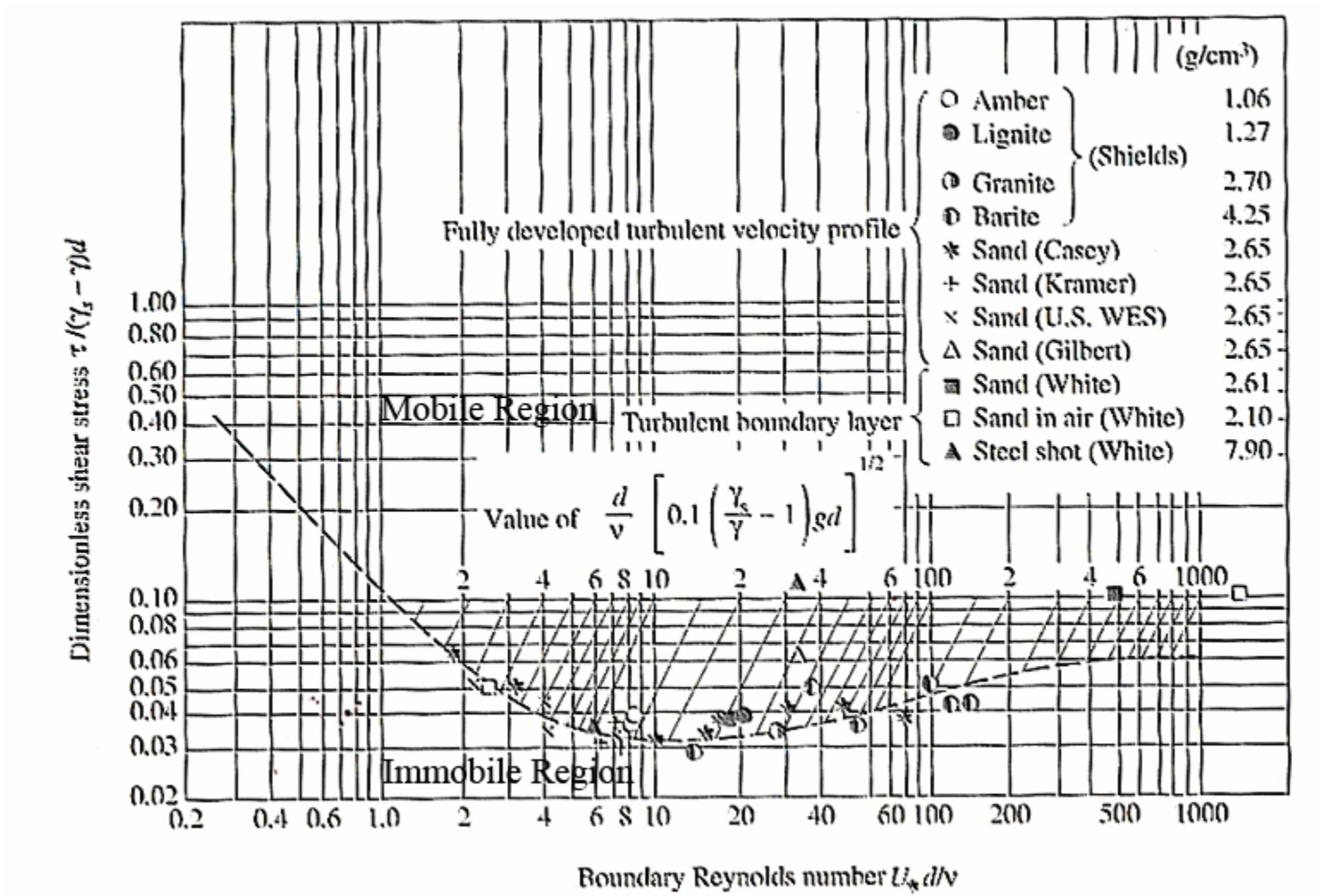

Figure 19. Shields diagram for incipient motion adopted from Yang 1996. Line denotes critical dimensionless shear stress. Region above line represents mobile sediments while region below line is for immobile sediments.

The Shields curve allows determination of whether a sediment will be mobile in a given steady flow. The line denotes dimensionless critical shear stress, so the region above the line corresponds to stresses high enough to move sediment, whereas the area below the curve corresponds to no motion. For natural sediments, a variety of particle sizes will be present, some of which will be mobile even if others are not. The development of the Shields Curve created a method by which critical shear for sediment motion could be estimated.

Several graphs were constructed to show the dependency of critical velocity on the grain diameter, with the following assumptions:

s = specific gravity of sediment = 2.65;

ρ = seawater mass density = 1025 kg/m^3;

ν = kinematic viscosity = 10^{-6} m^2/s;

f = friction factor = 0.018.

The relationship between sediment diameter and the corresponding critical velocity for sediment motion is displayed in Figure 20.

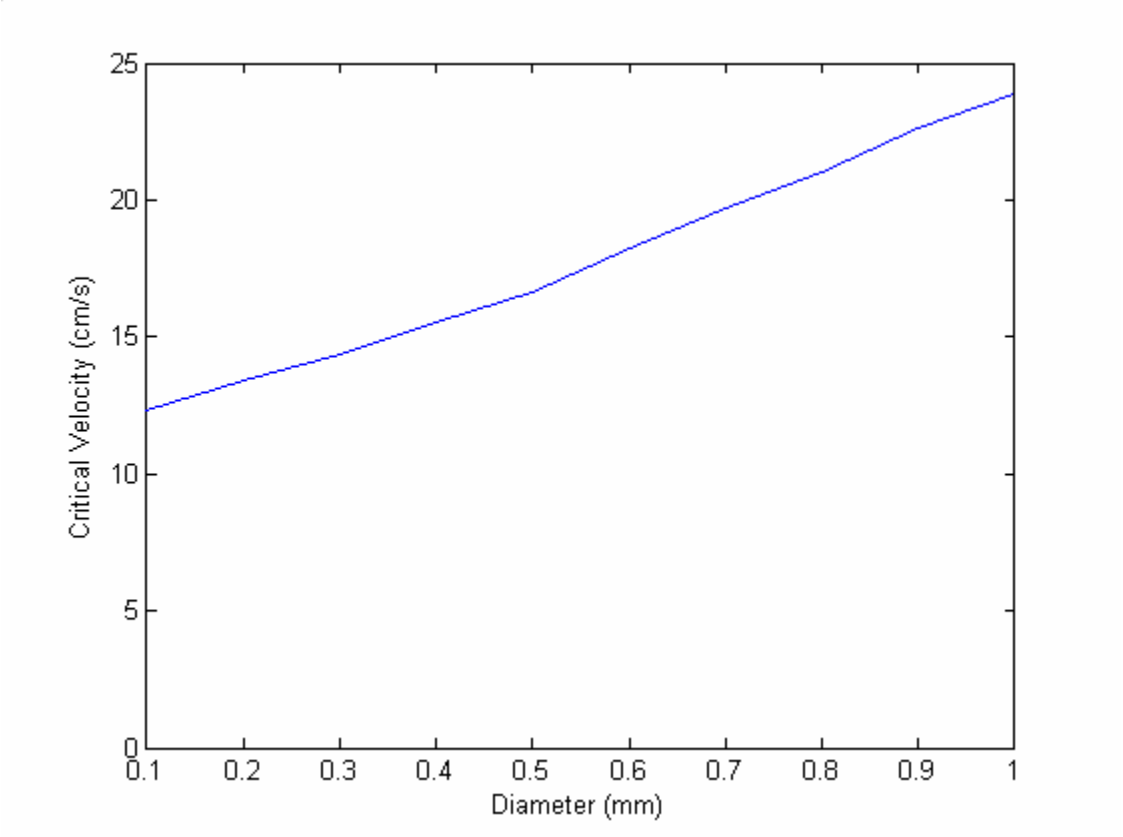

Figure 20. Relationship between the diameter of a particle and the critical velocity required for incipient motion according to the Shields Diagram.

Typical median sediment diameters in the mound crest was 350 μm and sediments of this size have an associated critical Shields parameter of 0.038 and critical velocity of approximately 15 cm/s.

Much of the work in the field of sediment transport that followed Shields (1936) was based on his curve and the assumption that sediment transport is proportional to some excess shear or excess Shields parameter; therefore, Shields and others have proposed formulae of the form:

$$q_b = k(\Theta - \Theta_c)^n \tag{18}$$

where,

q_b = bed load transport [M/T-L];

Θ = actual Shields parameter calculated using flow characteristics and particle diameter;

Θ_c = critical Shields parameter for incipient motion;

k & n = empirical calibration coefficients;

Meyer-Peter & Muller (1948) proposed an empirical relationship for dimensionless bed load transport, Φ_B. It was later modified by Nielsen (1992) to better approximate experimental data. The modified formula is given as:

$$\Phi_B = 12(\Theta - \Theta_c)\sqrt{\Theta} \tag{19}$$

where,

$$\Phi_B = \frac{q_b}{d\sqrt{(s-1)gd}} \tag{20}$$

q_b = bed load transport rate [L^3/T-L];

d = sediment diameter [L];

s = specific gravity of sediment, assumed to be 2.65;

g = acceleration of gravity [L/T^2].

The Nielsen formula gives non-dimensional sediment transport as a function of the excess Shields parameter. This non-dimensional transport is easily converted to give a volumetric rate for sediment transport. The dependency of the non-dimensional and the volumetric sediment transport rates on flow speed is displayed in Figure 21 below.

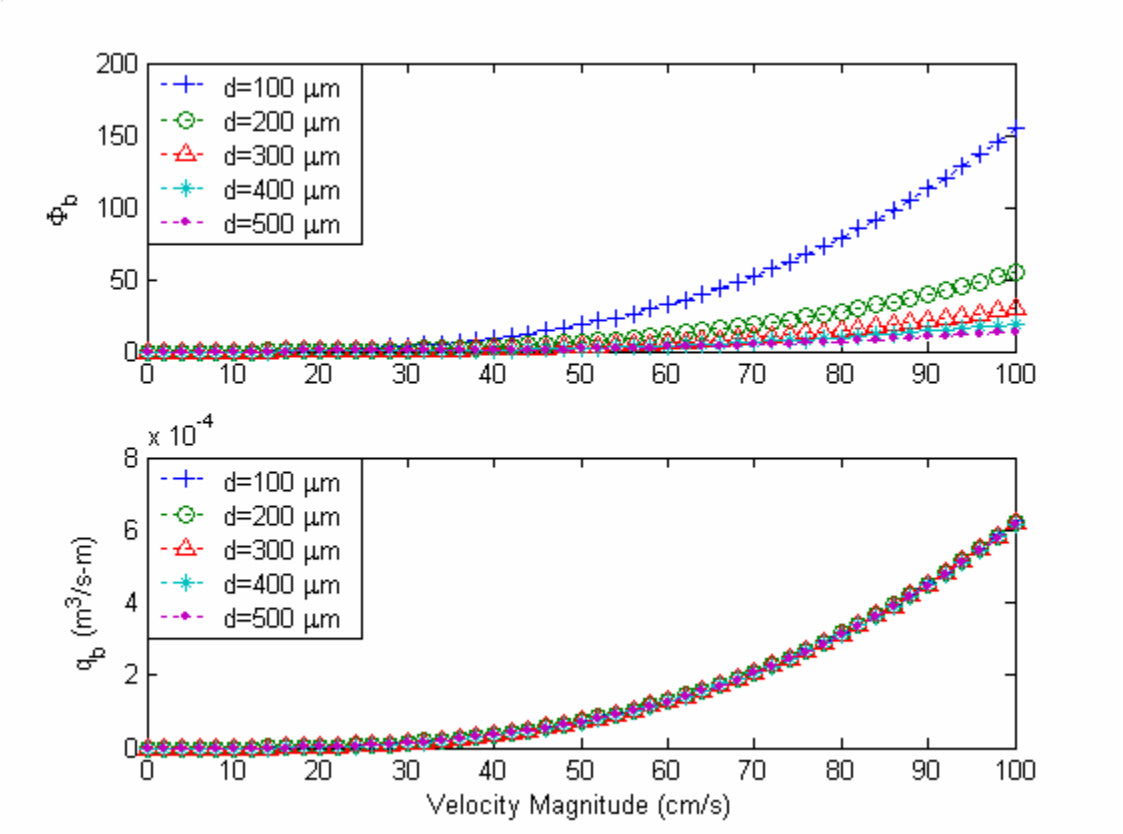

Figure 21. Dimensionless (top) and volumetric (bottom) sediment transport rates as a function of magnitude of velocity according to the Nielsen formula.

Looking at the nondimensional sediment transport Φ_b, a dependency on sediment diameter is displayed; however, when that term is dimensionlized to give a volumetric transport rate the dependency on diameter disappears. This can be explained by substituting Equation (19) into Equation (20) and solving for q_B.

$$q_b = \frac{12\sqrt{(s-1)g}}{(\gamma_s - \gamma)^{3/2}}\left[\tau^{3/2} - \tau_c \tau^{1/2}\right] \tag{21}$$

Equation (21) shows that q_b is proportional to an excess shear, and diameter does not explicitly appear in the equation. The diameter will affect the values for actual shear, τ, through the friction factor, f, and the quantity for critical shear, τ_c. In the graph above, f

was taken as a constant for each sediment size so the diameter only influences critical shear, and that influence diminishes as shear increases. This explains the trend displayed in Figure 21 of volumetric transport rates being independent of d_{50}. When this method is applied to actual data, with varying friction factors, a larger dependence of diameter on sediment transport will be displayed.

The Nielsen method was one of three methods used to estimate the bed load sediment transport rate over the crest of the mound. The Nielsen formula was applied using data from the ADV and ADCP with the following steps:

1. Burst averaged velocity, U, was determined for each burst from the ADV;
2. The orbital velocity, u_w, was calculated from the standard deviation of velocity for each burst taken from the ADV located over the mound. Mean frequency, ω, was taken from the ADCP located off the mound for the same period (according to linear wave theory ω is constant although the depth changes);
3. Friction factor, f, for each burst calculated using the approach of Swart (1974) where:

$$f = \exp\left[5.213\left(\frac{2.5d_{50}}{A}\right)^{0.194} - 5.977\right] \tag{22}$$

$$A = \frac{|u_w|}{\omega} = \text{excursion length [L]}; \tag{23}$$

Friction factors ranged from 0.01-0.03 with the average being 0.018;

4. Shear stress computed using the magnitude of the mean velocity and Equation (17);
5. Shields parameter, Θ, calculated for each burst using Equation (14);

6. Critical Shields parameter, Θ_c, determined for the sediment size considered using the Shields Diagram (Figure 19);
7. Shields parameters substituted in the Nielsen method, Equations (19) and (20), and a burst averaged sediment transport rate calculated for each burst.

This methodology assumes that sediment transport characteristics displayed during a three-minute period are representative of those for the rest of that hour. This is acceptable since wave and current conditions do not typically change dramatically over an hour.

This methodology was used for 3 sediment sizes: d_{50}=100 μm, d_{50}=350 μm, and d_{50}=500 μm. The percentage of the time that each sediment fraction was mobile for each deployment was found. A sediment was termed mobile if the near-bed horizontal velocity measured by the ADV was in excess of the critical velocity calculated using the Shields Diagram and Equation (17). The results of this analysis are summarized in Table 7.

Table 7. Average friction factor calculated using Swart's method and critical velocity for sediment entrainment found using Shields Diagram. Percentage of the time the critical velocity is exceeded for each deployment and sediment size considered is also displayed.

	Deployment 2 (1215 good bursts)			**Deployment 3 (1585 good bursts)**		
Sediment Size	**Average Friction factor**	**Critical Velocity (cm/s)**	**% Mobility**	**Average Friction factor**	**Critical Velocity (cm/s)**	**% Mobility**
100 μm	0.012	14.5	66.8 %	0.012	14.1	49.4 %
350 μm	0.018	14.7	66.5 %	0.019	14.2	48.6 %
500 μm	0.021	15.4	64.3 %	0.022	14.9	46.2 %

Critical velocity varies between deployments due to differences in the average friction factor. This approach also neglects bed forms, which would modify the results. Bed forms increase roughness height, cause eddies on the lee side of the form, increase form drag and sediment suspension, and cause an overall increase in sediment transport. Several options exist for predicting bed forms based on flow characteristics. A graphical approach was presented in Nielsen (1992) in which eight bed form regimes were noted on a plot of grain roughness Shields parameter versus current Shields parameter (Figure 22). Those two Shields parameters are given as:

$$\theta_{2.5} = \frac{0.5 f \rho u_w^2}{\rho(s-1)gd} \tag{24}$$

$$\overline{\theta} = \frac{0.5 \rho 0.003 \overline{U}^2}{\rho(s-1)gd} \tag{25}$$

where,

$\theta_{2.5}$ = grain roughness Shields parameter [-];

$\overline{\theta}$ = current Shields parameter [-];

u_w = wave orbital velocity = standard deviation of 3-minute velocity magnitude time series [L/T];

$\overline{U}$ = mean current velocity [L/T].

A plot of those the Shields parameters noting the occurrence of bed forms is displayed in Figure 22.

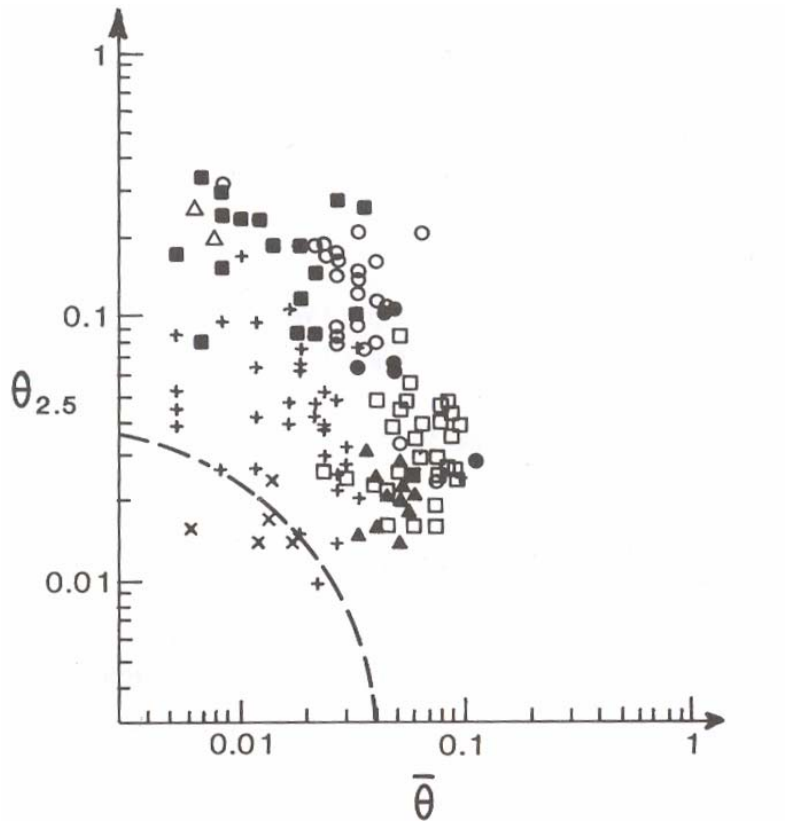

Figure 22. Ripple types in terms of wave and current Shields Parameters. 'x' denotes flat bed while other symbols denote different types of ripples. The curve corresponds to the initiation of ripple formation, $\theta_{2.5} + \overline{\theta} = 0.04$. Figure adopted from Nielsen (1992).

Figure 21 indicates ripple formation when the sum of the two Shields parameters exceed 0.04. Nielsen (1992) notes that for Shields parameters above 1 the ripples tend to disappear. An effort to predict bed forms was made by plotting results derived from the ADV velocity data on the same set of axes and noting the percentage of the time the data exceed the curve for ripple formation. This plot is given in Figure 23.

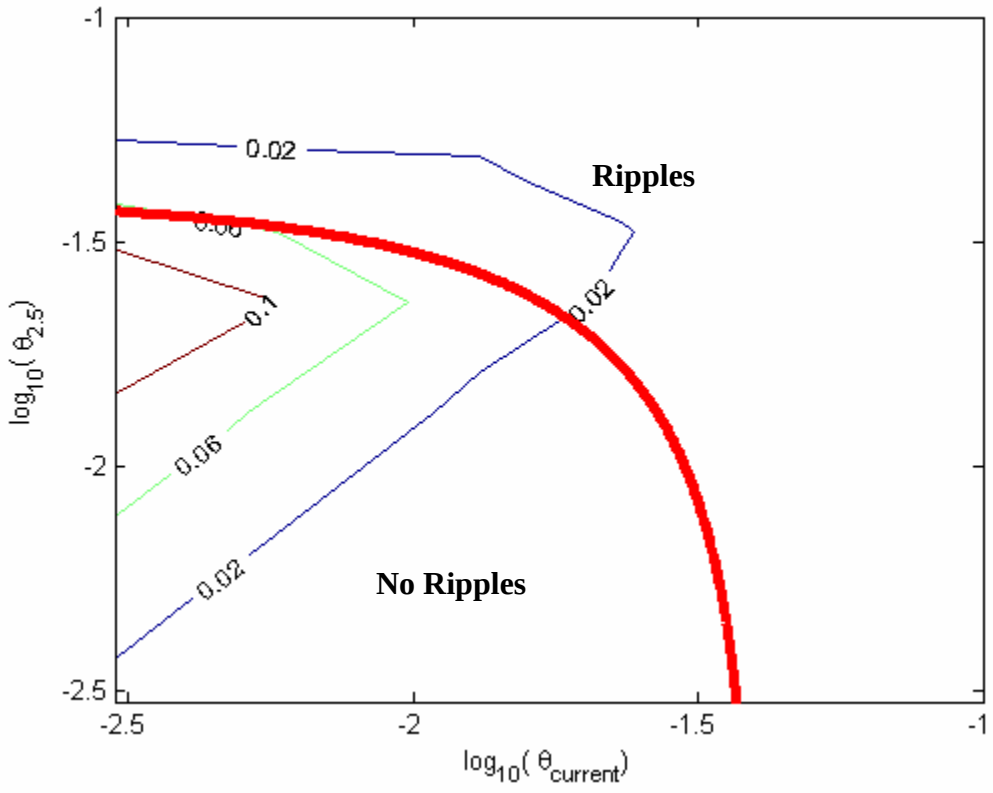

Figure 23. Logarithmic values of the wave-induced and current-only Shields parameter for the site. The area to the right of or above the line is indicative of sediment motion and the formation of ripples. For this site ripples are formed or maintained approximately 17% of the time.

For the Brunswick site, velocity characteristics are favorable for the formation and maintenance of bed forms approximately 17% of the time, which is a small portion of the deployment period. There are no data for which the Shields parameter exceeds 1 (0 on the log scale), the point were bed forms are washed away. The relatively low occurrence of bed forms is encouraging since they were not considered for this study.

A prediction of the magnitude of sediment transport was also made using the Nielsen formula. Figure 24 shows the average sediment transport rate for each 3 minute burst during both deployments.

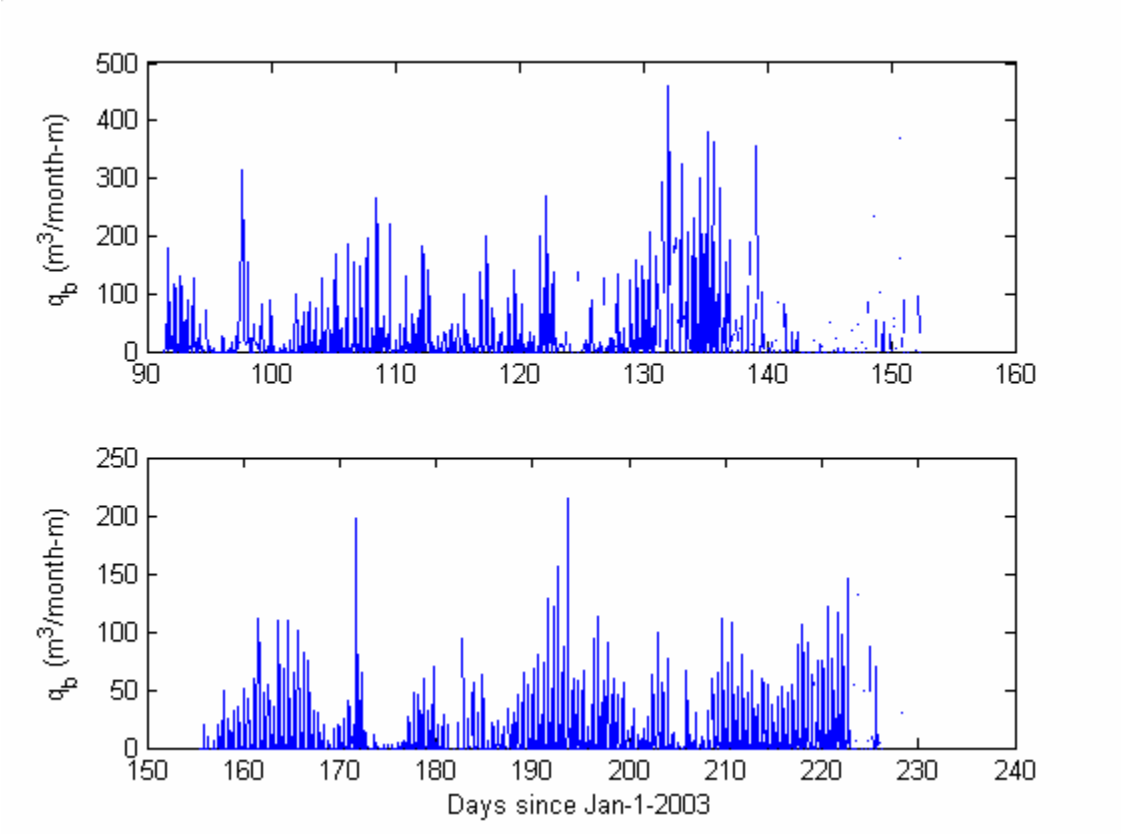

Figure 24. Bed load transport rate for a 350 μm sediment calculated using Nielsen method and the mean velocity from each three-minute burst. The average transport rate for Deployment 2 (top) is 29.2 m^3/month-m, and the average transport rate for Deployment 3 (bottom) is 10.8 m^3/month-m. Data points near the end of the record were eliminated during the quality control procedures.

Similar graphs were constructed for the other size fractions. The deployment-averaged transport rates for each size fraction are summarized in Table 8.

Table 8. Average bed load transport rate predicted using the Nielsen method. Transport rate is an average over a 3-minute burst determined for several sediment sizes.

Sediment Size	**Deployment 2 Average q_b (m^3/month-m)**	**Deployment 3 Average q_b (m^3/month-m)**
100 μm	15.8	5.9
350 μm	29.2	10.8
500 μm	35.6	13.1

The table suggests that larger particles are transported at a rate nearly double that of the smallest particles considered, which is counterintuitive. The reason larger particles tend to have larger volumetric transport rates according to Nielsen's method is due to an associated increase in friction factor. The increased friction factor yields a larger shear stress and an increase in computed transport rate. Looking back at Table 7, the average friction factor nearly doubles between a 100 μm and 500 μm sediment, while the critical velocity for sediment motion only increases by about 6%. It seems that the trend displayed for friction factors is too strong while that for critical velocity is too weak, which leads to the large increase of sediment transport with increased diameter particles. Transport rates for Deployment 2 are also larger than Deployment 3 due to larger velocities experienced during the earlier deployment, which translated to greater mobility of sediments. In order to illustrate the directional distribution of transport, sediment transport roses were constructed for each sediment size fraction and deployment. They are presented and discussed in Chapter 5.

4.4.2 Soulsby Bed Load Transport Method

Soulsby (1997) developed a formula to approximate bed load transport in a combined wave-current environment. This method was derived by integrating the Nielsen bed load formula over a single wave cycle. Note that if wave forcing is zero, the Soulsby formula reverts to the Nielsen equation. The Soulsby formula is given as:

$$q_{bx,y} = \Phi_{x,y}\left[g(s-1)d_{50}^3\right]^{1/2} \tag{26}$$

where,

$$\Phi_{x1} = 12\theta_m^{1/2}\left(\theta_m - \theta_{cr}\right) \tag{27}$$

$$\Phi_{x2} = 12\left(0.95 + 0.19\cos 2\phi\right)\theta_w^{1/2}\theta_m \tag{28}$$

Φ_x = maximum of Φ_{x1} and Φ_{x1}

$$\Phi_y = \frac{12\left(0.19\theta_m\theta_w^2 \sin 2\phi\right)}{\theta_w^{3/2} + 1.5\theta_m^{3/2}} \tag{29}$$

q_{bx} = component of q_b in the direction of the mean current [L^3/T-L];

q_{by} = component of q_b perpendicular to the mean current [L^3/T-L];

q_b = mean volumetric bed load transport rate per unit width [L^3/T-L];

θ_m = mean Shields parameter over a wave cycle [-];

θ_w = amplitude of oscillatory component of θ due to waves [-];

$\theta_{\max}$ = maximum Shields parameter from combined wave-current stresses [-];

θ_{cr} = critical Shields parameter for initiation of motion [-];

ϕ = angle between current direction and direction of wave travel [degrees].

An illustration of the current, wave, and bed load components of Soulsby's method is shown in Figure 25.

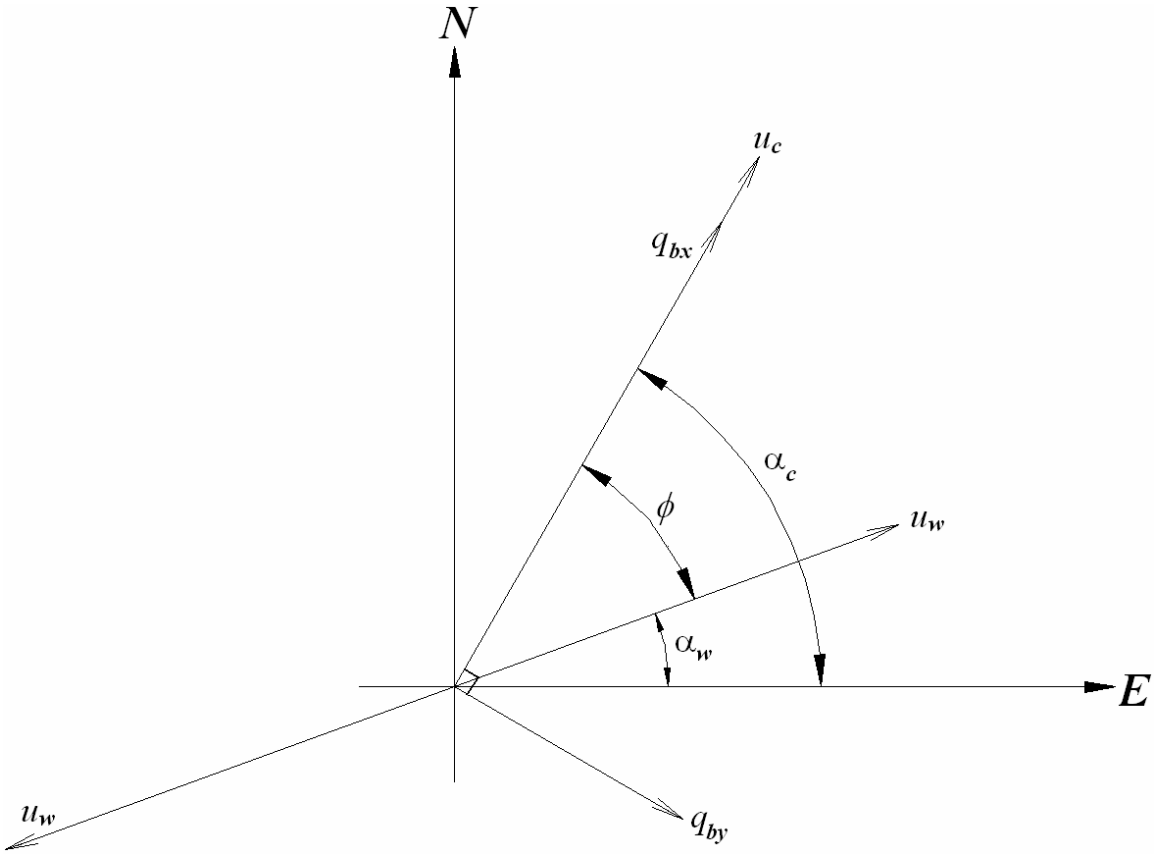

Figure 25. Illustration of the Soulsby methodology. Sediment transport component q_{bx} is in the same direction as the mean current, u_c, and the second component, q_{by}, is perpendicular to the mean current.

The Soulsby method was developed for use with near-bed velocities computed from known wave information. This was not needed for this study since the near bed velocities were measured directly by the ADV.

Data from the ADV and ADCP were used in the Soulsby formula. Recall that the ADV was deployed over the crest of the mound in 2.5 m of water. The ADCP was located approximately 500 m away from the ADV in 6 m of water. The following process was used for applying the Soulsby method:

1. Shields parameter calculated for every velocity record within burst;

2. Maximum Shields parameter within burst taken as θ_{max};
3. Critical Shields parameter, θ_{crit}, determined using Shields diagram. If $\theta_{max} > \theta_{crit}$ then sediment transport occurs;
4. Mean of all Shields parameter within burst taken as θ_m;
5. Oscillatory Shields parameter, θ_w, evaluated using the standard deviation of the velocity for the burst;
6. Direction of mean velocity vector, α_c, for the burst taken from ADV, where:

$$\alpha_c = \arctan\left(\frac{\overline{V_N}}{\overline{V_E}}\right) \tag{30}$$

$\overline{V_N}$ = burst averaged north component of velocity [L/T];

$\overline{V_E}$ = burst averaged east component of velocity [L/T];

7. Incident wave direction, α_w, taken from the ADCP. Wave direction is calculated from the peak of the energy spectrum. Angle between current and wave directions taken as ϕ;
8. All calculated parameters substituted into the Soulsby equations and a burst averaged sediment transport rate calculated;
9. Average transport rate for each size fraction over each deployment was calculated. The results are displayed in Table 9 below.

Table 9. Average bed load transport rate predicted using Soulsby's method. Transport rate is an average over a 3-mintue burst determined for several sediment sizes.

Sediment d_{50}	**Deployment 2 (April 2—June 4, 2003)**		
	Average q_{bx} (m^3/month-m)	**Average q_{by} (m^3/month-m)**	**Average q_b (m^3/month-m)**
100 μm	36.3	-0.23	36.3
350 μm	63.5	-0.39	63.5
500 μm	76.2	-0.47	76.3
	Deployment 3 (June 5—August 22, 2003)		
	Average q_{bx} (m^3/month-m)	**Average q_{by} (m^3/month-m)**	**Average q_b (m^3/month-m)**
100 μm	17.1	-0.20	17.1
350 μm	30.4	-0.35	30.5
500 μm	37.1	-0.43	37.1

Since the Soulsby formula was derived from the Nielsen formula, their transport trends are very similar. Like the results from Nielsen's equation, transport rates increase as sediment size increases due to an associated increase in friction factor. Larger transport rates are also predicted for the spring deployment over the summer. Recall, the Nielsen equation was applied using the burst averaged velocity, so it is a current-only bed load predictor. The Soulsby equation includes wave effects in the bed load calculations, so it should predict transport at higher rates when waves are present. By comparing the two methods, the relative importance of waves can be seen. When considering waves (i.e. the Soulsby method), the transport rate is on average 2-3 times larger than transport considering only currents. This underscores the importance of including waves in the transport calculations. Soulsby's method also includes wave forcing in the prediction of transport direction, but the component of transport perpendicular to the current, q_{by}, is very small compared to the component in the current direction, q_{bx}; therefore, net

predicted directions of transport are no different from the Nielsen current only method for this case.

4.5 Suspended Load Predictions

Suspended sediment transport is sediment movement within the water column, not in close proximity to the sea floor. The wash load is the portion of the suspended sediment that is not in equilibrium with the system and is usually introduced to a system by rivers (Nielsen 1992). Wash load stays in suspension and does not settle back to the seafloor; therefore, it will not be considered for this study. As waves pass over the mound, sediments can become entrained into the water column. Upon entrainment, the sediment can then be advected by wind- or tide-driven currents. Several methods were explored to determine the rate and direction of sediment transport in suspension for the site considered here.

4.5.1 Rouse Concentration Profile

Rouse (1937) developed a theoretical equation to describe the suspended sediment concentration vertical profile. While this method was not used to estimate suspended sediment transport rate, it was used as a comparison tool to evaluate the validity of the measurements reported by the OBS instruments. The Rouse suspended sediment profile equation is given as:

$$c = c_b \left(\frac{D - z}{z} \frac{b}{D - b} \right)^{z^*} \tag{31}$$

where,

c = suspended sediment concentration at a distance z above the bed [M/L^3];

c_b = reference concentration at a distance b above the bed [M/L^3];

z = distance above the bed [L];

D = water depth [L];

b = distance above the bed where the reference concentration is measured [L];

$$z^* = \text{Rouse Number} = \frac{w_s}{kU_f} \tag{32}$$

w_s = sediment fall speed [L/T];

k = von Karman Constant=0.4;

U_f = shear velocity [L/T];

The controlling parameter in this equation is the Rouse number, which is dependent on sediment fall speed and shear velocity. Figure 26 is a graph of the Rouse concentration equation for various values of z^*.

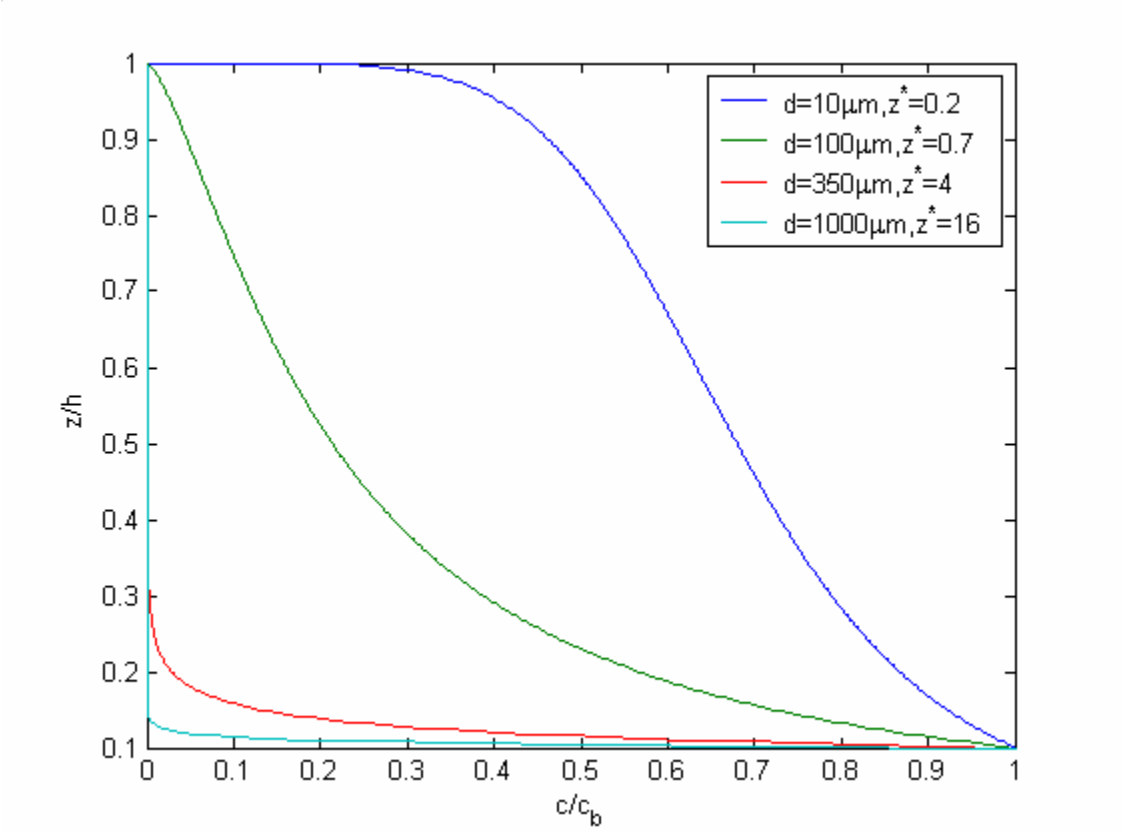

Figure 26. Rouse concentration distribution for a mean velocity of 30 cm/s.

The figure shows the dependency of concentration on the Rouse number. Larger values of z^* result in rapid decay of concentration with elevation in the water column, while smaller values of z^* result in slower decay over the vertical. This rapid decay occurs with coarse sand or flows with little to no turbulence, while a slower decay occurs in the presence of fine sand or a highly turbulent flow. Higher velocities, which lead to larger shear velocities, cause the Rouse number to decrease, which in turn causes slower decay of concentration over the vertical.

4.5.2 Optical Backscatter Method

Since the LISST provided little to no valid data useful for suspended sediment calculations, a volumetric suspended sediment size distribution could not be computed. The suspended sediment flux was computed using concentration data from the OBS and velocity measurements from the ADV. Using these two data sources, the suspended sediment transport could be described as:

$$q_{ss}(t) = \int_0^h c(z,t)u(z,t)dz \tag{33}$$

where,

$q_{ss}(t) =$ instantaneous suspended sediment transport rate [M/T-L];

$c(z,t) =$ time-dependent concentration profile [M/L^3];

$u(z,t) =$ time-dependent velocity profile [L/T];

$h =$ water depth [L].

The OBS instruments measured concentrations at three different points in the water column. The depths at which each OBS measured as well as the dynamic turbidity range of each instrument are shown in Figure 27.

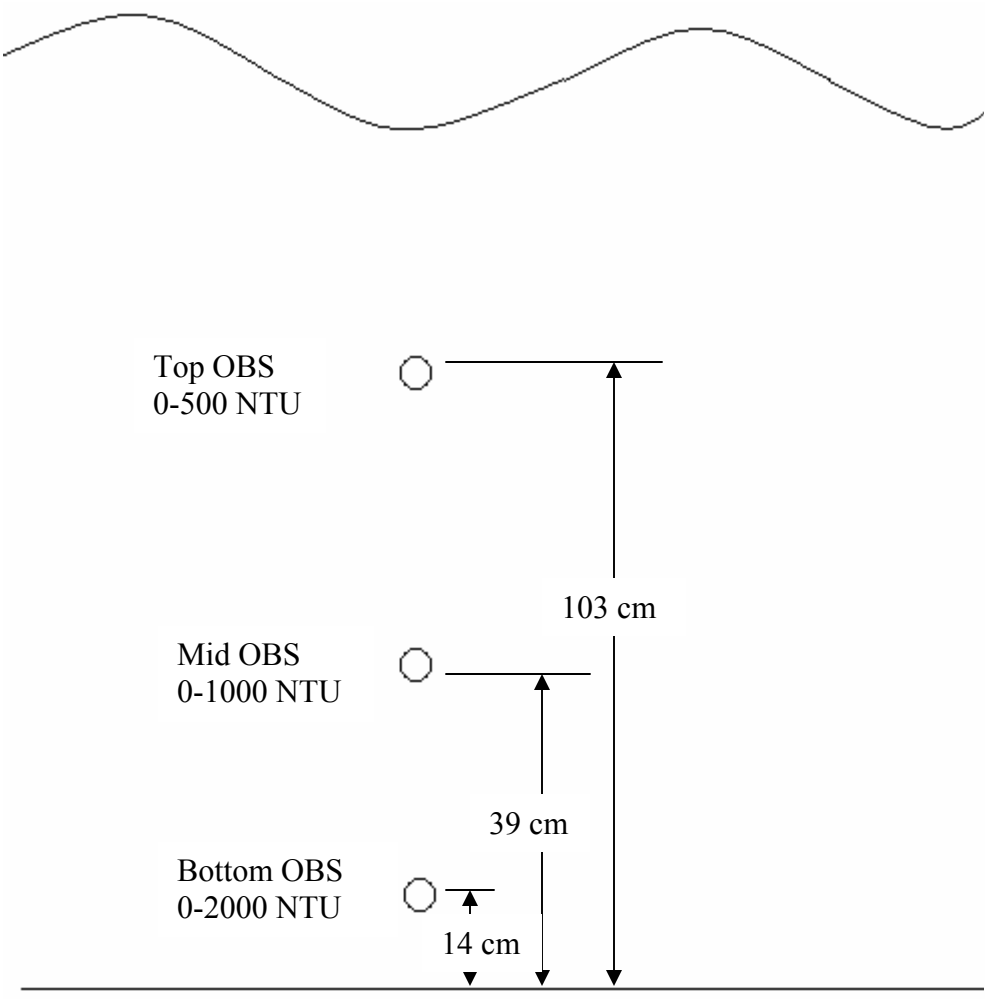

Figure 27. Elevation of OBS instruments above the seafloor with their corresponding dynamic turbidity range.

The water depth in which the OBS instruments were deployed was approximately 2.5 m on average, with a mean tidal fluctuation of ±1 m. The response of each instrument to changing concentration was recorded as a voltage. The average concentration over a three-minute burst was calculated by converting the output of each OBS (voltage) to concentration units by applying calibration curves (Cartwright and Friedrichs 2004).

The 3-minute averaged concentration profiles measured by the OBS were then inspected to insure that they were of good quality. According to the Rouse model and

intuition, one would expect concentration to either decrease or possibly remain constant with increasing elevation above the bed, but not increase. Figure 28 was constructed to view the type of profile that most often occurred according to measurements made by the OBS instruments. The concentration measured by each OBS was normalized by the average concentration measured by all OBS instruments. The mean of each of these normalized concentrations were then computed and a plot versus the elevation of each instrument was constructed.

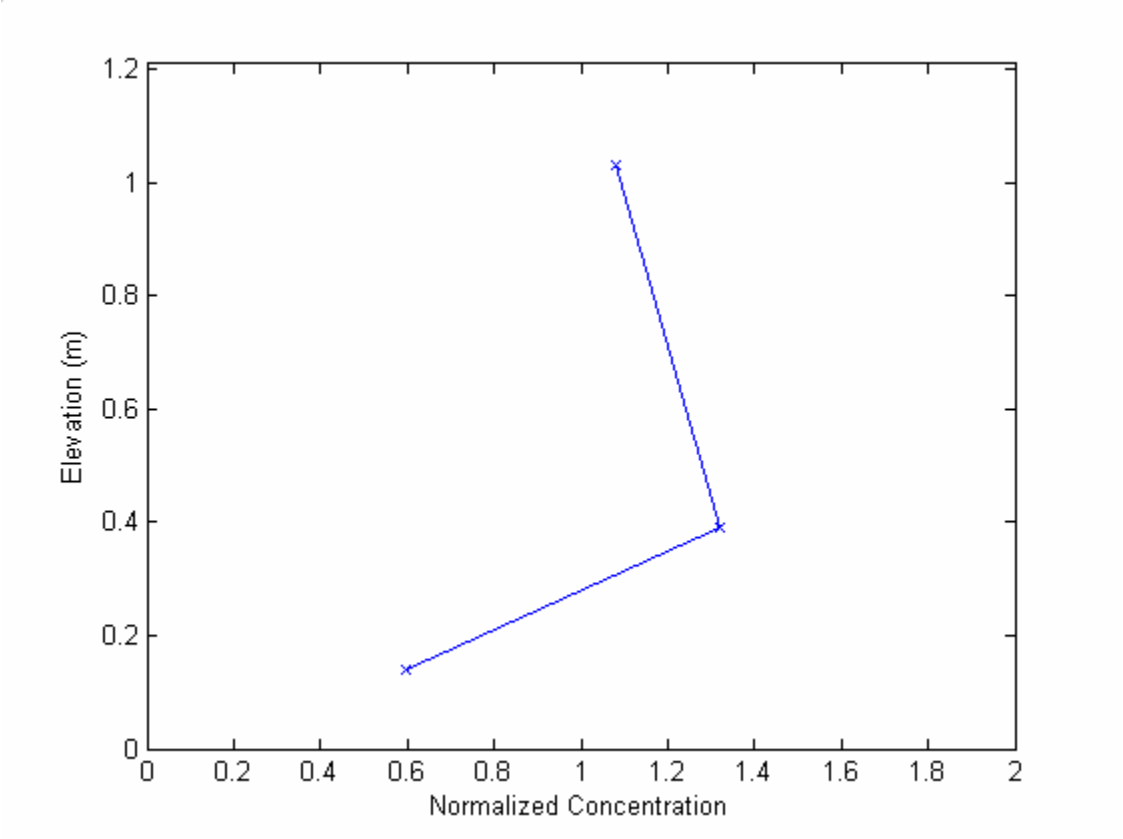

Figure 28. Concentration profile normalized by the average concentration measured by the three OBS instruments. OBS instrument elevations are denoted by 'x' on the graph.

The figure shows that concentration between the bottom and middle OBS instruments tends to increase with increasing height in the water column, which contradicts intuition and theoretical expectations. This trend was displayed for both deployments. The calibration and post processing were conducted by VIMS, and those procedures were not well documented. It is possible that some invalid data were not discarded during post processing; however, this is purely speculative. There were several instances noted, where the bottom OBS was damaged during the deployment and had to be repaired. It is possible that some data were collected during times when the OBS was damaged, but there is no certain way of knowing.

It is also possible that the instruments worked correctly and the profile looks incorrect simply due to a mix up in instrument location (i.e. maybe the middle instrument data is actually data for the near bottom concentration), but the fact remains that the concentration profiles are suspect; therefore, an alternative to the integral method as defined by Equation (34) was chosen. The alternative was to average the OBS measurements together and assume a uniform concentration profile over the vertical. If the instrument locations were wrong this would also give an accurate estimate of the average concentration over the vertical. This averaging would also remove some of the uncertainty in the measurements by eliminating random error. Since only a point measurement of velocity was available, an assumed depth-averaged current profile was also used to calculate suspended sediment transport rates. The assumption is that the ADV is measuring the free stream velocity (velocity outside the boundary layer), and that this mean velocity is approximately equal to the depth averaged current. The depth for a

given burst was calculated using the data from the pressure transducer on the ADV. With these assumptions, suspended sediment flux becomes:

$$q_{ss} = \int_0^h c(z,t)u(z,t)dz \approx \bar{c} * \bar{u} * h \tag{34}$$

This equation was applied to each burst of data to give a burst-averaged suspended sediment flux. The suspended sediment transport rate for each burst was calculated using the OBS data and converted from a mass to volume basis to facilitate comparisons. The results of those calculations are shown in Figure 29 and Figure 30.

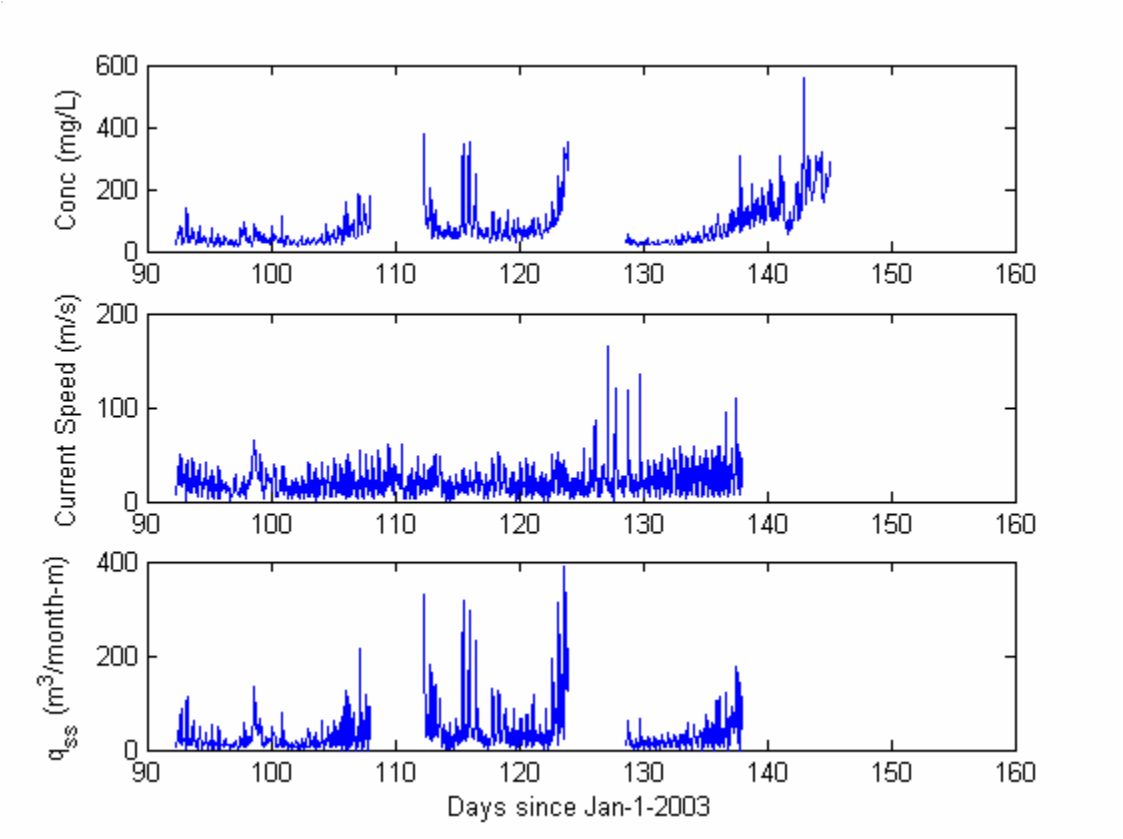

Figure 29. Suspended sediment transport rate (bottom) calculated using the average concentration derived from OBS measurements (top) and magnitude of the mean velocity from the ADV (middle) for Deployment 2.

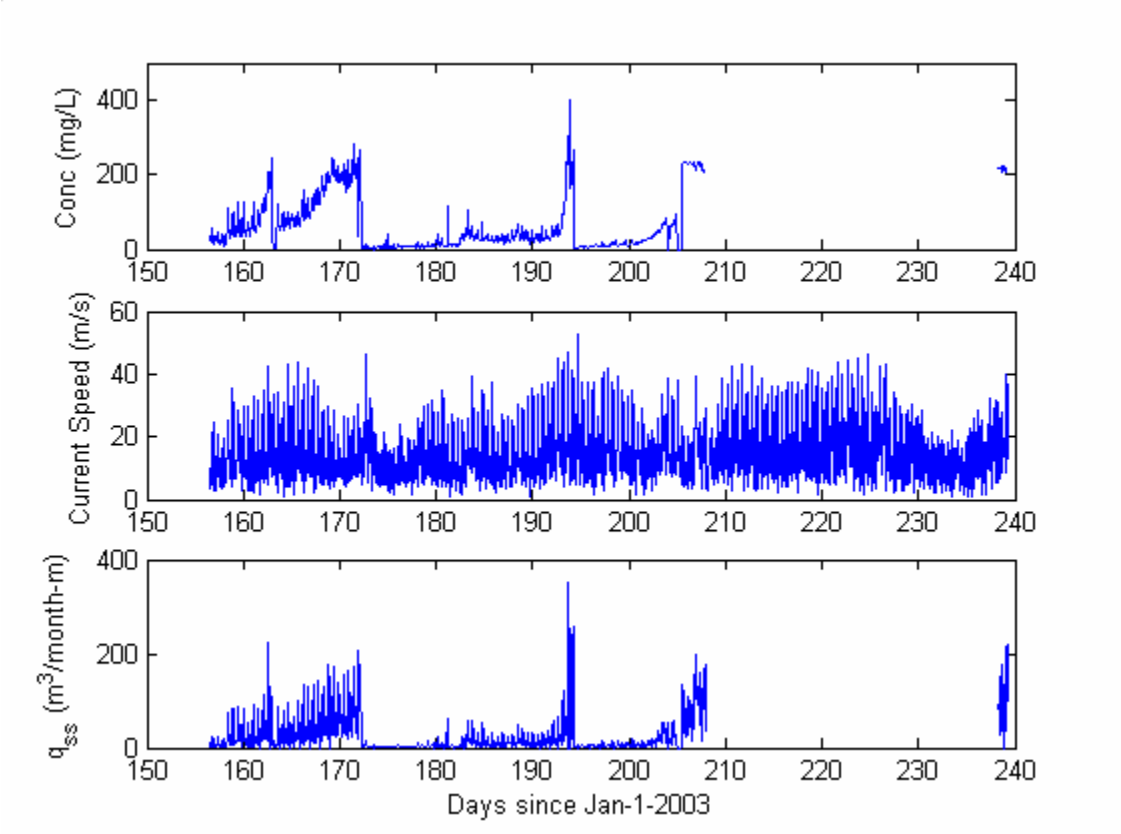

Figure 30. Suspended sediment transport rate (bottom) calculated using the average concentration derived from OBS measurements (top) and mean velocity from the ADV (middle) for Deployment 3.

Looking at the concentration plot in Figure 29 and Figure 30 there are several instances when concentration builds up over time then drops off. These instances correspond with fouling and subsequent cleaning of the transducer faces, and this building trend, due to fouling, causes the suspended sediment transport estimates to become inflated. After each instrument cleaning it takes several days before fouling begins to cause the measured concentrations to increase; therefore, to get a more reasonable measure of suspended sediment flux, only the first 5 days after instrument cleaning will be considered for the transport calculations. Looking only at the first 5 days

after each cleaning the average suspended sediment transport rate for Deployment 2 and 3 is 33.4 m^3/month-m and 13.7 m^3/month-m, respectively.

4.6 Total Load Transport Predictions

Total load is the sum of bed load and suspended load transport. Methods have been developed for estimating the bed and suspended load separately (e.g. Van Rijn 1984), while others simply estimate the total load directly based on flow characteristics (e.g. Ackers and White 1973). Here total load computed using Van Rijn's (1984) formula is discussed and results presented. The total load was also estimated using a combination of the Soulsby (1997) bed load formula and OBS suspended load measurements. The results of each method will then be compared.

4.4.1 Van Rijn Total Load

Van Rijn (1984) developed a total load sediment transport method for riverine environments. This method has since been used in current dominated oceanic environments (e.g. Smith 2003). The method can be applied for depths between 1-20 m, d_{50} between 100 and 2000 μm, and velocities between 0.5 and 5 m/s. Bed and suspended load are computed separately, but they can be summed to give total load transport rates:

$$q_b = 0.005\overline{U}h\left[\frac{\overline{U}-\overline{U}_{cr}}{[(s-1)gd_{50}]^{1/2}}\right]^{2.4}\left(\frac{d_{50}}{h}\right)^{1.2} \tag{35}$$

$$q_s = 0.012\overline{U}h\left[\frac{\overline{U}-\overline{U}_{cr}}{[(s-1)gd_{50}]^{1/2}}\right]^{2.4}\left(\frac{d_{50}}{h}\right)(D_*)^{-0.6} \tag{36}$$

$$q_t = q_b + q_s = \text{total load transport rate} \tag{37}$$

where,

$$\overline{U}_{cr} = 0.19(d_{50})^{0.1} \log_{10}\left(\frac{4h}{d_{90}}\right),\ 100 \le d_{50} \le 500\ \ \mu\text{m} \tag{38}$$

$$\overline{U}_{cr} = 8.50(d_{50})^{0.6} \log_{10}\left(\frac{4h}{d_{90}}\right),\ 500 \le d_{50} \le 2000\ \ \mu\text{m} \tag{39}$$

$$D_* = \left[\frac{g(s-1)}{\nu^2}\right]^{1/3} d_{50} \tag{40}$$

$\overline{U}$ = depth-averaged current [L/T];

$\overline{U}_{cr}$ = critical velocity required for sediment transport [L/T];

d_{90} = sediment diameter for which 90% is finer by weight [L];

h = water depth [L].

ν = kinematic viscosity [L^2/T];

The values for d_{50} and d_{90} on Mound C were, 350 μm and 1400 μm respectively (Cartwright and Friedrichs 2003). Figure 31 was developed to show how the Van Rijn bed load equation depends on various sediment sizes and depths.

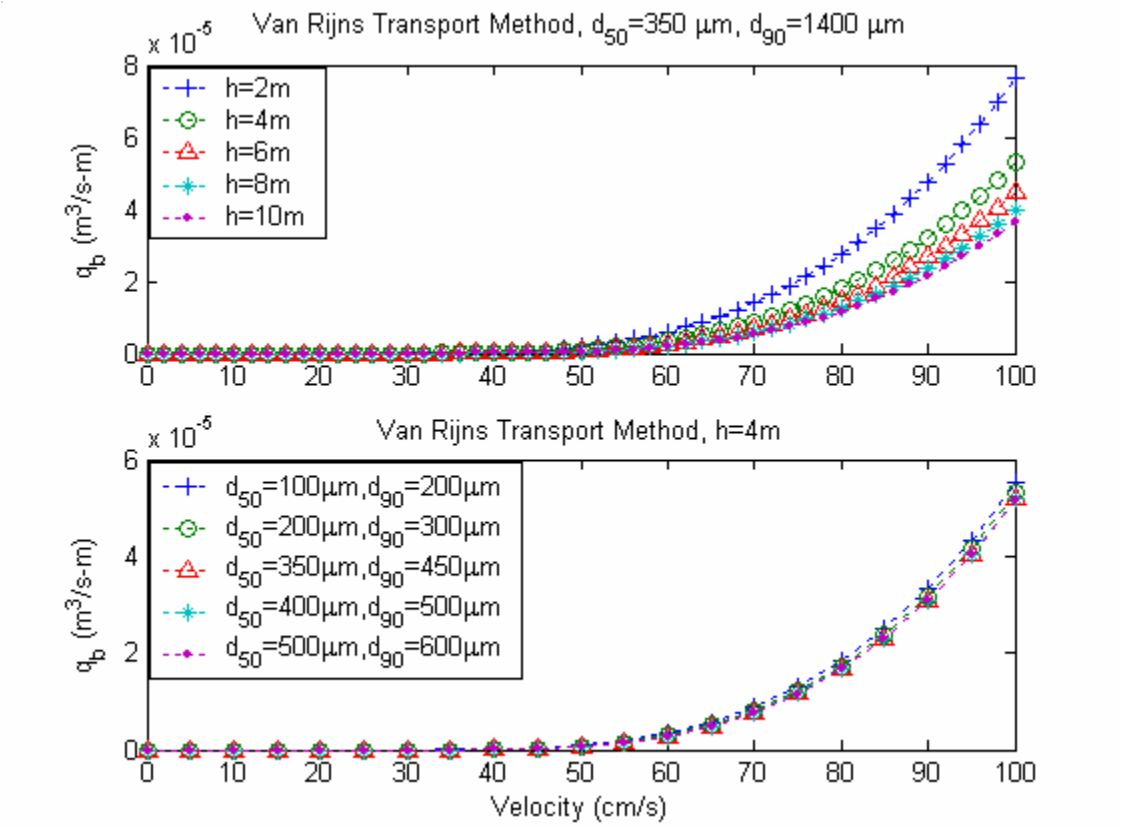

Figure 31. Bed load transport predictions according to the van Rijn method. Top graph is bed load transport rate as a function of water depth and magnitude of uniform velocity. Sediment d_{50}=350 µm, and d_{90}=1400 µm. Bottom graph is the volumetric sediment transport rate as a function of sediment size and depth uniform magnitude of velocity. Water depth is 4 m.

Water speed tends to decrease deeper in the water column due to the presence of a fixed boundary, the bottom, and viscosity; therefore, the velocity magnitude near the bottom is proportional to, but smaller than, the free stream velocity. Figure 31 shows that for increasing water depths the sediment transport rate decreases. This is expected since for a given depth-averaged current, increasing water depths translate to a decrease in the near-bottom velocity. This trend is illustrated by the following empirical formula (Soulsby 1990):

$$U(z) = \left(\frac{z}{0.32h}\right)^{1/7} \overline{U} \qquad \text{for } 0 < z < 0.5h \tag{41}$$

$$U(z) = 1.07\overline{U} \qquad \text{for } 0.5h < z < h \tag{42}$$

If depth increases or free stream velocity decreases then a decrease in the near bottom velocity results which in turn causes less sediment to become mobilized or entrained into the water column.

Figure 32 displays how the Van Rijn suspended load equations vary with sediment size and depth.

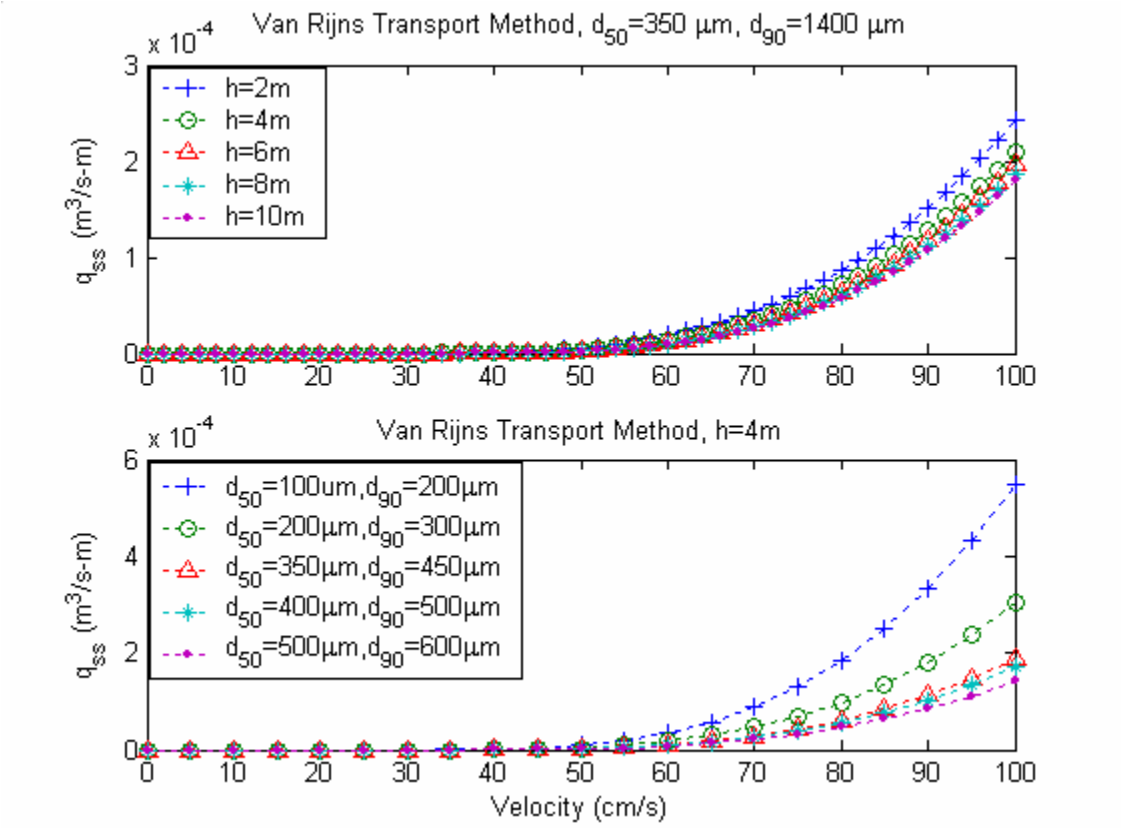

Figure 32. Suspended sediment transport predictions according to the Van Rijn method. Top graph is volumetric suspended sediment transport rate as a function of mean horizontal velocity and depth. Sediment d_{50}=350 µm, and d_{90}=1400 µm. Bottom graph is the volumetric suspended sediment transport as a function of magnitude of velocity and sediment size. Water depth is 4 m.

Van Rijn's suspended load equation includes a dependence on sediment diameter, unlike the bed load equation. In the suspended load regime, the larger particles tend to be transported at a smaller rate than the smaller particles. This is due to the greater settling velocity of larger diameter particles. Suspended sediment transport is a weak function of depth for this method, but does increase slightly as depth decreases.

The Van Rijn model was developed using a depth averaged current. This current could be derived by averaging the velocity profile as measured by an ADCP. Since there was no ADCP over the mound, no velocity profile is available; therefore, the mean velocity for each burst as recorded by the ADV was used as input to the Van Rijn model. The sediment transport rates were calculated for each 3-minute burst and averaged over the deployment. The results of those calculations are summarized in Table 10.

Table 10. Average bed load, suspended load, and total load transport rates predicted using the Van Rijn method. Sediment transport rates are for several sediment sizes average over each deployment.

		Deployment 2 (April 2—June 4, 2003)		
Sediment d_{50}	**Sediment d_{90}**	**Average q_b (m^3/month-m)**	**Average q_{ss} (m^3/month-m)**	**Average q_t (m^3/month-m)**
100 μm	**1000 μm**	0.432	4.443	4.875
350 μm	**1400 μm**	0.307	1.157	1.464
500 μm	**1800 μm**	0.298	0.844	1.142
		Deployment 3 (June 5—August 22, 2003)		
100 μm	**1000 μm**	0.038	0.397	0.436
350 μm	**1400μm**	0.019	0.074	0.093
500 μm	**1800 μm**	0.018	0.052	0.070

The results from the Van Rijn method show that there is dependence of sediment size on transport rates. This dependence is most apparent in the suspended load regime where

smaller sediments are transported with the highest rates. The size dependence is not as large for the bed load regime. In this regime, larger particles are transported at reduced rates due to larger required critical velocity to initiate sediment motion. This trend is the opposite of that exhibited by the Nielsen method. The bed load transport rates predicted using Van Rijn's method are, on average, two orders of magnitude less than that predicted by the Nielsen equation. Van Rijn's formula does not explicitly consider friction factor like Nielsen and has a stronger dependence of critical velocity on sediment diameter. The total load rate was determined by simply summing the bed load and suspended load transport rates. The Van Rijn method also predicts that the transport rates for the spring deployment are larger than that for the summer, which is due to larger velocities in the earlier deployment. The mound evolution predicted using each of these methods is presented in the next chapter.

4.4.2 Estimation of Total Load from Soulsby Bed Load and Suspended Load Predictions/Estimates

The last two estimates of total load were derived from a combination of Soulsby's Bed Load Method and suspended sediment measures from the OBS, and Soulsby plus Van Rijn's Suspended Load estimates. Combining these methods will in theory give us the best estimate of mound deflation since they incorporate wave- and current-induced bed load with suspended sediment load estimates. The results of the Soulsby-Van Rijn combination are given in Table 11.

Table 11. Total load estimation made by summing Soulsby bed load and Van Rijn suspended load predictions.

Sediment d_{50}	**Deployment 2 Average q_{total} (m^3/month-m)**	**Deployment 3 Average q_{total} (m^3/month-m)**
100 μm	40.7	17.5
350 μm	64.6	30.6
500 μm	77.1	37.0

Looking at the table, the influence of the friction factor on Soulsby's method dominates since transport rates are increasing with sediment size. The Soulsby-OBS combination results are displayed in Table 12. Since the OBS measurements were only for one size fraction, the estimated rates for the combination of that method with the Soulsby method are also for one size fraction.

Table 12. Total load estimation made by summing Soulsby bed load predictions and OBS suspended load measurements

Sediment d_{50}	**Deployment 2 Average q_b (m^3/month-m)**	**Deployment 3 Average q_b (m^3/month-m)**
350 μm	96.9	44.2

Now that transport rates for each method, deployment, and sediment size have been determined, using these results to predict the overall response of the dredged material mound will be undertaken. Predictions of the predominant sediment transport direction and the rate at which the mound deflates are made. These estimates are also compared to bathymetric survey data for comparison. These efforts are discussed in detail in Chapter 5.

CHAPTER 5

LONG-TERM MOUND MIGRATION TRENDS

Now that predictions of sediment transport based on field measurements have been made, the long-term evolution (i.e., on the order of months) of the mound is investigated. In Chapter 4 the rate of sediment transport was predicted using several methods. In this chapter, the predictions are applied to the mound to estimate the rate of deflation and the direction of mound migration. A continuity approach is employed to describe changes in mound height, and the results are compared to available survey data. The effect of velocity asymmetry on sediment transport is also discussed.

5.1 Direction of Mound Migration

In order to find the direction of mound migration, sediment transport roses were constructed using the predictions from each method. Each rose consists of three axes. The radial axis shows the magnitude of sediment transport. The θ axis shows the direction in which sediment is traveling. The contours (i.e., the vertical axis) show the percentage of the time a sediment fraction is mobile in a particular direction at a particular rate. The sediment transport rose is an excellent graph for displaying the predominant direction of transport and for estimating the percent mobility in a direction. The rose for the 350 μm sediment for the spring deployment (Deployment 2) using predictions from the Soulsby method is shown in Figure 33.

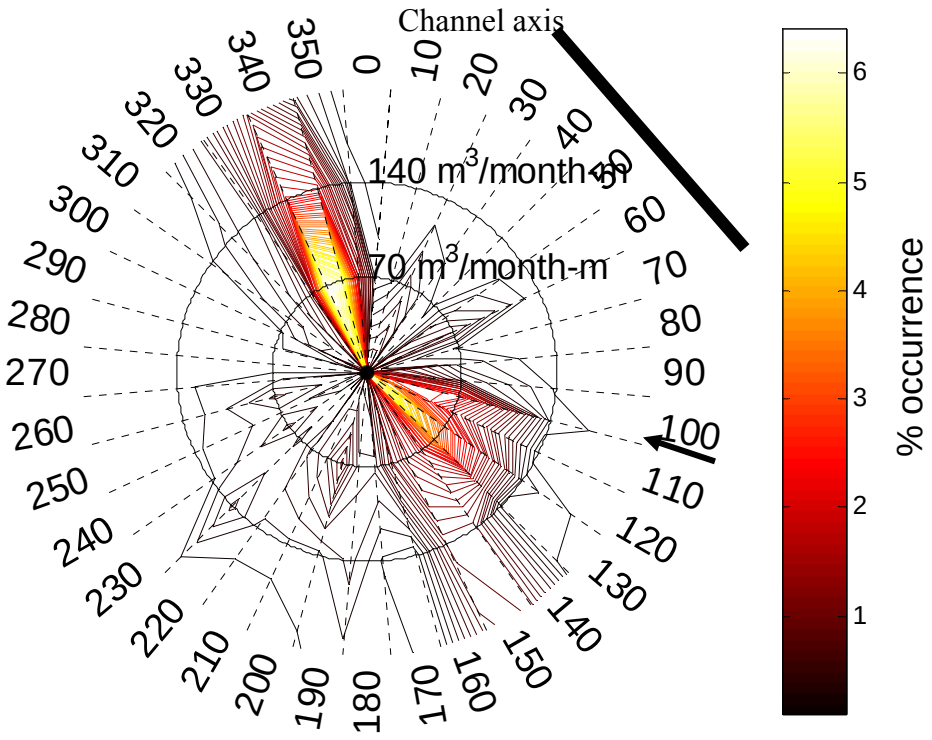

Figure 33. Sediment transport rose constructed using the Soulsby method for 350 μm sediment for the spring deployment (Deployment 2). The predominant transport direction for this rose is 335° clockwise from magnetic North. The rose indicates the direction toward which the sediment is traveling. The arrow is the average incident wave direction, which is 105°, taken from the ADCP. Channel axis is at an angle of 320° with respect to magnetic North.

The Soulsby method predicts sediment transport vectors from wave and current information, but the sediment transport mostly follows the mean flow at the Brunswick site. By plotting all of the vectors on the same rose, a predominant direction of sediment transport can be seen by noticing the direction in which the percent occurrence is the highest. In this case the predominant sediment transport direction was 335° measured clockwise from magnetic North, which is nearly parallel to the channel axis, and biased

toward the onshore direction. Roses were also constructed for 100 and 500 μm sediments and the results were qualitatively similar.

The northern edge of Jekyll Island lies just south of the entrance channel at a bearing of about 307^{o} from the mound with respect to magnetic North. Although sediments are not traveling directly toward Jekyll Island, it is encouraging that sediment predictions are biased toward the onshore direction, rather than offshore. It is possible that the direction in which the sediments are traveling could change once outside the area considered in this study. This cannot be determined without further study and hydrodynamic modeling which is beyond the scope of this project.

Placing the dredged material farther downdrift of the entrance channel *might* decrease the probability of sediments falling back into the entrance channel and increase the likelihood of indirect nourishment of Jekyll Island. The farther mounds are placed from the entrance channel the less likely sediments are to end up back in the channel which increases the chances of the sediments making their way onshore. Mounds placed farther from the channel could also be impacted less by the mean flows along the channel axis and could be influenced more by onshore wave action; however, this is speculative, and there is a trade off in that as dredging distances increase so do costs associated with placement.

Separate sediment transport roses were also constructed for the summer deployment (Deployment 3). The rose constructed from predictions from the Soulsby method and a 350 μm sediment is shown in Figure 34.

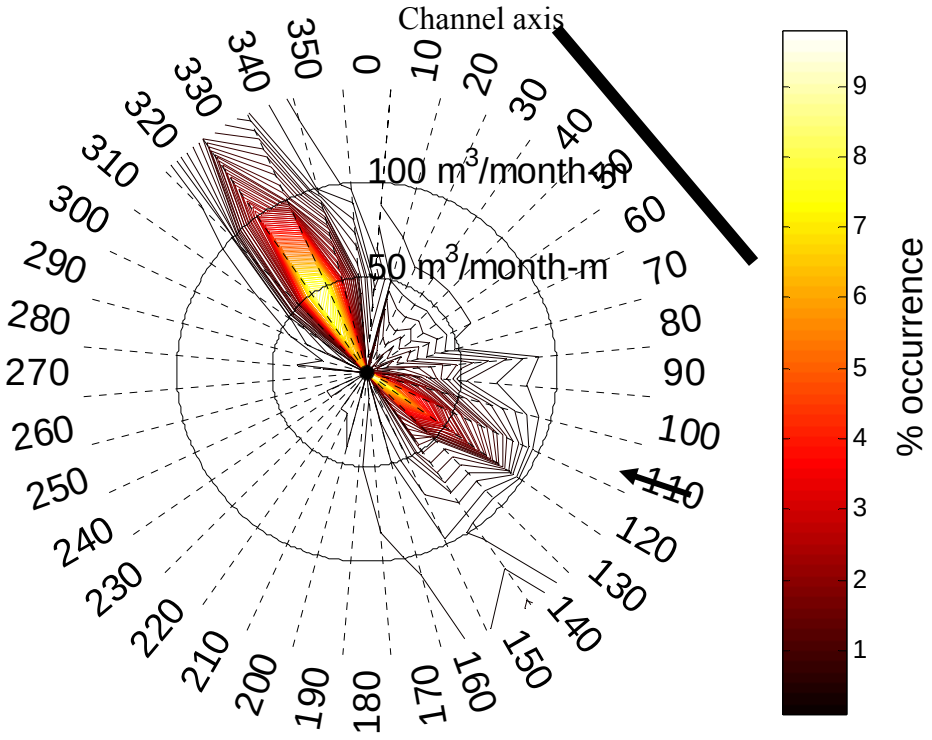

Figure 34. Sediment transport rose constructed using the Soulsby method for 350 μm sediment for the summer deployment (Deployment 3). The predominant transport direction for this rose is 325° clockwise from magnetic North. The rose indicates the direction in which the sediment is traveling toward. The arrow is the average incident wave direction, which is 112°, taken from the ADCP. Channel axis is at an angle of 320° with respect to magnetic North.

The direction of transport for summer is 325° measured clockwise from magnetic North, which is 10° west of the direction found for the spring. This slight difference may be due to seasonal changes in wave direction. The incident wave direction for the spring and summer deployments were 105° and 112° respectively. A weighted average wave direction (weighted by the energy flux) was also calculated and found to be 99 ° and 112 ° for the spring and summer deployments, respectively. Note for the later deployment the wave directions is more closely aligned with the entrance channel as is the sediment

transport direction. Again, the transport roses for all three sediment sizes displayed similar results for predominant transport direction.

The transport rose for summer has smaller values on the radial axis as compared to spring. This is due to the fact that for the later deployment, sediments are mobile a smaller percentage of the time due to an associated decrease in velocities over the crest of the mound. This decrease in velocity is expected as deflation of the mound occurs and may also be due to some seasonal effects since summer wave heights were less than those in the spring. It is worth noting, however, that for the later deployment there is a stronger bias toward onshore transport. For each of the transport formulae considered, mean flows dominated sediment transport; therefore, the transport roses for each of the other methods were qualitatively similar to those constructed for the Soulsby method.

5.2 Rate of Evolution of Mound

The sediment transport methods described in the previous chapter were applied to each valid burst of data and the results averaged over each deployment period to yield time-averaged, gross sediment transport rates. The evolution of the mound was then determined assuming the crest could be represented by a 600 m X 600 m box as shown in Figure 35.

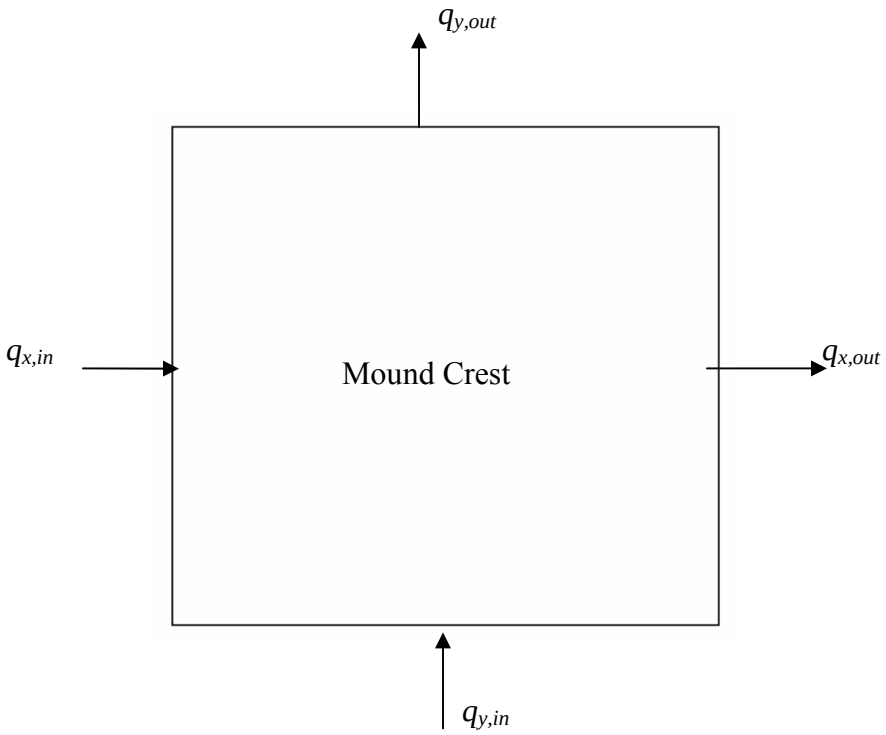

Figure 35. Crest of the mound was represented as a 600 m X 600 m box for the sediment balance as shown. Sediment input is assumed zero and all mobilized sediments are lost.

The change of mound height over time was determined using the time-averaged gross sediment transport rates and the following equations:

$$\frac{dh}{dt} = \left(\frac{dq_x}{dx} + \frac{dq_y}{dy} \right) \frac{1}{1-\varepsilon} \tag{43}$$

where,

$h =$ mound height [L];

$q_x =$ sediment transport in the x direction [L^3/T-L];

$q_y =$ sediment transport in the y direction [L^3/T-L];

ε = porosity [-].

The high relief of the mound over the seafloor hinders sediments, especially those in the bed load regime, from being deposited on the crest of the mound; therefore, $q_{x,in}$ and $q_{y,in}$ are assumed to be zero. With this assumption, in finite difference form, Equation (43) becomes:

$$\frac{\Delta h}{\Delta t} = \left(\frac{q_{x,out}}{\Delta x} + \frac{q_{y,out}}{\Delta y} \right) \frac{1}{1-\varepsilon} \tag{44}$$

where,

Δh = mound deflation rate [L];

Δt = time elapse for the deployment [T];

$q_{x,out}$ = sediment transport rate away from the mound in the x direction [L^3/T-L];

$q_{y,out}$ = sediment transport rate away from the mound in the y direction [L^3/T-L].

If the x and y dimensions of the box are assumed equal and the porosity of the mound is assumed to be 0.3, then the change in mound height and mound volume can be written as:

$$\Delta h = \frac{\Delta t}{0.7w} \left[q_{x,out} + q_{y,out} \right] \tag{45}$$

$$\Delta V = \Delta h * w^2 \tag{46}$$

where,

ΔV = volume of sediment leaving the mound [L^3];

w = width of the mound [L].

Using the rates derived from each method, the assumption that all mobilized sediments leave the mound, and Equations (45) and (46), the volumetric rate of deflation and the associated change in height were calculated and are given in Table 13 below. For

bed load predictions, Soulsby's method is most appropriate since it accounts for both waves and currents. Van Rijn's formula is a total load method, yet it displays the lowest associated transport, which is likely due to the fact that it does not account for wave action. Other total load estimations were made by combining the Soulsby bed load prediction with measurements from the OBS and with the portion of the Van Rijn method which predicts suspended load. The results of each of these combinations are also given in Table 13.

Table 13. Volume of sediment leaving the mound, and mean rate of deflation assuming the crest of the mound lies within a 600 m X 600 m box.

Method	**Deployment 2 (April 2—June 4, 2003)**		**Deployment 3 (June 5—August 22, 2003)**	
	ΔV **(m^3/month)**	**Deflation Rate (m/month)**	ΔV **(m^3/month)**	**Deflation Rate (m/month)**
OBS Measurements	$3.6*10^4$	0.10	$1.5*10^4$	0.042
Nielsen	$3.4*10^4$	0.094	$1.3*10^4$	0.036
Van Rijn	$1.7*10^3$	0.0048	$1.1*10^2$	0.00031
Soulsby	$7.2*10^4$	0.20	$3.5*10^4$	0.098
Soulsby + OBS	$10.8*10^4$	0.30	$5.0*10^4$	0.14
Soulsby + Van Rijn Suspended Load	$7.3*10^4$	0.20	$3.5*10^4$	0.098

Each method employed for this study indicates that the average volume of sediment leaving the mound is on the order of 10^4 m^3/month, not considering the Van Rijn total load method. The associated depth change ranged from 4-30 cm/month. It is expected that as the mound deflates, the associated velocity over the mound would decrease, causing less transport. The summer months of the year also tend to have smaller wind speed and wave heights when compared to the spring months, so this would also cause sediment transport rates to decrease. This trend is displayed by looking at Deployment 3

compared to Deployment 2, where the mean deflation rate is reduced by at least 50% for each method.

Bathymetric survey data of the mound were studied for comparison to predictions. Three surveys were conducted after placement of the dredged material in winter 2002. These surveys were conducted in February, April, and July of 2003. Data were collected from a boat using a 234 kHz interferometric swath sonar system integrated with GPS and a sensor for removing vessel motion. Water level fluctuations due to astronomical and wind-driven tides were also removed. Survey track lines were spaced 20 m apart with approximately 50 soundings taken per square meter. After collection of the data it was processed using several survey software packages and fit to a 4 m uniform grid. For more details about the collection of the survey data see the report by McNinch (2003). The survey data from February are shown in Figure 36 below.

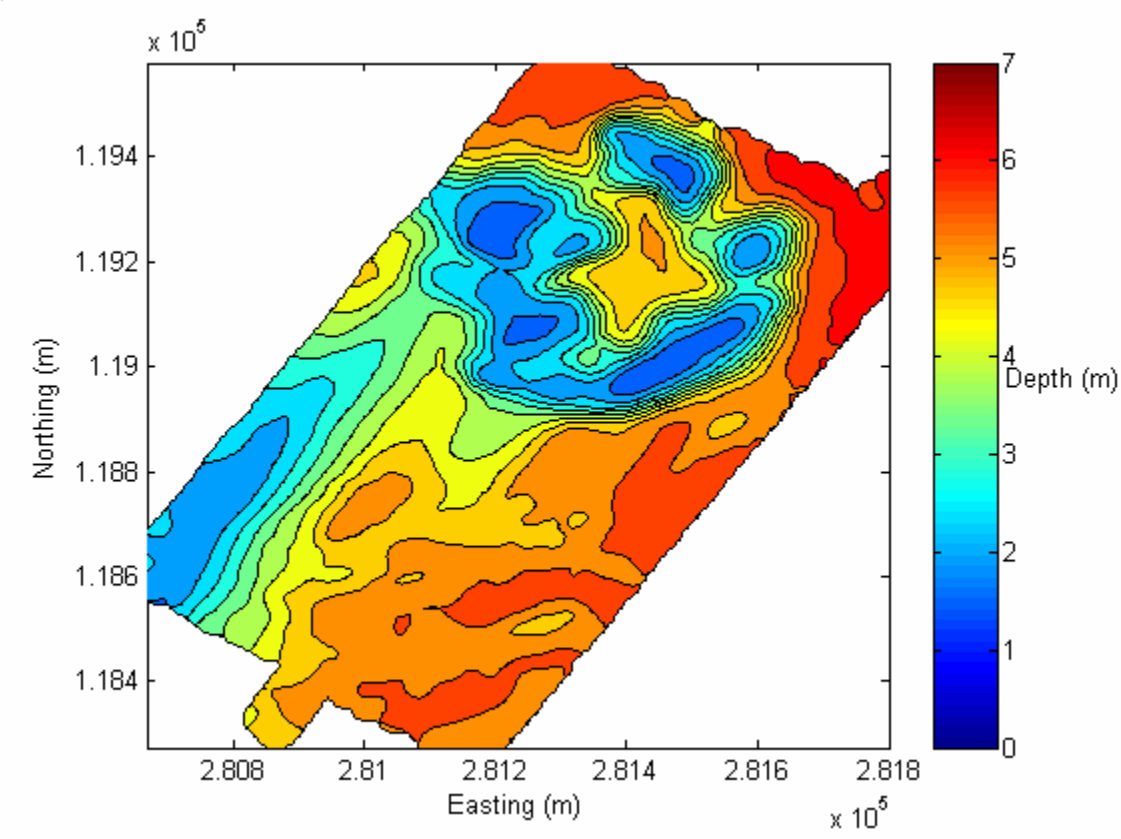

Figure 36. Survey results for Mound C on February 3-8, 2003 survey. Depth is approximately 1.5 m over the crest of the mound and 6 m (MLLW) offshore of the mound.

The change in depth between surveys was calculated in order to give a rate which could be compared to the predictions; however, these plots displayed uniform accretion rates of 10-21 cm away from the mound in 6+ m of water and little to no erosion over the crest of the mound. The erosion and accretion volumes being mismatched along with the unlikelihood of uniform accretion over such a large area suggests that there was a datum problem; therefore, an adjustment was made. A constant, equal to the amount of accretion, was added to the entire domain such that no accretion/erosion was observed off of the mound in the deeper water. This adjustment gave the expected trend of erosion over the crest of the mound, accretion in the low areas around the mound, and no change

in the deeper water off of the mound. The resulting contour plots after the datum corrections are displayed below: February to April change is given in Figure 37, April to July change in Figure 38, and overall change in Figure 39.

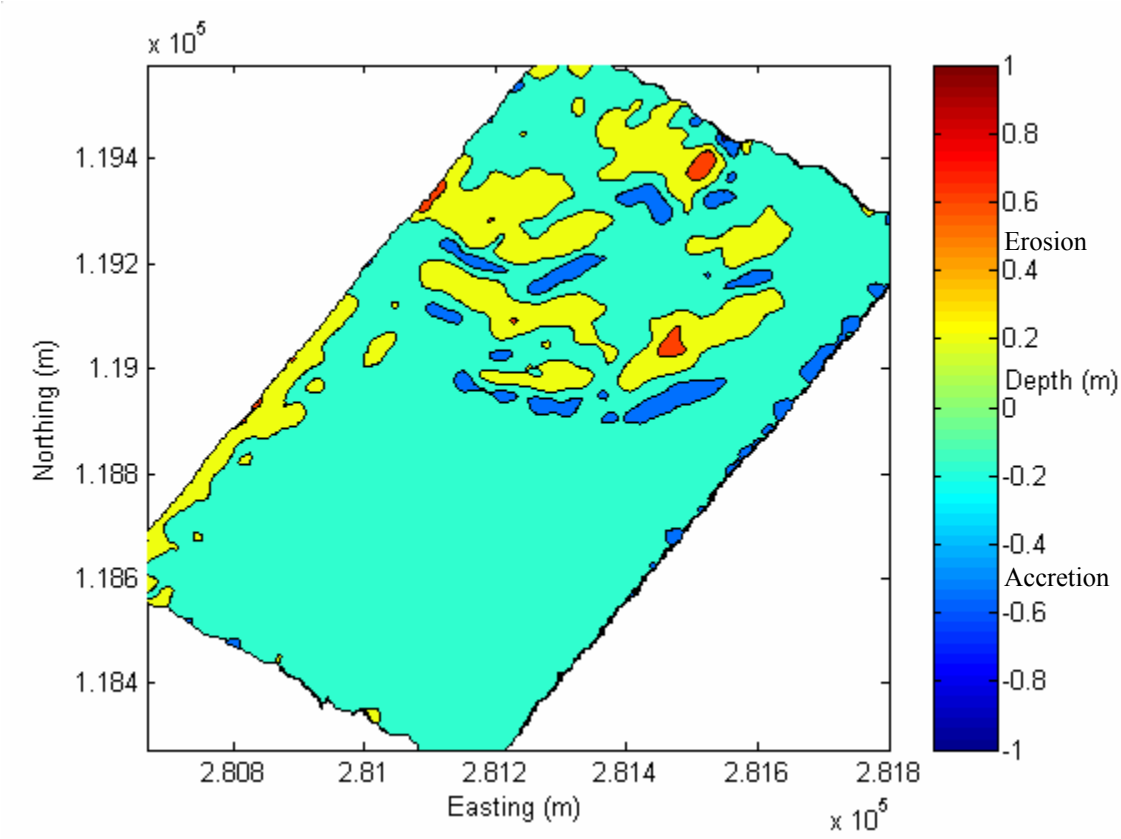

Figure 37. Change experienced within the dredged material placement site between the February and April 2003 survey. Ten centimeters were added to the entire domain to force the change in depth away from the mound to zero.

In the period between February and April, the erosion over the crest areas of the mound is between 20 cm (yellow) and 60 cm (red). Accretion tends to occur between the high relief areas of the mound with a magnitude of approximately 50 cm (blue). Similar trends were also observed for the April to July 2003 survey but at reduced rates as shown in Figure 38.

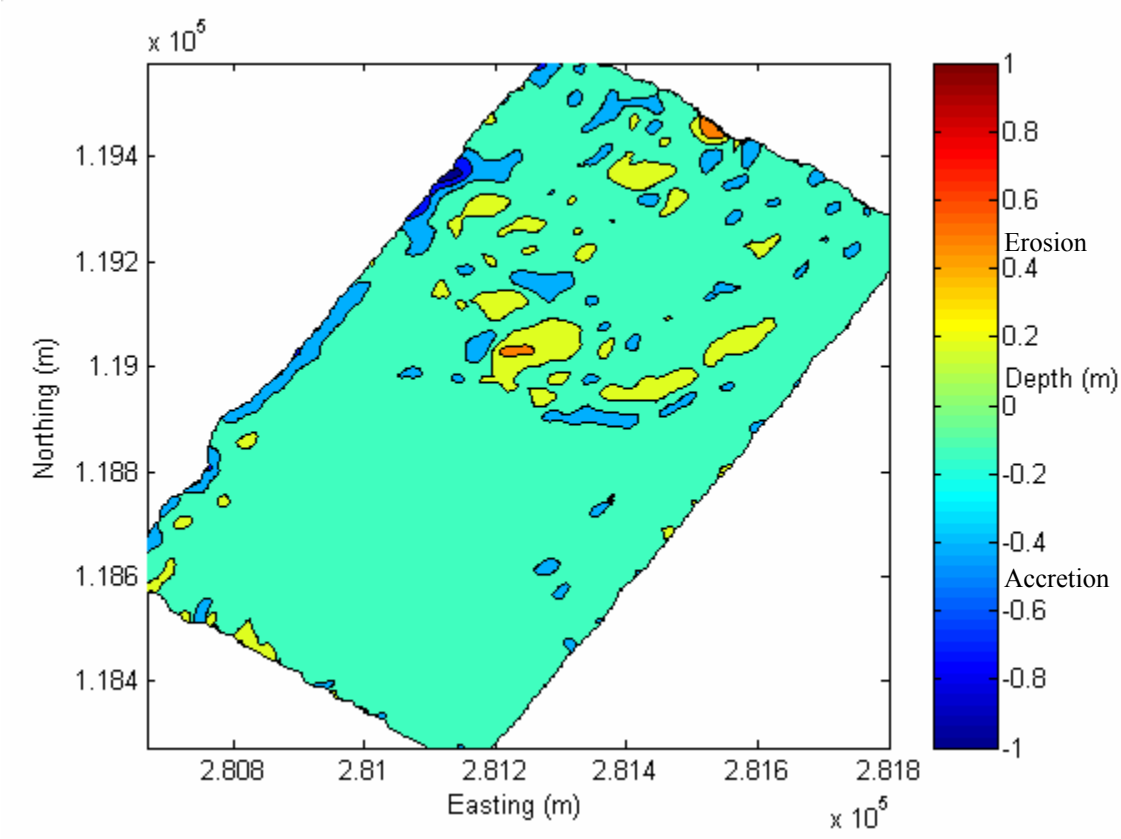

Figure 38. Change experienced within the dredged material placement site between the April and July 2003 survey. Fourteen centimeters were added to the entire domain to force the change in depth away from the mound to zero.

The average erosion rate experienced between each survey within the 600 m X 600 m box located around the crest was calculated and found to be 4 cm/month between the February and April survey and 1 cm/month for the April to July survey. According to the survey results, the rate of mound deflation decreases as time passes which is similar to the trend displayed by the predictions. A plot of the overall change in depth from February to July is displayed in Figure 39.

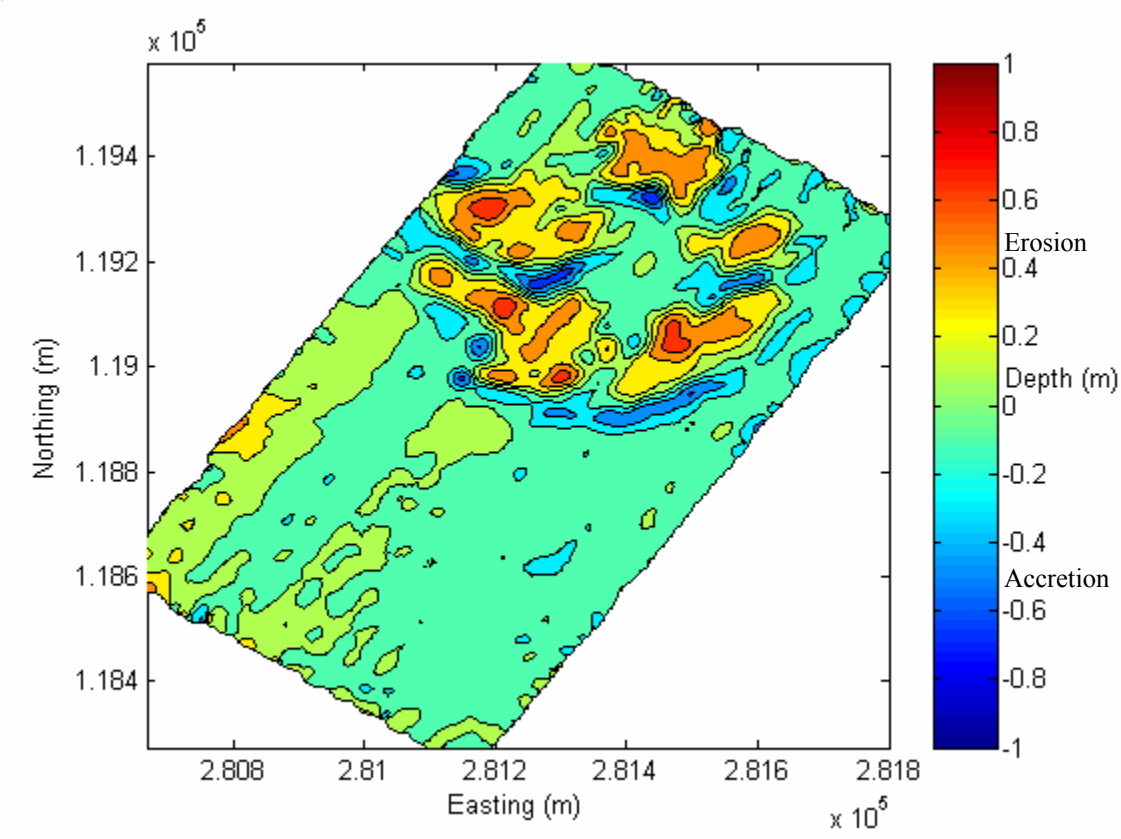

Figure 39. Change experienced within the dredged material placement site between the February and July 2003 surveys. Twenty-one centimeters were added to the entire domain to force the change in depth away from of the mound to zero.

The maximum erosion occurred over crest areas of the mound while accretion trends dominated in the areas of deeper water just around the mound crest. Overall, the average rate of sediment loss in the crest area from February to July was calculated as 2 cm/month. The results of the survey are lower than the predictions based on the sediment transport formulae. This is due to the fact that the sediment transport predictions were taken at the location on the mound where the most transport occurs, and averaged over the entire crest. Looking at the survey and focusing only on the area of the crest where

the instruments were located, an erosion rate of approximately 20-45 cm/month is observed, which matches more closely with the sediment transport predictions.

5.3 Effect of Velocity Asymmetry

As waves approach shallow water and begin to shoal and break, asymmetry of the free surface about the mean water level occurs. This asymmetry of the water surface, often termed skewness, is also reflected in the velocity underneath a wave train. Velocity skewness is defined by Doering et al. (2000) as the horizontal asymmetry of a wave in the cross-shore direction, which is a direct reflection of the shape of a wave. Mathematically it is defined as:

where,

$$S = \frac{\overline{u^3}}{\left(u_{rms}\right)^3} = \frac{\overline{u^3}}{\left(\sigma^2\right)^{3/2}} \tag{47}$$

S = skewness of time series [-];

$\overline{u^3}$ = velocity records within a time series cubed and time averaged [L^3/T^3];

u_{rms}^3 = cube of the root-mean-square velocity of a time series [L^3/T^3];

σ^2 = variance of velocity time series [L^2/T^2].

For a linear wave, skewness is zero, while for a non-linear wave skewness is a non-zero value. The shapes of the free surface for linear and non-linear waves are shown in Figure 40.

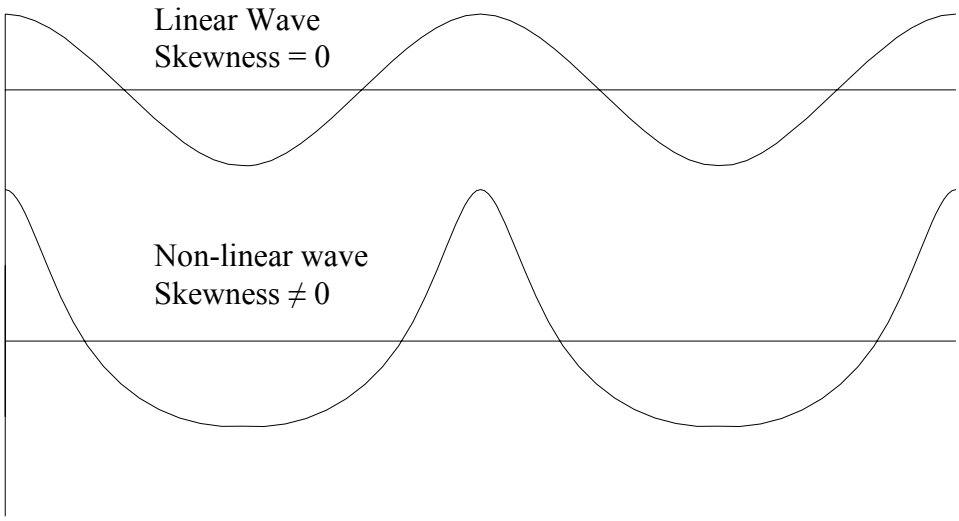

Figure 40. Sketch of the free surface of a linear, non-skewed wave (top), and a non-linear, skewed wave (bottom).

Notice that for the skewed wave the crest is larger or more "peaky." This asymmetry tends to cause a net transport in the wave direction due to larger associated forward velocities under the crest when compared to backward velocities under the trough. As waves shoal and begin to break, the crests also begin to pitch forward which introduces additional asymmetry.

Since waves shoal as they approach and travel over the mound, it is possible that velocity skewness has an added effect on sediment transport trends. Several graphs were constructed to see if a relationship between skewness and relative depth or skewness and wave steepness existed at this site. Figure 41 was constructed using data from both the ADV and ADCP. Skewness of each velocity component for each burst was calculated. The north component of skewness was not considered because it was zero for most of the deployment. The west component was used, as opposed to the east component, because

waves travel in a westerly direction toward the shoreline. The wave height and depth over the mound were calculated from ADV data while wave length over the mound was found using wave period information from the ADCP and Equations (48) and (49) shown below.

$$L_{mound} = \frac{2\pi}{k} = \text{wavelength over the mound [L];} \tag{48}$$

$k = \text{wave number [1/L];}$

$$\omega^2 = gk \tanh(kh) = \text{dispersion relationship from linear wave theory [1/T}^2\text{];} \tag{49}$$

$\omega = \text{wave frequency given by ADCP [1/T];}$

$g = \text{acceleration due to gravity [L/T}^2\text{];}$

$h = \text{depth over the mound given by ADV pressure sensor [L].}$

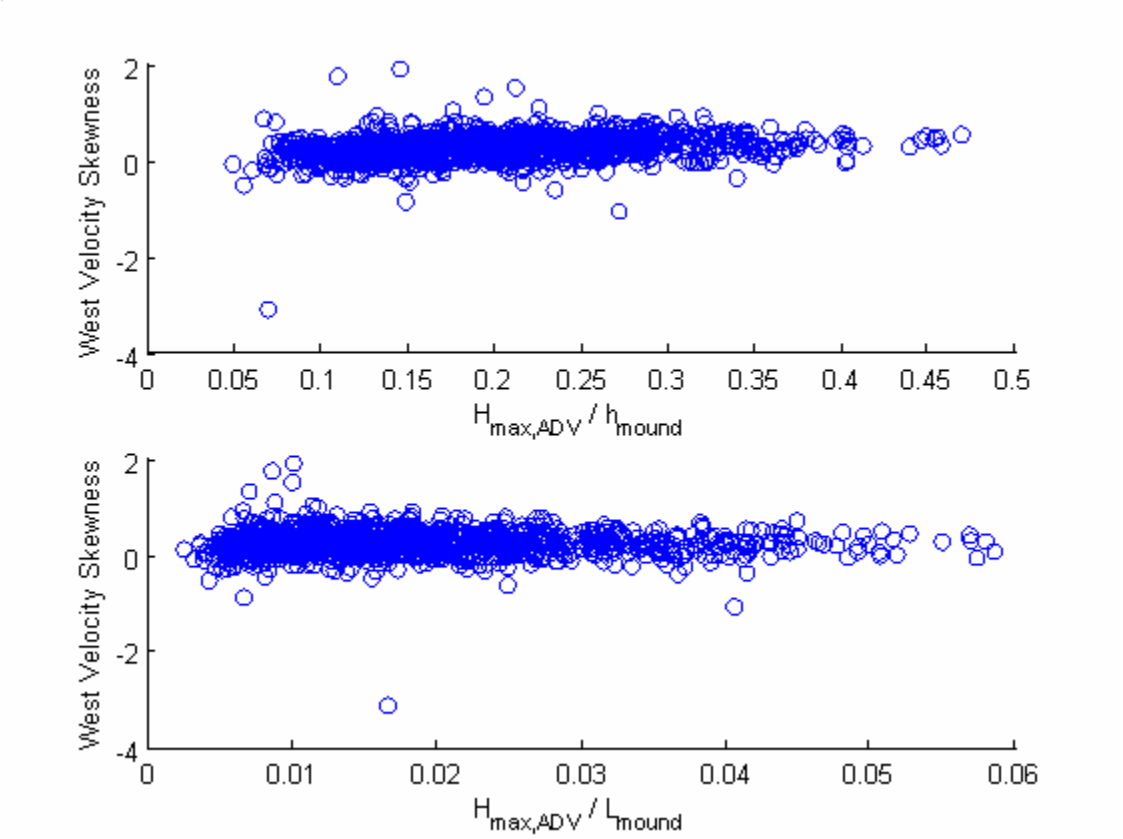

Figure 41. Skewness of west component of velocity as a function of relative depth (top) and wave steepness over the mound (bottom). Only west skewness is graphed because that is the direction in which waves travel to reach shore. Graphs suggest that there is no relationship between the variables for the range experience at the Brunswick site.

There is no apparent relationship between velocity skewness and relative depth or wave steepness displayed in Figure 41. In general, it is accepted that as waves approach a relative depth of 0.78 they are said to be breaking. It is likely that no relationship between velocity skewness and relative depth is displayed here because when the majority of waves pass over the instrument location, they are not close to the H/h ratio of 0.78. The accepted breaking value for wave steepness, H/L, is 1/7 and this value is not approached at this location either.

The Soulsby equation, which is the most suited for this site, does not take skewness into account for the sediment transport predictions. Recall that the major parameters driving the Soulsby equation are the mean Shields parameter, θ_m and, the oscillatory Shields parameter, θ_w (see Section 4.4.2). Inspecting these parameters reveals that it is possible to have a non-skewed wave train with the same oscillatory and mean Shields parameters as a skewed wave train. If this situation exists, the Soulsby equation would give the same sediment transport rate for each. Theory dictates that the skewed wave train would have larger sediment transport, so if it had been incorporated into the method, the sediment transport predictions may have been different. Skewness is typically thought to be a function of relative depth and wave steepness, but looking at Figure 41 suggests that skewness is not dependent on either parameter for the range of values experienced at this site.

CHAPTER 6

CONCLUSIONS

The United States Army Corps of Engineers (USACE) is responsible for maintaining navigability of entrance channels serving 400 ports on the U.S. coast (USACE 1999). One of these ports is located at Brunswick, GA, where periodic dredging is necessary to maintain adequate depth for safe passage of ships into and out of the port regardless of tidal stage. Dredged material removed the Brunswick Entrance Channel has traditionally been placed far from shore, removing it from the littoral cycle, until recently, when some material was placed in nearshore mounds. This study focused on five months of field data collected during 2003 describing sediments and hydrodynamics at one of these nearshore dredged material mounds near Brunswick, Georgia.

The project was motivated by several facts:

- Sediment must be removed from the Brunswick Entrance Channel in order to maintain its navigability;
- Disposing of sediments from the entrance channel in the offshore is expected to cause erosion on the downdrift side of the channel, specifically along Jekyll Island, as is observed;
- Placing sediment directly on the beach is impractical due to the presence of fines in the material and an increase in associated project costs.

For these reasons nearshore placement is a potentially viable alternative. Nearshore placement is desired so that the resulting mounds might make available sediments to the littoral cycle, providing nourishment to the beaches on the downdrift side on the channel.

The objective of the study was to use the measurements along with appropriate predictive methodologies to describe the sediment transport trends at a placed mound. Results of the study are then available for use in calibration and verification of numerical models developed and applied by the USACE. The ultimate goal is to use the results of this study in conjunction with the USACE model to assess the feasibility of nearshore placement of dredged material offshore of Brunswick, Georgia. If successful this method might then be used to plan nearshore placement at other locations.

Data describing waves, currents, and suspended sediment concentrations were collected over the mound at Brunswick using a variety of acoustic and optical instruments. Sediment size data were also available from sediment cores taken from several locations on the mound. Several quality control procedures were undertaken to ensure that only valid data points were considered. Four predictive techniques were used to describe sediment transport trends, including one based solely on measurements. One method described bed load and suspended load separately, while the remaining two methods predicted only bed load. One of these bed load only methods considered only mean currents. The other bed load method incorporated not only waves and currents, but also instances in which they were non-collinear. Fluorescent tracer material was also placed on the crest of the mound to give an additional method for estimating sediment transport trends.

All results assume that no sediment is deposited on the mound after dredging (i.e. the mound serves as a sediment source only). If this assumption is incorrect then the mound evolution rates calculated here are overestimations. With this assumption, sediment transport direction does not affect the rate of evolution; however, the direction of transport was studied by creating sediment transport roses. Bathymetric survey data from the mound were also compared to the predictions for comparison and validation.

A summary of the results are:

1. Sediment transport is nearly parallel to the channel and biased toward the onshore direction;
2. As sediments leave the mound they are not headed directly toward Jekyll Island, but transport is biased toward the shore. The ultimate fate of sediments eroded from the mound cannot be determined using only the measurements described here. More complex large-scale modeling is needed to make this determination;
3. Placing the mound further downdrift of the channel may decrease the likelihood of dredged material returning to the entrance channel and could increase the chance of sediments making their way to Jekyll Island;
4. An optimal time of placement is not evident since the predominant transport direction is independent of time for the period considered. Placement of dredged material in autumn or winter would take advantage of larger wave climate when compared to the spring and summer. This pattern could increase the rate and likelihood of sediments re-entering the littoral cycle.

5. Transport direction is independent of sediment size. Three sand size fractions were considered and all were predicted to move in the same onshore direction. Transport rate predictions are dependent on sediment size;
6. Tracer results suggest that the fine fraction is winnowed rather quickly (days to weeks) while the sand-sized fraction appears to be moved over a longer term period (on the order of months to years);
7. Transport rates are time-dependent with more significant movement occurring in the spring compared to the summer months. The reduction in sediment transport rates over time are due to reduced velocities over the mound. This decrease in velocity is likely due to mound deflation and seasonal reductions in velocity;
8. The mound was predicted to deflate between 4-30 cm/month depending on the predictive methodology used while bathymetric survey data suggests that the average rate of erosion is 20-45 cm/month at the instrument location;

Improvements can be made to the predictions in several ways. First, a year-round deployment would be helpful to better describe the seasonal dependence of currents, waves, and transport. Future sampling of the fluorescent sediment tracer would also be helpful to give an additional source of validation as well as a picture of true transport trends for the site. Improvements to the OBS measurements should be explored so that accurate suspended sediment profiles can be used for suspended sediment estimations. Data from the LISST would have also been helpful to describe the size distribution of suspended sediments; however, at present it is very difficult to obtain data from the optical instruments due to the large fouling potential of these waters. Finally, some

improvements in predictive equations and methodologies should be explored. A methodology is desired which can accurately predict the transport rates of differing sediment sizes while taking into account non-collinear waves and currents, bed forms, and the effects of velocity skewness.

REFERENCES

Ackers, P. and W. R. White (1973). "Sediment transport: new approach and analysis." ASCE Journal of Hydraulics Division 99(11): 2041-2060.

Ahrens, J. P. and E. B. Hands (1998). "Parameterizing beach erosion/accretion conditions." Coastal Engineering: 2383-2394.

Bagnold, R. A. (1956). "The flow of cohesionless grains in fluids." Philosophical Transaction of the Royal Society, 249(964): 235-297.

Bijker, E. W. (1967). Some considerations about scales for coastal models with movable bed. Delft Hydraulics Laboratory Publication No. 50. Delft, The Netherlands.

Carter, H. S. (1970). Georgia tropical cyclones and their effect on the state. United States Department of Commerce: 33pp.

Cartwright, G. M. and C. T. Friedrichs (2003). Dredged Sediment Movement and Fate Project Brunswick Harbor, Georgia Vibracore Samples May 2003. Report to Evans-Hamilton, Inc. and the United States Army Corps of Engineers, Vicksburg, MS, Contract No. DACW39-99-D-008.

Cartwright, G. M. and C. T. Friedrichs (2004). Dredged sediment movement and fate project Brunswick Harbor, Georgia dredge plume survey December 2002. Report to Evans-Hamilton, Inc. and the United States Army Corps of Engineers, Vicksburg, MS, Contract No. DACW39-99-D-008.

D & A Instruments (2000). OBS-3a Instruction Manual, D & A Instruments, Port Townsend, WA. http://www.d-a-instruments.com

Dean, R. G. and R. A. Dalrymple (1991). Water Wave Mechanics for Engineers and Scientists. Advanced Series on Ocean Engineering, vol 2, World Scientific, Singapore.

Dean, R. G. and R. A. Dalrymple (2002). Coastal Processes with Engineering Applications, Cambridge University Press, New York.

Doering, J. C., B. Elfrink, D. M. Hanes, G. Ruessink (2000). Parameterization of velocity skewness under waves and its effect on cross-shore sediment transport. 27th Internation Conference on Coastal Engineering, Sydney.

Douglass, S. L., D. T. Resio, and E.B. Hands (1995). Impact of near-bottom currents on dredged material mounds near Mobile Bay. Dredging Research Program, United States Army Corps of Engineers, Vicksburg, MS: 1-39.

Environmental Tracing Systems (ETS) Limited (2004). Dredged Sediment Dispersal Study, Brunswick, Georgia, USA. Report to Evans Hamilton, Inc. and the United States Army Corps of Engineers, Vicksburg, MS, Contract No. DACW39-99-D-008.

Green, M. O. and J. D. Boon, III (1993). "The measurement of constituent concentrations in nonhomogeneous sediment suspensions using optical backscatter sensors." Marine Geology 110: 73-81.

Griffin, M. M. and V. J. Henry (1984). Historical changes in the mean high water shoreline of Georgia, 1857-1982. Georgia Department of Natural Resources, Environmental Protection Division and Georgia Geologic Survey: 96pp.

Hands, E. B. (1992). Monitoring of Alabama Berms. Dredging Research: Technical Notes, United States Army Corps of Engineers, Vicksburg, MS: 14pp.

Hayes, M. O. (1994). Georgia Bight. Geology of the Holocene Barrier Island System. R. A. Davis (ed.). Springer-Verlag, Berlin: 233-304.

Hoyt, J. H. and V. J. Henry (1967). "Influence of island migration on barrier island sedimentation." G. S. A. Bulletin, 82: 59-66.

Hubbard, D. K. and G. Oertel (1979). "The role of waves and tidal currents in the development of tidal-inlet sedimentary structures and sand body geometry: Examples from N. Carolina, S. Carolina, and Georgia." Journal of Sedimentary Petrology 49(4): 1073-1092.

Kingery, F. A. (1973). Textural analysis of shelf sands off the Georgia coast, California State University. Masters of Science unpublished thesis.

Komar, P. D. and M. C. Miller (1973). "The threshold of sediment movement under oscillatory water waves." Journal of Sedimentary Petrology 43(4): 1101-1110.

Kraus, N. C. (1992). Prediction of cross-shore movement of dredged material berms. Dredging Research--Technical Notes, United States Army Corps of Engineers, Vicksburg, MS: 1-16.

Kraus, N. C., M. Larson, and D. L. Kriebel (1991). "Evaluation of beach erosion and accretion predictors." Proceedings of Coastal Sediments 1991, ASCE: 572-578.

McCowan, J. (1894). "On the highest wave of permanent type." Philos. Mag. J. Sci. 38.

McNinch, J. E. (2003). Bathymetric Change on Mixed-Sediment Mounds: Brunswick Georgia. Report to Evans Hamilton, Inc. and the United States Army Corps of Engineers, Vicksburg, MS, Contract No. DACW39-99-D-008.

Meade, R. H. (1976). "Sediment problems in the Savannah River Basin." Proceedings of Symposium at Hickory Knob State Park, McCormick, South Carolina, Oct 14-15, 1975, Clemson University, South Carolina, 105-129.

Meyer-Peter, E. and R. Muller (1948). Formulas for bed-load transport. International Association of Hydraulic Structures Research, Stockholm.

Moritz, H. R., B. H. Johnson, and N.W. Scheffner (2000). Numerical models for predicting the fate of dredged material placed in open water. Handbook of Coastal Engineering. J. B. Herbich. New York, McGraw-Hill, 16.1-16.27.

Munoz-Perez, J. J., J. M. Gutierrez-Mas, J. M. Parrado, and L. Moreno (1999). "Sediment transport velocity by tracer experiment at Regla Beach (Spain)." Journal of Waterway, Port, Coastal, and Ocean Engineering, ASCE: 332-335.

Nielsen, P. (1992). Coastal Bottom Boundary Layers and Sediment Transport. Advanced Series on Ocean Engineering, Vol 4, World Scientific, Singapore.

Quick, M. C., K. Kingston, and S. Lei (1986). "Onset of sediment motion under waves and currents." Canadian Journal of Civil Engineering 14: 196-206.

R. D. Instruments (1996). Acoustic Doppler Current Profiler Principles of Operation: A Practical Primer, San Diego, CA.

Rouse, H. (1937). "Modern conceptions of the mechanics of turbulence." Transactions of the ASCE, 102: 436-543.

Scheffner, N. W. (1996). "Systematic analysis of long-term fate of disposed dredged material." Journal of Waterway, Port, Coastal, and Ocean Engineering 122(3): 127-133.

Sequoia Scientific Incorporated (2004). LISST-100 Particle Size Analyzer User's Manual, Version 4.2, Redmond, WA.

Shields (1936). "Anwendung der Aehnlichkeitsmechanik und Turbulenzforchung auf die Geschiebebewegung." Mitt Preuss Versuchsanstalt fur Wasserbau und Schiffbau 26.

Smith, S. J. (2003). Estimates of sediment transport and channel infilling on the Chukchi Sea, Alaska. Proceedings Coastal Sediments 2003. St. Petersburg Florida, ASCE.

Sontek (2001). SonTek/YSI ADVField/Hydra Acoustic Doppler Velocimeter (Field) Technical Documentation, San Diego, CA.

Soulsby, R. L. (1990). Tidal-current boundary layers. The Sea. Ocean Engineering Science, Vol. 9B, eds B. LeMehaute' and D. M. Hanes, Wiley, New York, 523-566.

Soulsby, R. L. (1997). Dynamics of Marine Sands Thomas Telford, 249pp.

Swart, D. H. (1974). Offshore sediment transport and equilibrium beach profiles. Delft Hydraulics Laboratory Publication No. 131. Delft, The Netherlands.

Swart, D. H. (1976). Predictive equations regarding coastal transports. 15th Coastal Engineering Conference, New York, ASCE, 1113-1132.

Tanner, W. F. (1960). "Florida coastal classification." Gulf Coast Assoc. Geological Society Transaction 10: 259-266.

United States Army Corps of Engineers (1971). National shoreline study: regional inventory report, South Atlanta Division: 367pp.

United States Army Corps of Engineers, Engineering Research and Development Center (2004). Data Report for Field Measurement Program in Support of Investigation of Dredged Sediment Movement and Fate at the Entrance to Brunswick Harbor, Georgia. Report prepared by Evans Hamilton, Inc., Contract No. DACW39-99-D-008.

United States Army Engineering Research and Development Center (1999). Research Brief: Comprehensive Open Water Site Management System, Technical Note DOER-N2: DMSMART-Dredged Material Spatial Management, Analysis, and Record Tool, Vicksburg MS.

Van Rijn, L. C. (1984). "Sediment transport, part I: bed load transport." Journal of Hydraulic Engineering, ASCE, 110(10): 1431-1456.

Van Rijn, L. C. (1984). "Sediment transport, part II: suspended load transport." Journal of Hydraulic Engineering, ASCE, 110(11): 1613-1641.

Vanoni, V. A. (1977). Sedimentation Engineering. ASCE Task Committee for the Preparation of the Manual on Sedimentation of the Sedimentation Committee of the Hydraulics Division.

Wren, D. G., B. D. Barkdoll, R. A. Kuhnle, and R. W. Derrow (2000). “Field techniques for suspended-sediment measurement.” Journal of Hydraulic Engineering, ASCE 126(2): 97-104.

Zenkovich, V. P. and M. L. Schwartz (1987). “Protecting the Black Sea-Georgian S.S.R. gravel coast.” Journal of Coastal Research 3(2): 201-211.